AD-A094 296 GENERAL ELECTRIC CO CINCINNATI OH AIRCRAFT ENGINE GROUP F/G 20/1
HIGH VELOCITY JET NOISE SOURCE LOCATION AND REDUCTION. TASK 3. --ETC(U)
DEC 78 P R KNOTT, P F SCOTT, P W MOSSEY DOT-OS-30034
UNCLASSIFIED R78AE0627-VOL-4 FAA-RD-76-79-3-4 NL

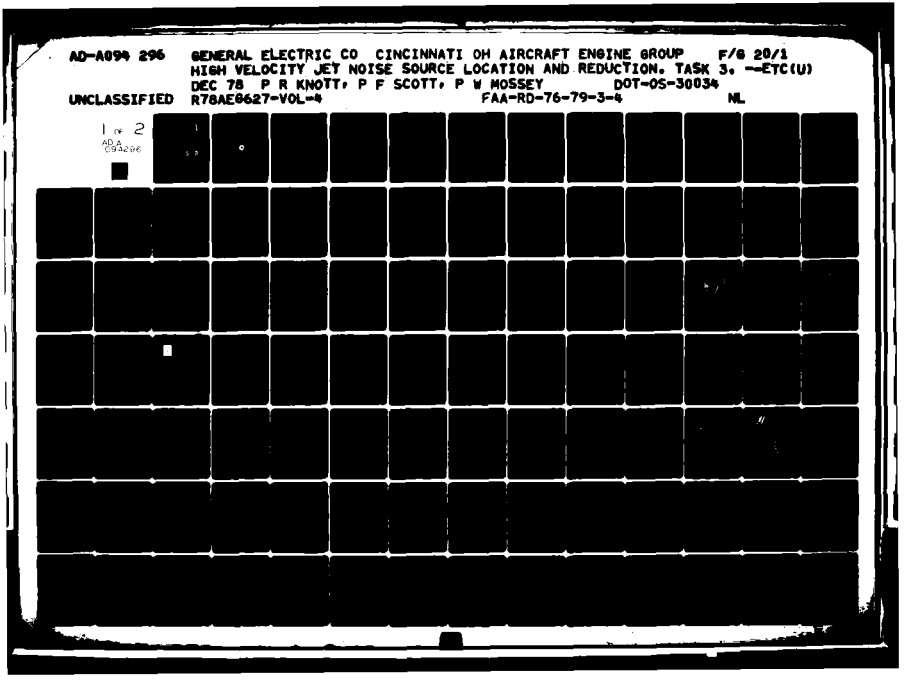

PHOTOGRAPH THIS SHEET

AD A094296

DTIC ACCESSION NUMBER

LEVEL III

INVENTORY

GENERAL ELECTRIC CO CINCINNATI OHIO AIRCRAFT ENGINE GROUP. HIGH VELOCITY JET NOISE SOURCE LOCATION AND REDUCTION. TASK 3. EXPERIMENTAL INVESTIGATION OF SUPPRESSION PRINCIPLES. VOLUME IV - LASER VELOCIMETER TIME DEPENDENT CROSS CORRELATION MEASUREMENTS. FINAL REPT. DEC.'78,

REPT. NO. R78AEG627 CONTRACT DOT-OS-30034 FAA-RD-76-79-3-4.

DISTRIBUTION STATEMENT A
Approved for public release;
Distribution Unlimited

DISTRIBUTION STATEMENT

ACCESSION FOR	
NTIS	GRA&I
DTIC	TAB
UNANNOUNCED	
JUSTIFICATION	
BY	
DISTRIBUTION /	
AVAILABILITY CODES	
DIST	AVAIL AND/OR SPECIAL
A	

DISTRIBUTION STAMP

DTIC
ELECTE
S JAN 29 1981 D
D

DATE ACCESSIONED

81 1 27 002

DATE RECEIVED IN DTIC

PHOTOGRAPH THIS SHEET AND RETURN TO DTIC-DDA-2

DOCUMENT PROCESSING SHEET

DTIC FORM OCT 79 70A

REPORT NO. FAA-RD-76-79, III - IV

R78AEG627

HIGH VELOCITY JET NOISE SOURCE LOCATION AND REDUCTION

TASK 3 - EXPERIMENTAL INVESTIGATION OF SUPPRESSION PRINCIPLES

Volume IV - Laser Velocimeter Time Dependent Cross Correlation Measurements

AUTHORS:

P.R. Knott
P.F. Scott
P.W. Mossey

GENERAL ELECTRIC COMPANY
AIRCRAFT ENGINE GROUP
CINCINNATI, OHIO 45215

DECEMBER 1978

FINAL REPORT

Prepared for

U.S. DEPARTMENT OF TRANSPORTATION
FEDERAL AVIATION ADMINISTRATION
Systems Research & Development Service
Washington, D.C. 20590

NOTICE

The contents of this report reflect the views of the General Electric Company which is responsible for the facts and the accuracy of the data presented herein. The contents do not necessarily reflect the official views or policy of the Department of Transportation. This report does not constitute a standard, specification or regulation.

1. Report No.	2. Government Accession No.	3. Recipient's Catalog No.
FAA-RD-76-79, III - IV		

4. Title and Subtitle	5. Report Date
High Velocity Jet Noise Source Location and Reduction Task 3 - Experimental Investigation of Suppression Principles Volume IV - Laser Velocimeter Time Dependent Cross Correlation Measurements	December 1978
	6. Performing Organization Code
7. Author(s) P.R. Knott P.W. Mossey P.F. Scott	8. Performing Organization Report No. R78AEG627
	10. Work Unit No.
9. Performing Organization Name and Address General Electric Company Group Advanced Engineering Division Aircraft Engine Group Cincinnati, Ohio 45215	11. Contract or Grant No. DOT-OS-30034
	13. Type of Report and Period Covered Technical Report October 1974-October 1977
12. Sponsoring Agency Name and Address U.S. Department of Transportation, Federal Aviation Administration Systems Research and Development Service Washington, D.C. 20590	14. Sponsoring Agency Code ARD-550

15. Supplementary Notes R.S. Zuckerman, Program Manager; this report is in partial fulfillment of the subject program. Related documents to be issued in the course of the program include final reports of the following Tasks: Task 1 - Activation of Facilities and Validation of Source Location Techniques; Task 1 Supplement - Certification of the General Electric Jet Noise Anechoic Test Facility; Task 2 - Theoretical Developments and Basic Experiments; Task 4 - Development/Evaluation of Techniques for "Inflight" Investigation; Task 5 - Investigation of "Inflight" Aero-Acoustic Effects; Task 6 - Noise Abatement Nozzle Design Guide.

16. Abstract Experimental investigations were conducted of suppression principles; including developing an experimental data base, developing a better understanding of jet noise suppression principles, and formulating empirical methods for the acoustic design of jet noise suppressors. Acoustic scaling has been experimentally demonstrated, and five "optimum" nozzles have been selected for subsequent anechoic free-jet testing.

In-jet/in-jet and in-jet/far-field exhaust noise diagnostic measurements were conducted using a Laser Velocimeter (LV). Measurements were performed on a conical nozzle and a coannular plug nozzle. Two-point, space/time measurements using a two-LV system were completed for the conical nozzle. Measurements of mean velocity, turbulent velocity, eddy convection speed, and turbulent length scale were made for a subsonic ambient jet and for a sonic heated jet. For the coannular plug nozzle, a similar series of two-point, laser-correlation measurements were performed. In addition, cross correlations between the laser axial component of turbulence and a far-field acoustic microphone were performed.

This volume is part of the four volume set that constitutes the Task 3 final report. The other volumes are:

Volume I - Verification of Suppression Principles and Development of Suppression Prediction Methods

Volume II - Parametric Testing and Source Measurements

Volume III - Suppressor Concepts Optimization

17. Key Words (Suggested by Author(s))	18. Distribution Statement
Laser Velocimeter, Real-Time, Velocity Measurements, Cross-Correlation	Document is available to the public through the National Technical Information Center Springfield, Virginia

19. Security Classif. (of this report)	20. Security Classif. (of this page)	21. No. of Pages	22. Price*
Unclassified	Unclassified	136	

* For sale by the National Technical Information Service, Springfield, Virginia 22151

METRIC CONVERSION FACTORS

Approximate Conversions to Metric Measures

Symbol	When You Know	Multiply by	To Find	Symbol
		LENGTH		
in	inches	*2.5	centimeters	cm
ft	feet	30	centimeters	cm
yd	yards	0.9	meters	m
mi	miles	1.6	kilometers	km
		AREA		
in^2	square inches	6.5	square centimeters	cm^2
ft^2	square feet	0.09	square meters	m^2
yd^2	square yards	0.8	square meters	m^2
mi^2	square miles	2.6	square kilometers	km^2
	acres	0.4	hectares	ha
		MASS (weight)		
oz	ounces	28	grams	g
lb	pounds	0.45	kilograms	kg
	short tons (2000 lb)	0.9	tonnes	t
		VOLUME		
tsp	teaspoons	5	milliliters	ml
Tbsp	tablespoons	15	milliliters	ml
fl oz	fluid ounces	30	milliliters	ml
c	cups	0.24	liters	l
pt	pints	0.47	liters	l
qt	quarts	0.95	liters	l
gal	gallons	3.8	liters	l
ft^3	cubic feet	0.03	cubic meters	m^3
yd^3	cubic yards	0.76	cubic meters	m^3
		TEMPERATURE (exact)		
°F	Fahrenheit temperature	5/9 (after subtracting 32)	Celsius temperature	°C

*1 in = 2.54 (exactly). For other exact conversions and more detailed tables, see NBS Misc. Publ. 286, Units of Weights and Measures, Price $2.25, SD Catalog No. C13.10:286.

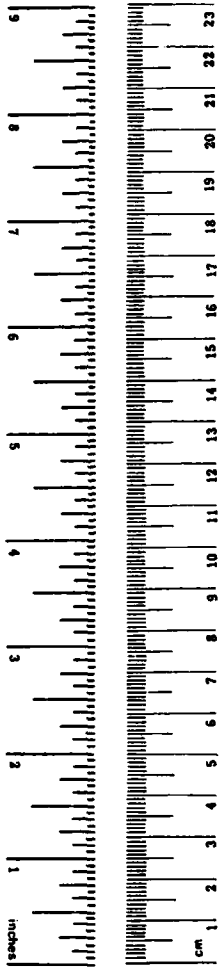

Approximate Conversions from Metric Measures

Symbol	When You Know	Multiply by	To Find	Symbol
		LENGTH		
mm	millimeters	0.04	inches	in
cm	centimeters	0.4	inches	in
m	meters	3.3	feet	ft
m	meters	1.1	yards	yd
km	kilometers	0.6	miles	mi
		AREA		
cm^2	square centimeters	0.16	square inches	in^2
m^2	square meters	1.2	square yards	yd^2
km^2	square kilometers	0.4	square miles	mi^2
ha	hectares (10,000 m^2)	2.5	acres	
		MASS (weight)		
g	grams	0.035	ounces	oz
kg	kilograms	2.2	pounds	lb
t	tonnes (1000 kg)	1.1	short tons	
		VOLUME		
ml	milliliters	0.03	fluid ounces	fl oz
l	liters	2.1	pints	pt
l	liters	1.06	quarts	qt
l	liters	0.26	gallons	gal
m^3	cubic meters	35	cubic feet	ft^3
m^3	cubic meters	1.3	cubic yards	yd^3
		TEMPERATURE (exact)		
°C	Celsius temperature	9/5 (then add 32)	Fahrenheit temperature	°F

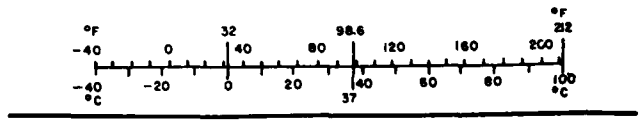

PREFACE

This report describes the work performed under Task 3 of the DOT/FAA High Velocity Jet Noise Source Location and Reduction Program (Contract DOT-OS-30034). The objectives of the contract were:

- Investigation, including scaling effects, of the aerodynamic and acoustic mechanisms of various jet noise suppressors.
- Analytical and experimental studies of the acoustic source distribution in such suppressors, including identification of source location, nature, and strength and noise reduction potential.
- Investigation of in-flight effects on the aerodynamic and acoustic performance of these suppressors.

The results of these investigations are expected to lead to the preparation of a design report for predicting the overall characteristics of suppressor concepts, from models to full scale, static to in-flight conditions, as well as a quantitative and qualitative prediction of the phenomena involved.

The work effort in this program was organized under the following major Tasks, each of which is reported in a separate Final Report:

Task 1 - Activation of Facilities and Validation of Source Location Techniques.

Task 2 - Theoretical Developments and Basic Experiments.

Task 3 - Experimental Investigation of Suppression Principles.

Task 4 - Development and Evaluation of Techniques for "In-flight" Investigation.

Task 5 - Investigation of "In-flight" Aero-Acoustic Effects on Suppressed Exhausts.

Task 6 - Preparation of Noise Abatement Nozzle Design Guide Report.

Task 1 was an investigative and survey effort designed to identify acoustic facilities and test methods best suited to jet noise studies. Task 2 was a theoretical effort complemented by theory verification experiments which extended across the entire contract period of performance.

The subject of the present, Task 3 report series (FAA-RD-76-79III -- I, II, III, and IV) was formulated as a substantial part of the contract effort to gather various test data on a wide range of high velocity jet nozzle suppressors. These data, together with supporting theoretical advances from Task 2, have led to a better understanding of jet noise and jet noise

suppression mechanisms, as well as to a validation of scaling methods. Task 3 helped to identify several "optimum" nozzles for simulated in-flight testing under Task 5, and to provide an extensive, high quality data bank leading to formulation of methods and techniques useful for designing jet noise suppressors for application in the Task 6 design guide as well as in future studies.

Task 4 was similar to Task 1, except that it dealt with the specific test facility requirements, measurement techniques, and analytical methods necessary to evaluate the "in-flight" noise characteristics of simple and complex suppressor nozzles. This effort provided the capability to conduct the "flight" effects test program of Task 5.

TABLE OF CONTENTS

TABLE OF CONTENTS (Continued)

TABLE OF CONTENTS (Concluded)

LIST OF ILLUSTRATIONS

LIST OF ILLUSTRATIONS (Continued)

LIST OF ILLUSTRATIONS (Concluded)

LIST OF TABLES

LIST OF SYMBOLS

a	Lens to object-plane distance
a'	Lens to image-plane distance
a_o	Ambient speed of sound
A_r	Area ratio
b	Beam separation distance
d	Diameter of central bright spot (Airy disc)
D	Incident beam diameter (Sections 4 and 5); also used as the diameter of a circular jet
D_{eq}	Equivalent Diameter - diameter based on the total area of the nozzle
D^2_{max}	The value of $\frac{\partial^2 Ru^2 p'}{\partial \tau^2}$ at τ that corresponds to $Ru^2 p'$ at its maximum
e	The fractional error in an estimate: $e = \frac{\hat{x} - x}{x}$
$E\{x\}$	Expected value operation in statistics: $E\{x\} = \int_{-\infty}^{\infty} x\, f_x(x)dx$
f	Lens focal length (Sections 4 and 5); also used as frequency
$f(\xi)$	Longitudinal turbulence correlation function
f_x	Probability density function
F_x	Probability distribution function: $F_x(x) = \int_{-\infty}^{x} f_x(\mu)d\mu$
h	Slit width (Sections 4 and 5); annular gap height for a coannular plug nozzle
I	Local intensity in laser beam (Sections 4 and 5); Acoustic intensity in the far-field
$\bar{K}$	Length ray vector

ℓ Length of beam intersection

L_x Integral turbulence length scale (see Figure 10-5)

m_n The n^{th} central moment of a probability distribution:

$$m_n = \int_{-\infty}^{\infty} (x - \mu_x)^n \; f_x(x)dx$$

M_c Convection Mach number (V_c/a_o)

M_j Ideal jet Mach number

n Number of wavelengths

p Static pressure

p' Acoustic pressure

P Width of slit image (Sections 4 and 5); probability (Sections 7 and 8)

P_r Pressure ratio (total to ambient)

r Distance between jet noise source and far-field observer; also used as a radial coordinate for nozzle geometry specification

R_L The correlation function of an eddy in the Lagrangian frame

$R_{xy}(\tau)$ The cross-correlation function between random variables x(t) and y(t+τ)

$\hat{R}_{xy}(\tau)$ An estimate of $R_{xy}(\tau)$

R_r Radius ratio

$R_{u^2p'}$ Total cross-correlation function defined as:

$$E\{u^2(\vec{y})\; p'(\vec{x},\vec{y};\tau)\} = u^2(y)\; p'(\vec{x},\vec{y};\tau)$$

When discussed as normalized:

$$\frac{\overline{u^2(\vec{y})\; p'(\vec{x},\vec{y};\tau)}}{\sqrt{(\bar{u}^2)^2\; \bar{p}'^2}}$$

R_{Total} Total cross-correlation function

S Fringe spacing

$S(R_{Total})$ Spectrum of $R_{u^2p'}$

$S(\frac{\partial^2 R_{Total}}{\partial \tau^2})$ Spectrum of $\frac{\partial^2 R u^2 p'}{\partial \tau^2}$

t Transit time between bright fringes (Sections 5 and 5); time

$t_{\alpha,N}$ Defined as Z_α except the probability is student T with N degrees of freedom

T_{ij} Lighthill's stress tensor (see Equation 6-3)

T_L The total time length of the data record used to estimate a correlation function

T_T Total temperature

u Dimensionless parameter (Sections 4 and 5); Instantaneous velocity

u' Turbulence velocity

$\bar{U}$ Mean velocity

v Dimensionless parameter (Sections 4 and 5)

$\bar{V}$ Particle velocity (Sections 4 and 5)

V_j Ideal jet velocity

V_o Jet noise source volume element

$VAR\{x\}$ The statistical variance of the random variable x:

$$VAR\{x\} = E\{(x - E\{x\})^2\}$$

$$= E\{x^2 - E^2\{x\}\}$$

V_c Convection velocity

V_j^{mix} Specific thrust or weight flow average velocity for a coannular nozzle configuration; or mixed velocity defined as:

$$(V_j^o \dot{\omega}^o + V_j^i \dot{\omega}^i)/(\dot{\omega}^o + \dot{\omega}^i)$$

V_y Velocity component perpendicular to the fringes

X Distance along optic axis of lens (Sections 4 and 5); coordinate along jet axis

$\vec{x}$ Position vector from origin to observer

$\vec{y}$ Position vector from origin to jet noise source element

Z_α The point on the unit Gausian distribution such that the area under the distribution is α:

$$\alpha = \int_{-\infty}^{Z_\alpha} \frac{1}{\sqrt{2\pi}} \exp\left(-\frac{1}{2}x^2\right) dx$$

α Included angle between laser beams; also see definition of Z_α

β Slit half angle of subtention

δ_{ij} Unity sensor

Δ Optical path length (Sections 4 and 5); the width of the time grid used to reconstruct the correlation function (Sections 7 and 8)

$\Delta\nu$ Scattering frequency

θ Observation angle

Θ Convection amplification factor (see Equation 6-5)

λ Wavelength of coherent radiation (Sections 4 and 5); the average rate of arrival of particles at the probe volume of the laser velocimeter

$\mu(t)$ The unit step function

$$\mu(t) = 1 \; ; \quad t \geq o$$

$$\mu(t) = 0 \; ; \quad t < o$$

$\mu_o(t)$ The Dirac delta function

μ_x The expected value or mean of the random variable x.

ξ The operation distance between LV probe volumes in a two-point velocity correlation measurement

ρ Fluid density

σ_x The standard deviation of the random variable x; also the turbulence level

τ Time

τ_o The retarded time (r/a_o)

τ_i The value of τ where $|R_{xy}(\tau)|$ is maximum

τ_{ij}	The viscous stress tensor
ω_f	Typical radian frequency of turbulence
ω_t	Radian frequency in the turbulence
$\dot{\omega}$	Weight flow

Super Scripts

i	Inner stream of coannular plug nozzle
o	Outer stream of coannular plug nozzle

1.0 SUMMARY

The High Velocity Jet Noise Source Location and Reduction Program (Contract DOT-OS-30034) was conceived to bring analytical and experimental knowledge to bear on understanding the fundamentals of jet noise for simple and complex suppressors.

Task 3, the subject of this report, involved the experimental investigation of suppression principles, including developing an experimental data base, developing a better understanding of jet noise suppression principles, and formulating empirical methods for the acoustic design of jet noise suppressors. Acoustic scaling has been experimentally demonstrated, and five "optimum" nozzles were selected for anechoic, free-jet testing in Task 5.

Volume I - Verification of Suppression Principles and Development of Suppression Prediction Methods - Some of the experimental studies (reported in Volume II) involved acquisition of detailed, far-field, acoustic data and of aerodynamic jet-flow-field data on several baseline and noise-abatement nozzles. These data were analyzed and used to validate the theoretical jet noise prediction method of Task 2 (referred to as M*G*B, designating the authors' initials) and to develop and validate the empirical noise-prediction method presented herein (referred to as M*S, designating the last name initials of the authors).*

The Task 2 theoretical studies conclude that four primary mechanisms influence jet noise suppression: fluid shielding, convective amplification, turbulent mixing, and shock noise. A series of seven suppressor configurations (ranging from geometrically simple to complex) were evaluated in Task 3 to establish the relative importance of each of the four mechanisms. Typical results of this evaluation of noise mechanisms are summarized in Figure 1-1 in terms of perceived noise level (PNL) directivity for a conical nozzle. In general, mechanical suppressors exhibit a significant reduction in shock

*The Task 3 empirical (M*S) method was initially intended for nozzle geometries which could not be modeled in the purely analytical Task 2 (M*G*B) method (a multielement nozzle with a treated ejector, for example).

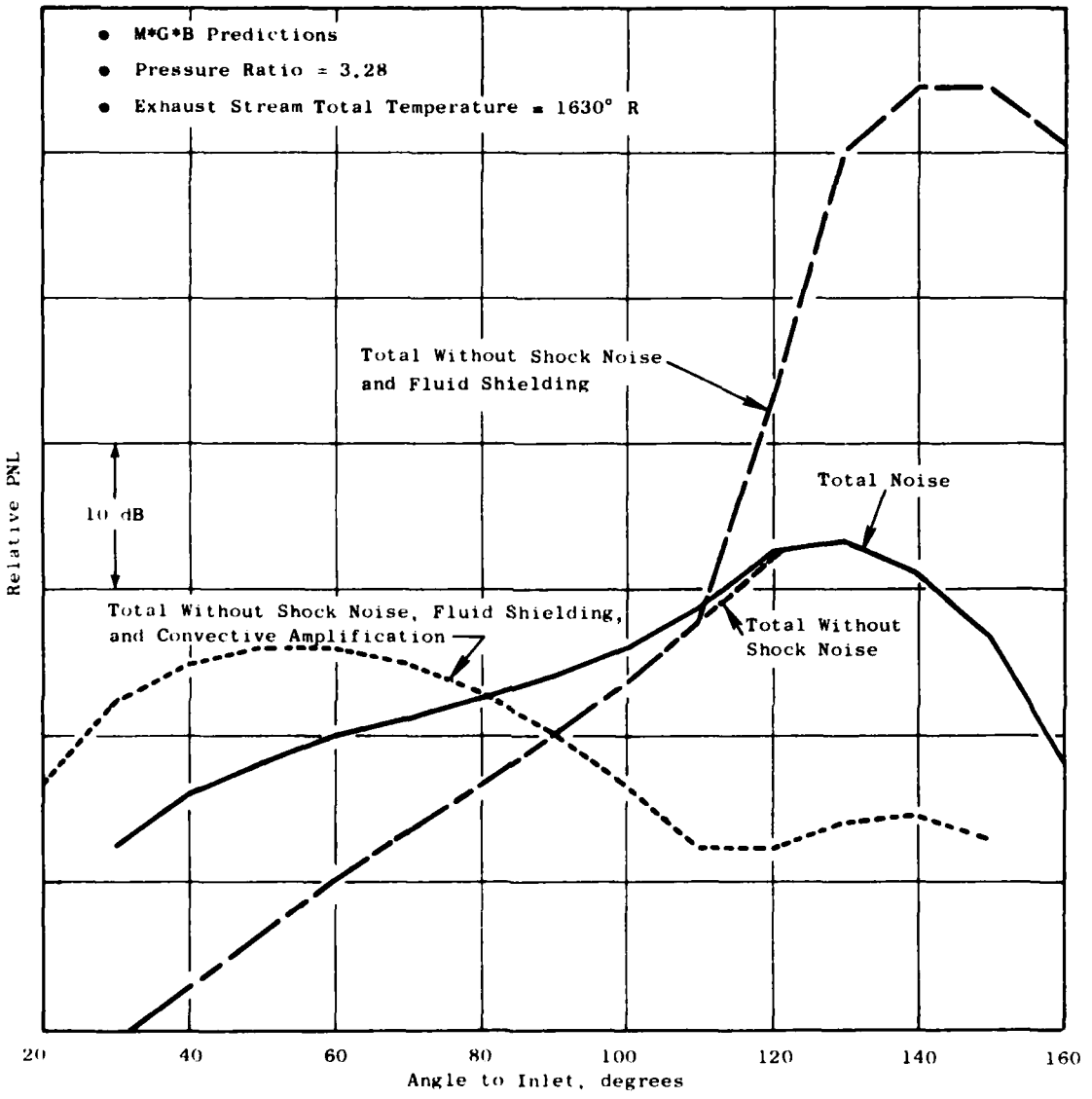

Figure 1-1. Evaluation of Noise Mechanisms for a Conical Nozzle.

noise relative to a baseline conical nozzle, reduce the effectiveness of fluid shielding (increase rather than suppress noise), reduce the effectiveness of convective amplification (reduce noise), and produce a modest reduction in turbulent mixing noise. The largest amount of shock noise reduction correlates with the suppressor which has the smallest characteristic dimension. Fluid shielding decreases because suppressors cause the mean velocity and temperature of the jet plume to decay faster than the conical baseline. A reduction in convection Mach number (and hence in convective amplification) occurs because a suppressor plume decays very rapidly. Turbulent mixing noise is reduced through alteration of the mixing process that results from segmenting the exhaust jet.

Aerodynamic flow-field measurements (mean-velocity profiles) were demonstrated to be useful in verifying the flow-field predictions which were calculated by the M*G*B (theoretical) noise-prediction program. Noise source location devices such as the Ellipsoidal Mirror (EM) were demonstrated to be less useful than the Laser Velocimeter (LV) for the M*G*M theory verification studies because the LV provides data which may be directly compared with predictions made using the M*G*M program. Axial and radial mean-velocity profiles are typical examples of such comparisons.

The empirical M*S jet noise prediction method has been developed to predict the static acoustic characteristics of multielement suppressors applicable to both advanced turbojets and variable-cycle engines (which are representative of power plants for future supersonic cruise aircraft). The effect of external flow on the M*S jet noise prediction is discussed in the Task 6 Design Guide Report. Inputs required to use the M*S computational procedure include: element type, element number, suppressor area ratio and radius ratio, chute-spoke planform and cant angle, and plug diameter. The prediction accuracy is estimated to be $\pm$3.3 Effective Perceived Noise Decibels (EPNdB) at a 95% confidence level. Figure 1-2 illustrates the correlation between measured and predicted EPNLs for all types of suppressors.

The merits of both the M*S and M*G*B computational techniques can be stated as follows. The empirical (M*S) jet noise prediction method, based on correlations of scale-model jet data, serves as a useful preliminary design

- Flyover calculation using static data corrected to free-field conditions.
- The "Reference" level is the predicted value of noise for each nozzle, at a specified set of thermodynamic conditions, plus an arbitrary value of 100 dB.

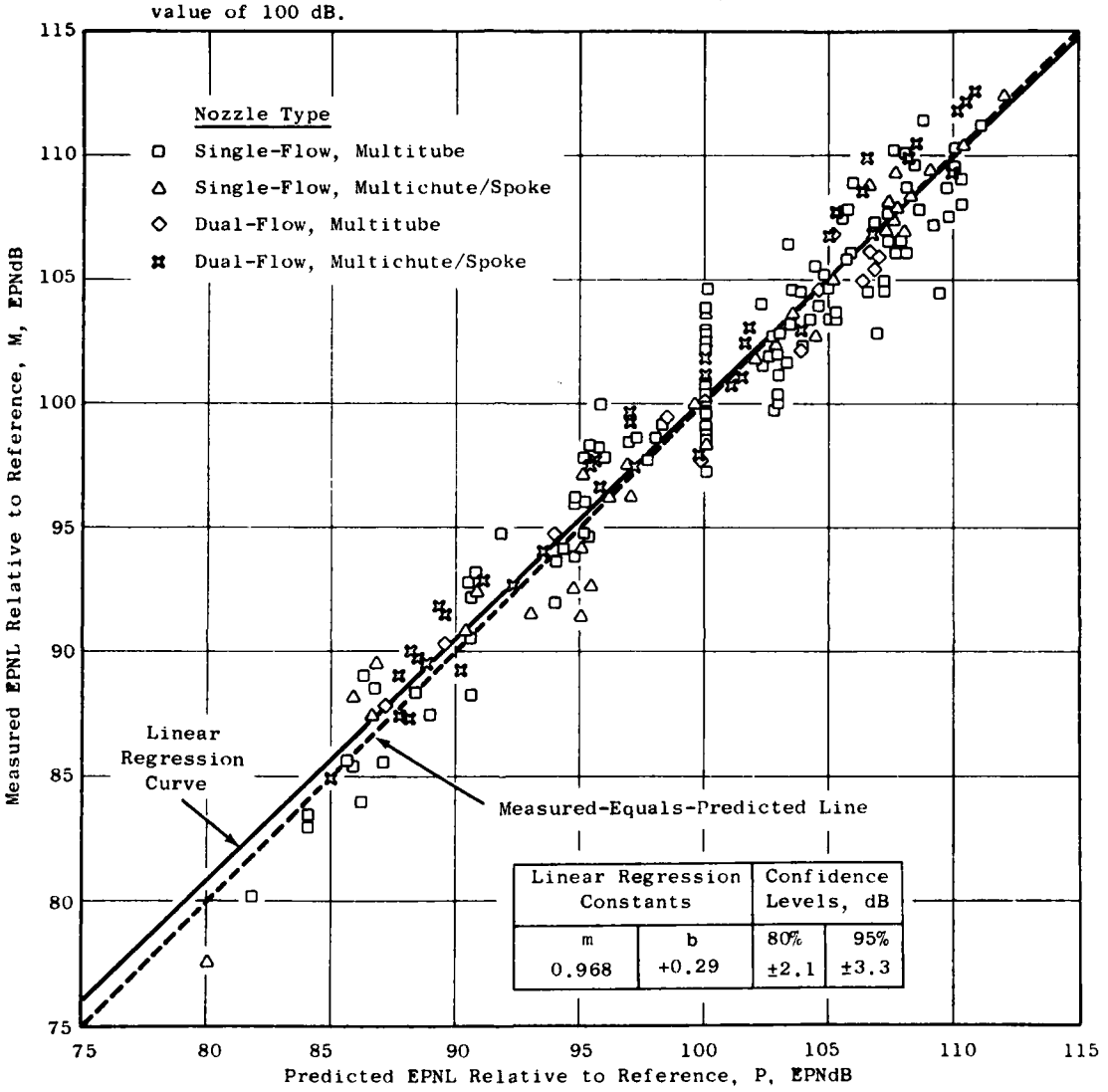

Figure 1-2. Correlation Between Measured and Predicted Effective Perceived Noise Level, EPNL, for all Types of Suppressor Nozzles.

and prediction tool for selecting the basic nozzle type (chute, spoke, multi-tube, etc.) and primary geometric parameters (element number, area ratio, etc.) for a given application. It is also useful in evaluating the acoustic performance of a given suppressor nozzle, provided the nozzle is one of the types from which the correlation was derived. Further, the method is useful for doing parametric studies since the computation procedure is relatively simple and economical of both computer time and cost. The theoretical (M*G*B) prediction method, on the other hand, is more suited to detailed design and analysis of a suppressor nozzle. It can supply detailed information on the jet plume flow development as well as the far-field acoustic characteristics. It is also capable of evaluating changes in nozzle planform shape, element placement and spacing, etc. In addition, the theoretical prediction model is a useful diagnostic tool, capable of assessing the relative roles the various mechanisms play in the noise suppression process, and can also serve as a source location analysis tool.

Volume II - Parametric Testing and Source Measurements - A parametric experimental series was conducted to provide far-field acoustic data on 47 baseline and suppressor nozzle configurations and to provide aerodynamic nozzle performance on 18 of the configurations. The data presented in this volume were taken for use in the current program as well as to provide an extensive, high-quality, data base for future studies. The impact of varying the area ratio and velocity ratio of dual-flow, baseline nozzle configurations was investigated, and the importance of shock noise was assessed. The impact of varying area ratio and element number was parametrically studied for both single and dual-flow suppressors; core plug geometry, velocity ratio, and weight flow ratio were evaluated for dual-flow suppressors. These studies establish absolute static suppression levels on the basis of normalized maximum PNL, for several families of suppressor nozzles, as illustrated in Figure 1-3.

Parametric testing identified the following primary trends for single-flow and for dual-flow suppressors during static operation:

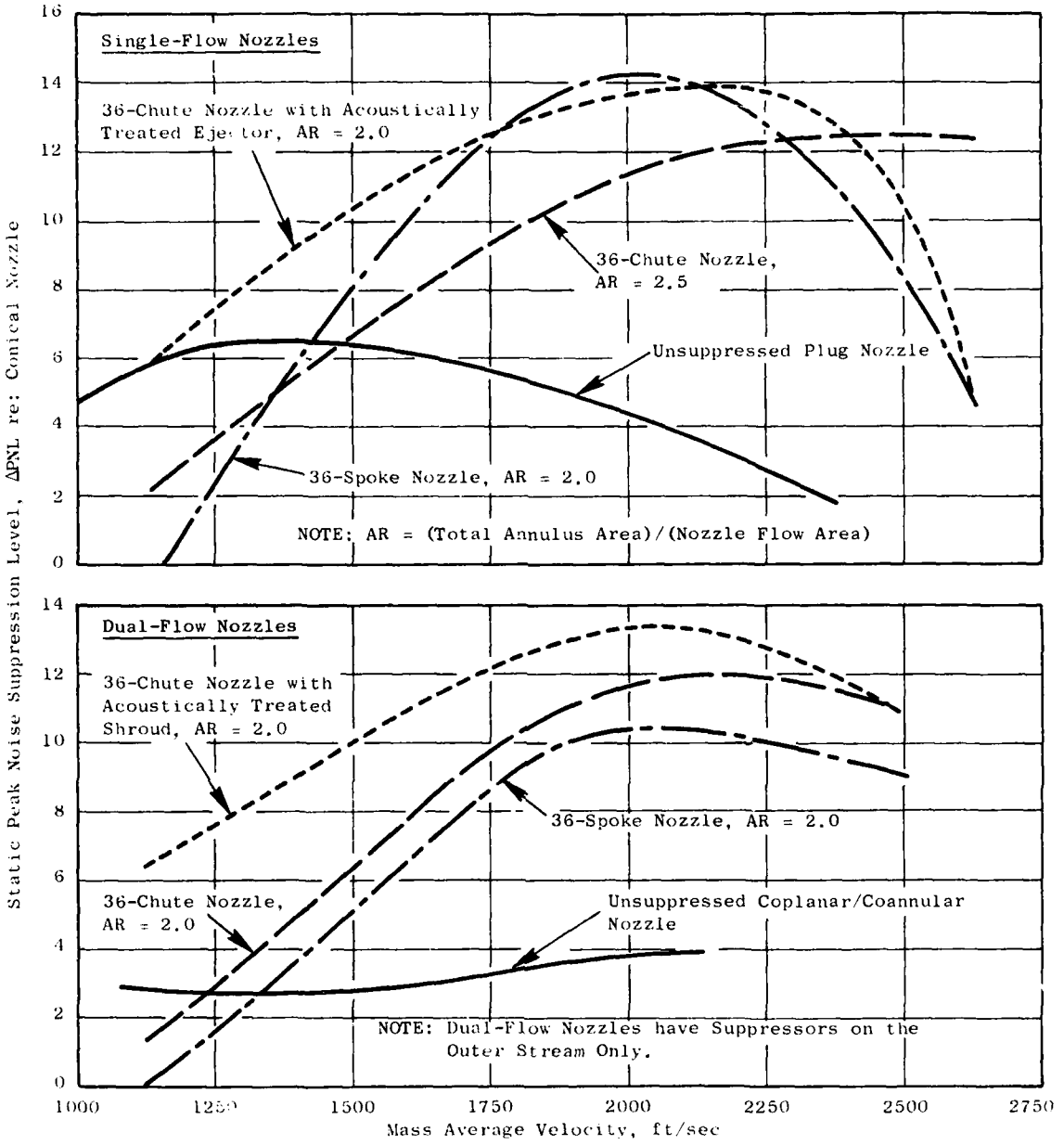

Figure 1-3. Typical Peak Static Noise Suppression Characteristics.

Single Flow

- Suppression increases with increasing area ratio at high jet velocity.
- Suppression decreases with increasing area ratio at low jet velocity.
- Suppression level is affected by element type (spoke systems suppress slightly better than chutes).

Dual Flow

- Suppression increases with increasing area ratio..
- Suppression increases with increasing element number at high jet velocity.
- Suppression level is affected by core plug geometry [by 2 to 3 decibels (dB)].
- Suppression increases 3 to 4 dB when a treated ejector is added to a suppressor configuration.

Selective, free-jet tests conducted on eight configurations indicate that suppression generally decreases in flight. Typical static versus free-jet results are shown in Table 1-1.

The aerodynamic performance test recorded on 18 of the configurations at both static and wind-on conditions is also included in this volume. Base pressure measurements were taken on several of the models in order to determine base drag (which is thought to be responsible for the poor aerodynamic performance of most mechanical suppressors in flight). These wind tunnel tests identified the following primary trends in aerodynamic performance:

- Performance decreases with increasing element number.
- Performance increases with increasing chute depth.
- Performance increases with increasing ratio of inner flow area to outer flow area.
- Performance is affected by element type (chutes perform better than spokes because spokes have higher base drag).

Table 1-1. Typical Summary of Nozzle Static and Projected Flight Peak PNL Suppression Characteristics.

- Suppression Levels are Relative to a Conical Nozzle at Equivalent Flight Conditions
- V_j = 2500 ft/sec

Configuration	Suppression Level, db	
	Static	Flight
Plug Nozzle - 0.789 Radius Ratio	1.3	3.0
Plug Nozzle - 0.85 Radius Ratio	2.3	3.7
8-Lobe Nozzle	5.6	5.6
AR = 2.5 36-Chute Nozzle	13.5	10.9
AR = 2.5 36-Chute Nozzle with Auxiliary Flow	12.5	9.4
104-Tube Nozzle	12.0	12.0

The base pressure correlations provide a procedure for predicting suppressor nozzle aerodynamic performance.

Volume III - Suppressor Concepts Optimization - Several studies were conducted to attempt an optimization of suppressor concepts. The end product of this overall effort was to design five nozzles for static and free-jet testing in Task 5. Trade studies of performance versus suppression, aircraft integration studies, and development of a figure of merit method of analysis all make up the activities in this "optimization" process.

Trade studies of suppression versus aerodynamic performance indicate that a properly selected and designed mechanical suppressor can attain a delta suppression to delta thrust coefficient ratio ($\Delta PNL/\Delta C_{f_g}$) of almost 3.0 (based on static suppression and wind-on aerodynamic performance).

The aircraft integration study consisted of ranking nine baseline and suppressor nozzles with respect to performance level, suppression level, weight, impact on aircraft mission range, and noise footprint. In general, suppression level was found to be the most important design variable, with performance and weight ranking second and third, respectively.

The appropriate figure of merit, considering all the design variables, was found to be aircraft range. However, use of range as the figure of merit requires that the aircraft mission be specified, and several techniques for cursorily ranking the suppressors based solely on suppression level, performance, and weight may also be identified. A summary of the range versus noise characteristics of typical nozzle configurations is presented in Figure 1-4. Once a noise goal is specified, adding a suppressor provides a significant range improvement over an unsuppressed system because adding a suppressor is less costly than reducing noise by enlarging the engine to reduce jet velocity.

The design of the five optimum nozzles was based on data from previous studies, performed by government and industry, on the M*G*B and M*S models discussed above and on the parametric data obtained in the acoustic and aerodynamic performance test series reported in Volume II. The configurations were designed and fabricated for open-throat, anechoic, free-jet testing in Task 5. The configurations chosen for evaluation were: (1) a 32-chute, single-flow

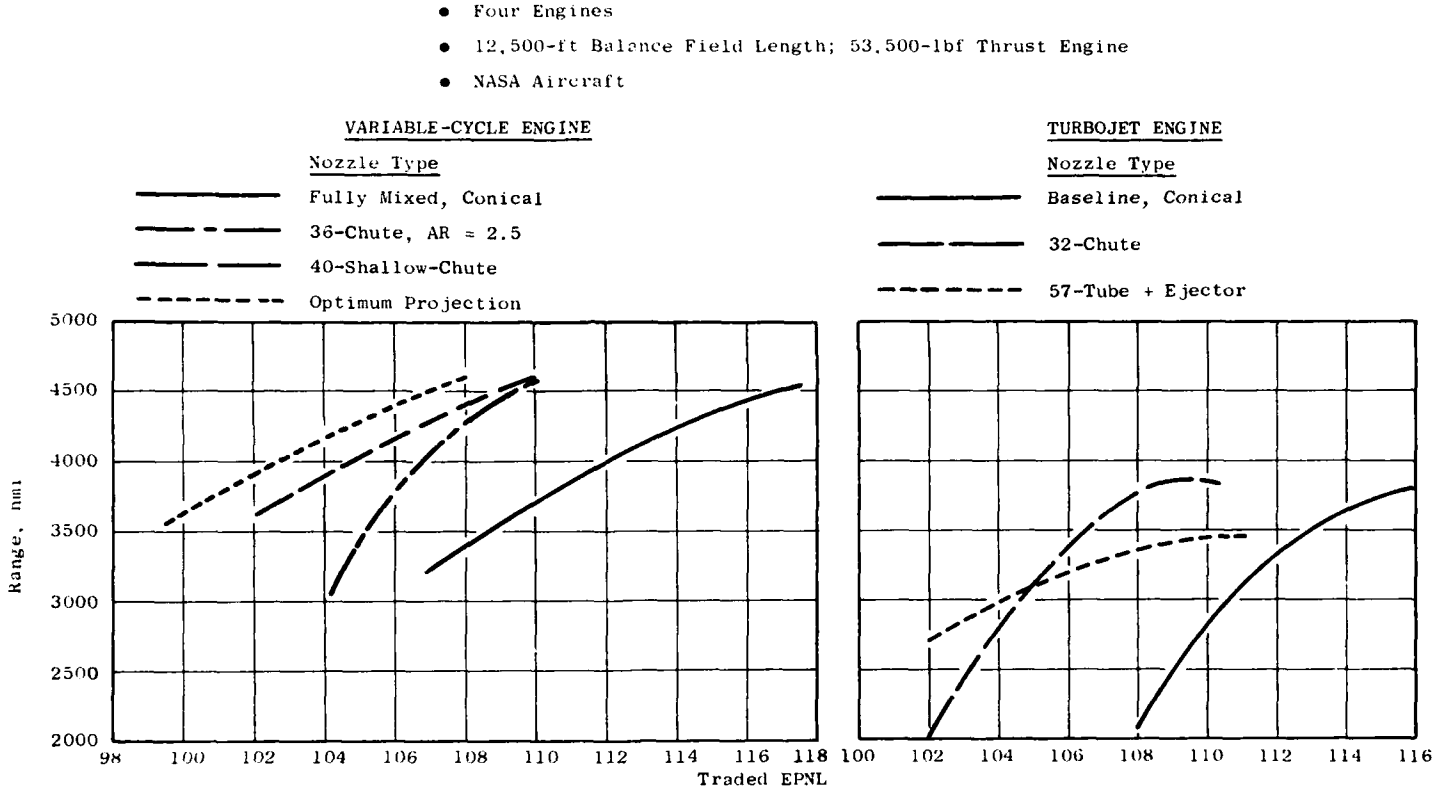

Figure 1-4. Summary of Range and Noise Characteristics for Several Baseline and Suppression Levels.

nozzle; (2) a 40-shallow-chute, dual-flow nozzle; (3 and 4) a 36-chute, dual-flow nozzle, with and without a treated ejector; and (5) a 54-element, co-planar-mixer, plug nozzle.

Demonstration of acoustic scaling for several suppressor configurations was conducted to assure the adequacy of using scale-model results to project full-scale suppression levels. Full-scale data were obtained on several suppressor configurations using J79 and J85 engines. The suppressors evaluated were: (1) a baseline conical nozzle, (2) a 32-chute nozzle with and without a treated ejector, (3) an 8-lobe nozzle, and (4) a 104-tube nozzle. Scale-model data were obtained for these same configurations to allow comparison of scale-model and full-scale results. In general, peak full-scale suppression levels projected from scale-model data were verified by the full-scale engine results. Directivity patterns were duplicated within $\pm$2 PNdB (the largest differences occurring with the conical nozzle configuration). Some spectral anomalies were observed for select cases; however, they were not of sufficient magnitude to invalidate the scale-model results. The conclusion resulting from this study is that full-scale noise levels can be predicted from scale-model test results using Strouhal scaling laws.

Volume IV - Laser Velocimeter Time Dependent Cross Correlation Measurements - In-jet/in-jet and in-jet/far-field exhaust noise diagnostic measurements conducted using a Laser Velocimeter (LV) are reported in this volume. Measurements were performed on a conical nozzle and a coannular plug nozzle. Two-point, space/time measurements using a two-LV system were completed for the conical nozzle. Measurements of mean velocity, turbulent velocity, eddy convection speed, and turbulent length scale were made for a subsonic ambient jet and for a sonic heated jet. For the coannular plug nozzle, a similar series of two-point, laser-correlation measurements were performed. In addition, cross correlations between the laser axial component of turbulence and a far-field acoustic microphone were performed.

Volumes I, II, III, and IV contain the results of a comprehensive effort to identify and integrate the theoretical studies, parametric test data, acoustic and performance diagnostic measurements, and system studies. A logical procedure has evolved for conducting suppressor design trade-offs.

2.0 INTRODUCTION

The first 20 years of commercial aircraft operation with jet propulsion have clearly demonstrated the need for effective high velocity jet noise suppression technology in order to meet community acceptance. Aircraft system studies show that an efficient jet noise suppression device is required if a commercial supersonic aircraft is to be economically viable as well as environmentally acceptable. The current state of the art of high velocity jet noise suppression would make a supersonic transport (SST), with advanced technology engines, meet 1969 noise rules (at best). This state of the art is represented by the material in References 1 through 6.

Reference 1 describes analytical and experimental investigations which were conducted in the early 1960's. This study established a basis for development of mathematical and empirical methods for the predictions of jet-flow-field, aerodynamic characteristics and for determining the directional characteristics of jet noise suppressors. This work was limited in the sense that the suppressors evaluated had only modest suppression potential, and the measurement techniques available did not allow the acquisition of high-frequency, spectral data necessary to establish full-scale, PNL suppression levels.

The development of commercial SST vehicles by the U.S. and by the British-French multinational corporation in the 1960's placed extreme emphasis on the need for effective and efficient noise suppression devices. Phase I of work, conducted by the Boeing and General Electric companies, is summarized in References 2 and 3. Primary emphasis was on jet noise suppressor development through model and engine testing applicable to an afterburning turbojet engine. Suppressor designs were based primarily on empirical methods. Phase II of this effort, References 4 and 5, continued the suppressor development with a stronger emphasis placed on the integration of analytical studies and experimental test data. Specifically, the Boeing Company concentrated on optimization of tube-type-suppressor systems and related semiempirical prediction methods. General Electric focused on the development both of chute and of tube-type-suppressor systems with primary emphasis placed on optimization of chute-type-suppressor nozzles.

Similar studies were conducted by the British and French in development of the Concorde, and typical results are summarized in Reference 6.

The design technology represented in References 1 through 6 is primarily semiempirical. The absence of general design rules based on engineering principles led to the Government's formulation of the High Velocity Jet Noise Program, Contract DOT-OS-30034, in 1973. The purpose has been to achieve fundamental understanding, on a quantitative basis, of the mechanisms of jet noise generation and suppression and to develop design methods.

This report presents the results of Task 3 of the contract. It provides the experimental data base which was used in conjunction with the supporting theories from Task 2 to develop a better understanding of jet noise and jet noise suppression.

The report is organized into four volumes (FAA-RD-76-79, III - I, II, III, IV) and is presented in a format consistent with the Task 3 work plan division of the subtasks. Volume I is entitled "Verification of Suppression Principles and Development of Suppression Prediction Methods." Volume II is a data report entitled "Parametric Testing and Source Measurements," and Volume III is an analysis report entitled "Suppressor Concepts Optimization," Volume IV, under this cover, is an analysis report entitled "Laser Velocimeter Time Dependent Cross Correlation Measurement."

Volume I uses the data base (Volume II) and the Task 2 theoretical model (Reference 7) to postulate the suppression mechanisms. Volume I also presents an independent, empirical, static jet-noise-prediction method which was developed from engineering correlations of the test data. Volume II presents the data and results of the parametric acoustic tests, the aerodynamic performance tests, and the Laser Velocimeter tests. Volume III presents the results of a trade study of performance versus suppression, an aircraft integration study, a "figure of merit" methodology, and a summary of the five "optimum" nozzles selected for testing in Task 5. An acoustic-scaling investigation was conducted to support the suppressor concepts optimization activities and is presented as an Appendix to Volume III. Volume IV presents the results of the in-jet/in-jet and in-jet/far-field cross correlation investigations.

The work reported in the present volume describes a number of new laser velocimeter processor and data handling concepts that are required for real-time cross-correlation type measurements. Of particular note are discussions of a filter bank laser velocimeter processor design approach, combined with the use of a quantized product-factoring computational concept for data handling that has enabled the successful measurement of two-point, space-time, cross-correlation measurements in realistic gas flows. A series of laser velocimeter cross-correlation measurements (using two laser velocimeters) are reported for a conical nozzle and a coannular plug nozzle at high velocities (2200 fps) and temperatures (16750° F) in which the exhaust jet turbulent length scale and convection speed were measured. Additionally, the laser was successfully used to determine regions of strong correlation between the velocity field and the acoustic far-field pressure for a coannular plug nozzle. These recent results indicate that the technology is now available for performing systematic and detailed jet noise source location diagnostic studies for jet nozzles operating at realistic velocity and temperature conditions.

3.0 GENERAL REMARKS ABOUT THIS REPORT

During the course of the last several years the General Electric Company has been engaged in a number of theoretical and experimental investigations aimed at developing a better understanding and quantification of jet exhaust noise of simple circular nozzles and complex mechanical type exhaust nozzle suppressors. The support for this work has come from a number of Government agencies (FAA/DOT, Air Force, and NASA) as well as from General Electric research and development funds. Both scientists and engineers at the General Electric Company, as well as engineers at a number of other industrial institutions, universities, research laboratories, and Government research centers have exerted and shared considerable time, talent and experience to solve and mitigate the aeroacoustic aspects of high-velocity and temperature exhaust-jet noise.

Typically, one-millionth of the total jet flow power is radiated as acoustic power, hence the difficulty to quantify and reduce jet noise. Realistic exhaust jets operate at high velocity and temperature. Therefore, complex and precise measurement and test facilities are required. The jet noise producing agents are aerodynamic in nature, and are airborne - hence rugged, but sensitive real-time aerodynamic and acoustic measurements of micro scale jet aerodynamic properties are necessary. Underscoring these problems is the fact that theoreticians are still probing for the most exact or best theoretical acoustic formulations for jet noise generation and for acceptable approximations for their solution. Considerable progress has been made in acoustic testing, theoretical acoustic modeling and engineering design procedures such as that reported in the various task reports under this program (Report Series FAA-RD-76-79).

One perplexing task in verifying the "exact" nature of jet noise generation is to develop the proper measurement tools, particularly those associated with measuring the aerodynamic real-time flow properties. This report discusses work carried out by the General Electric Company to develop a real-time velocity measurement system, the laser velocimeter.

Section 4.0 of this report contains descriptions and discussions of the fundamentals of laser velocimetry, and its unique problems. Section 5.0 contains an up-to-date description of General Electric's laser velocimeter system, including some unique real-time velocity processing features currently not available in the open literature. The theoretical aeroacoustic motivation for performing real-time velocity measurements is discussed in Section 6.0, where a perspective is given for performing real-time, two-point, space-time measurements for the purpose of measuring jet global turbulent structure properties, and for setting a frame work for noise source location studies. Sections 7.0 and 8.0 contain the theoretical statistical considerations necessary for performing real-time velocity measurements and cross-correlations with the discontinuous output of the laser velocimeter. Particular attention is devoted in these sections to define the concepts developed at GE which successfully permitted accurate measurement of mean and turbulent velocities, turbulent spectra, and two-point space-time cross-correlation measurements with two lasers, or with one laser and an acoustic microphone. The concepts discussed in Sections 7.0 and 8.0 will provide a basis for future investigators to assemble the type of computational algorithms necessary for processing real-time data samples in an economic fashion. Section 9.0 describes the laser velocimeter test arrangement used in performing many of the reported advanced LV diagnostic measurements. Section 10.0 contains the results of a number of key LV jet plume studies, including: discussions of some high lights of mean and turbulent velocity measurements performed on high velocity and temperature shocked and shock free conic nozzle flows, LV measured turbulence spectra, a comprehensive series of two-point space-time measurements on a conic nozzle and an inverted flow coannular plug nozzle for turbulent length scale and convection velocity, and a series of LV to farfield acoustic cross-correlation measurements on a coannular plug nozzle. The emphasis of all experiments was to illustrate the capability for performing diagnostic type velocity measurements in realistic high velocity (supersonic) high temperature nozzle flows. The measurements reported are believed to be unique and important for future investigations of this kind. Section 11.0 contains a summary and recommendations for future work in utilizing the laser velocimeter for jet noise diagnostics.

4.0 THE LASER VELOCIMETER AND APPLICATIONS TO JET NOISE DIAGNOSTICS

This section reviews the need for and the fundamentals of laser velocimetry, the historic background of the technique, and unique problems and solutions in the application of laser velocimetry to jet noise diagnostics.

4.1 THE NEED FOR A NON-INTRUSIVE DIAGNOSTIC METHOD

Historically, in diagnostics of ambient, subsonic jets, a variety of instrumentation has been available which creates relatively little disturbance on the local or global jet properties. Thus, miniature pitot-static probes, very small, streamlined microphones, hot wire anemometers, etc. were adequate. Such has not been the case for a hot, supersonic jet. Various non-disturbing techniques using optical effects such as Schlieren photography, holography, correlated two-beam refraction and laser velocimetry have been attempted by industrial and educational researchers throughout the world. Ten years of experience has shown that the most viable diagnostic techniques must be accurate and highly localized. This accounts for the outstanding acceptance of laser velocimetry.

4.2 HISTORICAL SKETCH OF LASER VELOCIMETRY

The concept of measuring the velocity of a gas flow by the Doppler shift of light has been known for a number of years. In 1948, Messrs, Bundy and Strong of the General Electric Research and Development Center published a report[8] on the measurement of gas velocity in a rocket exhaust, using the Doppler shift of light emitted by a trace of vapor of an alkali metal seeded in the flame. The concept, however, was limited to velocity measurements of hot gases where thermal excitation is sufficient to cause the alkali metal seeding material to radiate at its resonance spectral line. In the 1960's, the invention of the laser provided a light source with enough output and coherence to make heterodyning techniques feasible. In 1964, Yeh and Cummins also published material on this subject[9]. However, improvements in utility and arrangement were needed. In 1969, a particular arrangement of the laser-powered Doppler technique, called "Differential Doppler" was first described

by C.M. Penney of the General Electric Co. Research and Development Center[10]. The geometry of this arrangement is such that measurements of fluid flow velocities can be made in situations where there is access at only one side of a stream. Further, the differential Doppler arrangement is easy to align and calibrate. Today the vast majority of users, worldwide, are employing the Differential Doppler method, rather than the original reference beam arrangement.

4.3 FUNDAMENTALS OF LASER VELOCIMETRY

The laser velocimeter is a noncontact air-speed-measuring instrument which consists of a laser, seed particles, mirrors, lenses and beamsplitters, a photodetector and a signal processor. Figure 4-1 is a schematic view of the basic differential Doppler arrangement. The laser beam is split into two equal power beams that are focused and crossed in space, where the air speed is to be measured. Interference "fringes" are formed here (they can be seen with a microscope and some smoke). The fringes are plane, parallel, light and dark sheets that, on edge, resemble a picket fence. A single dust particle (seed) passing through this region scatters light in a sinusoidal burst, detected by a phototube. This is analogous to running alongside a picket fence, rapping it with a stick. The frequency of the sine burst is measured by a signal processor. Figure 4-2 is a simplified schematic diagram of the measuring process. A "counter-timer" is shown here, but there are other techniques. Figure 4-3 is a cross section to show how the basic components might be arranged for a single component, back-scatter system. Back-scatter means that only a small amount of the particle's scattered light is collected, and in the back direction.

4.3.1 The Differential Doppler Method

The LV technique can take the form of one of two optical configurations: reference-scatter (direct Doppler), Figure 4-4; or differential Doppler (dual scatter), Figure 4-5). The ease of alignment and usage plus the inherent increase in a signal-to-noise ratio have made the differential Doppler configuration predominant in the literature and the method chosen by General Electric.

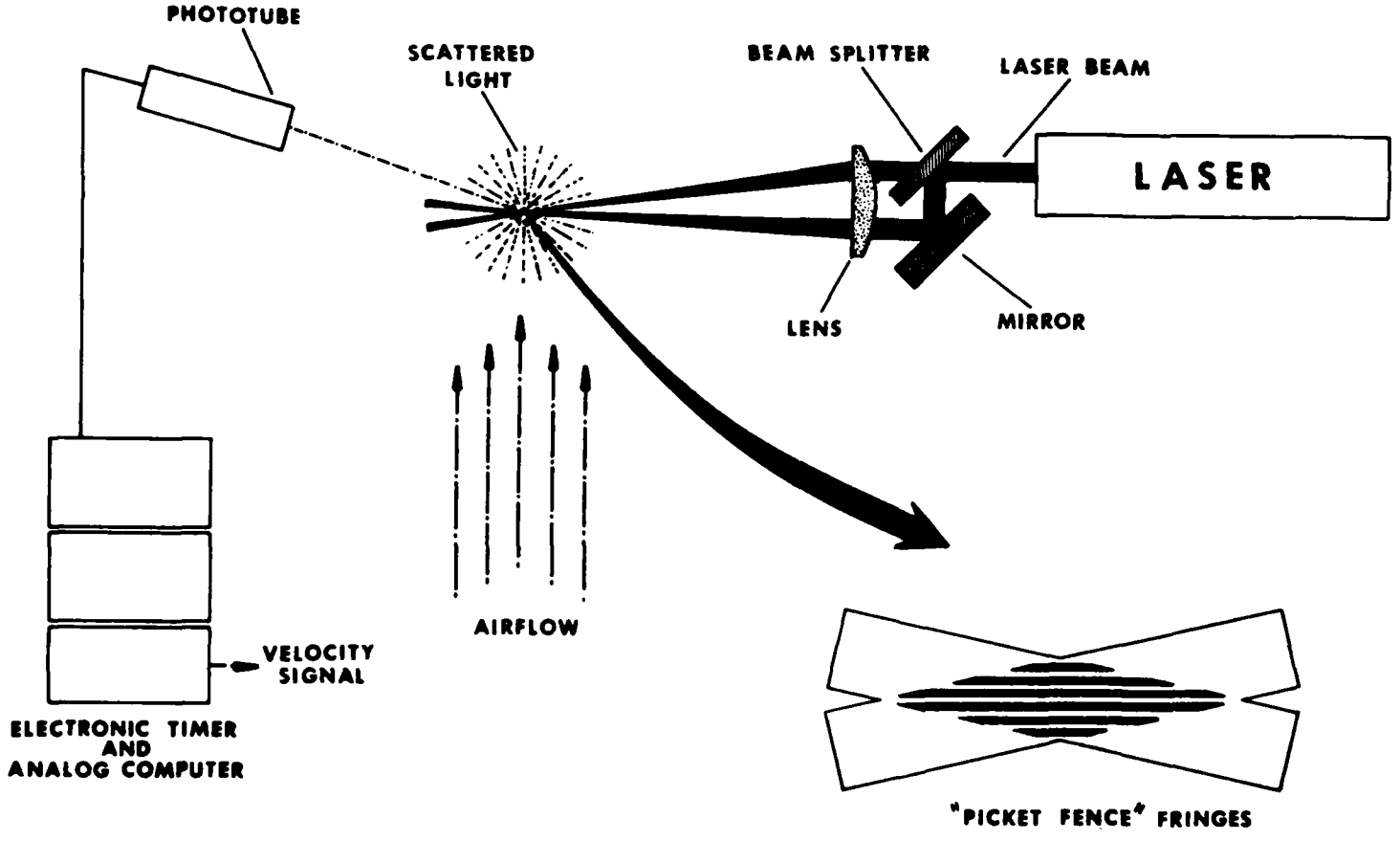

Figure 4-1. Schematic View of Laser Velocimeter.

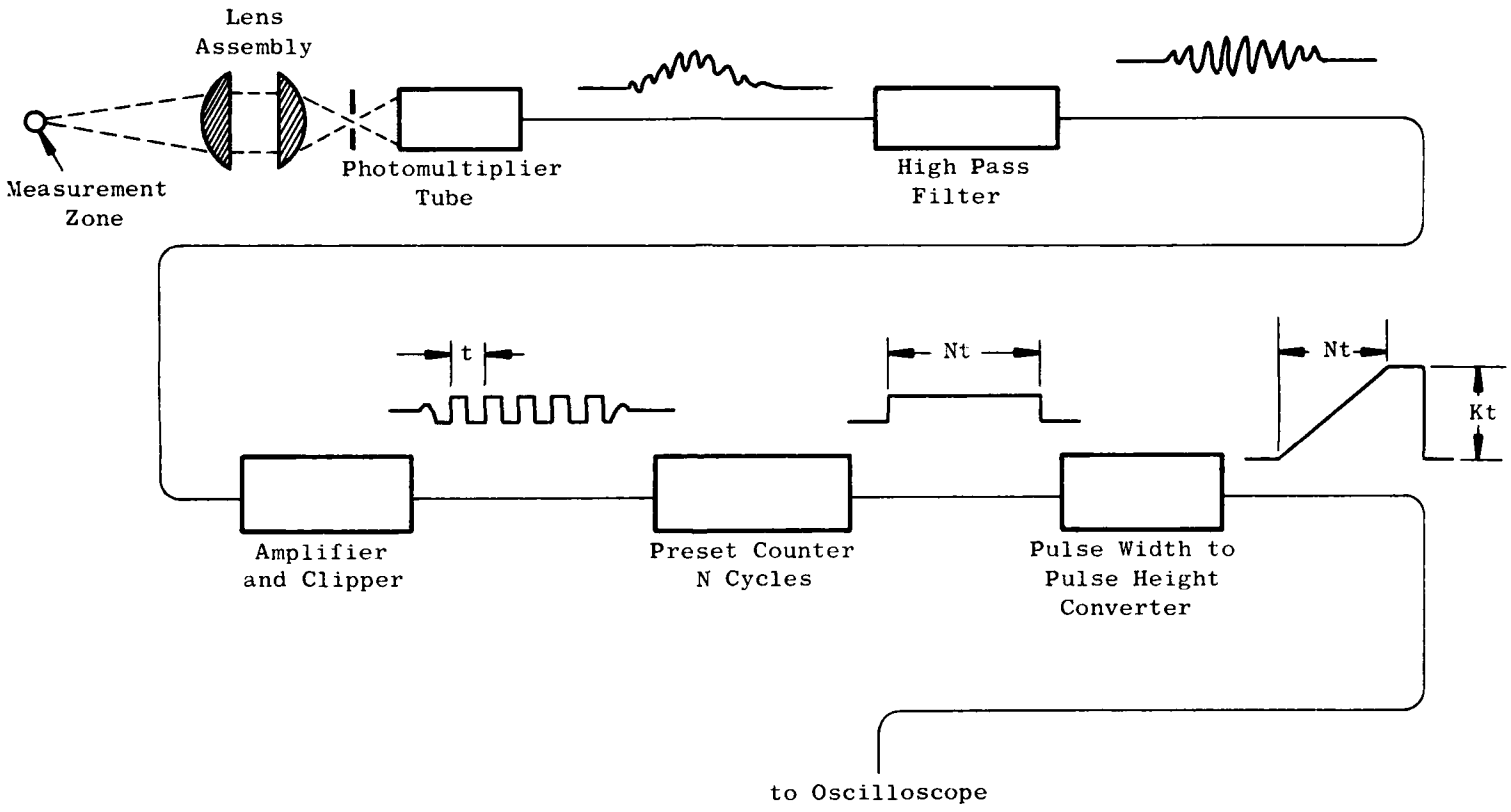

Figure 4-2. Schematic Diagram of an Elementary LV Measuring Process.

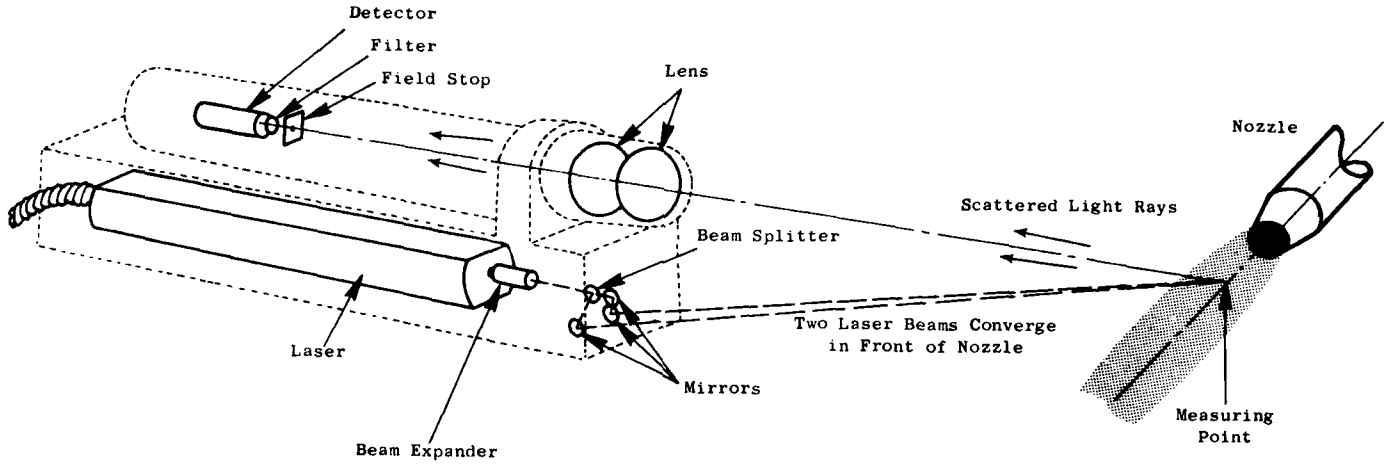

Figure 4-3. General Arrangement of a Backscatter LV.

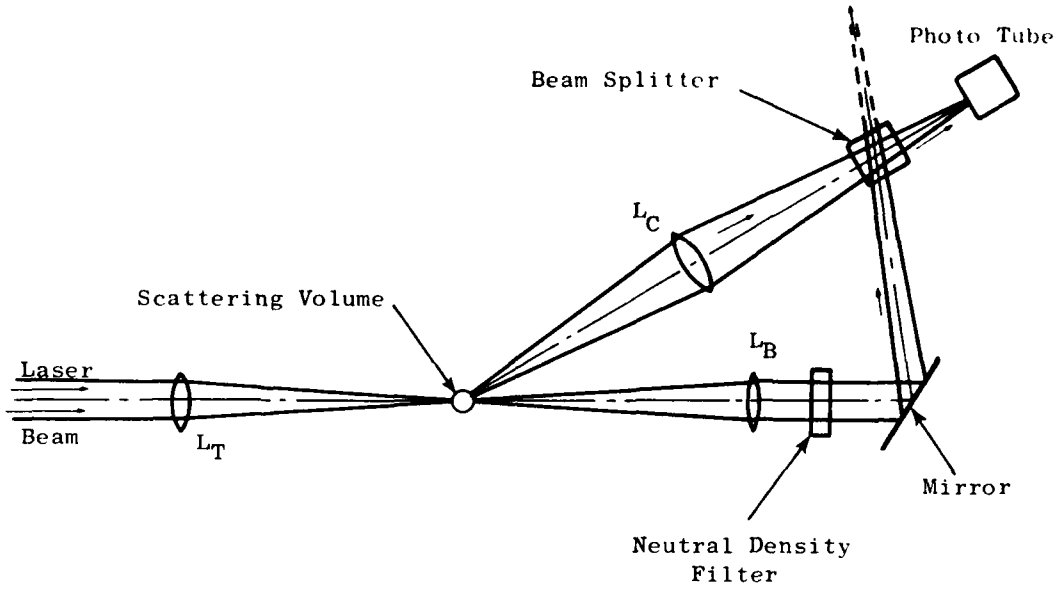

Figure 4-4. Reference-Scatter or Direct Doppler Arrangement.

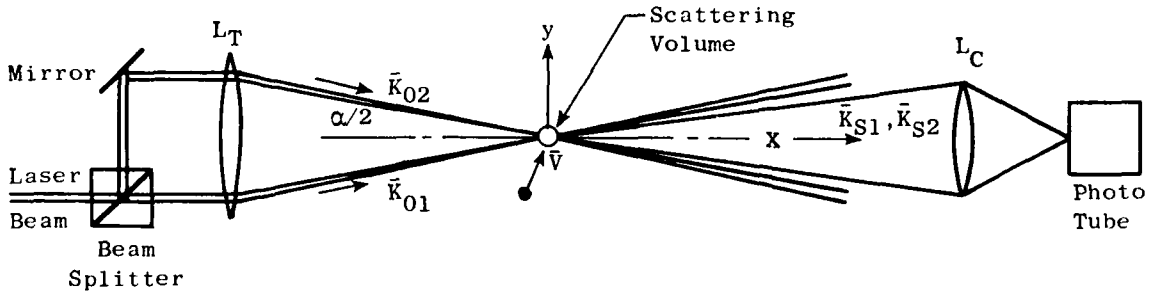

Figure 4-5. Dual-Scatter or Differential Doppler Arrangement.

An analysis of the differential Doppler method can be understood by considering the interference pattern created by two intersecting beams of coherent radiation, each having a wavelength λ_o. Referring to the scattering volume formed by the cross beams (Figure 4-6), constructive interference occurs when the optical path length, Δ, between the two beams differs by an amount $n\lambda_o/2$ for n odd. Similarly, destructive interference occurs when $\Delta = n\lambda_o/2$ for n even. Planes of constant optical path length difference between the two beams are parallel to the plane that bisects the two beams. Thus, the fringe spacing, S, is given by:

$$S = \frac{\lambda_o}{2}\left(\frac{1}{\sin\frac{\alpha}{2}}\right) \qquad 4\text{-}1$$

As the particle passes through these fringes at velocity $\bar{v}$, light is scattered only when it is in a bright fringe; hence, the scattering frequency, $\Delta\nu$, is simply:

$$\Delta\nu = \frac{\Delta\omega}{2\pi}$$

$$= V_y/S$$

or

$$\Delta\nu = \frac{2\ V_y\ \sin\ \alpha/2}{\lambda_o} \qquad 4\text{-}2$$

where V_y is the velocity component perpendicular to the fringes. The interference pattern considerations are easier to visualize when analyzing the LV as a velocity-measuring device, since the pattern can be thought of as a light grid placed in the flow to define an accurate displacement increment, S. Then, the local velocity normal to the fringes is simply S/t, where t is the transit time between bright fringes.

4.3.2 LV Spatial Resolution

The size of the scattering volume is an important consideration in designing the LV, since it determines the dimension over which any velocity fluctuations and gradients in the flow are averaged in the measurement. This

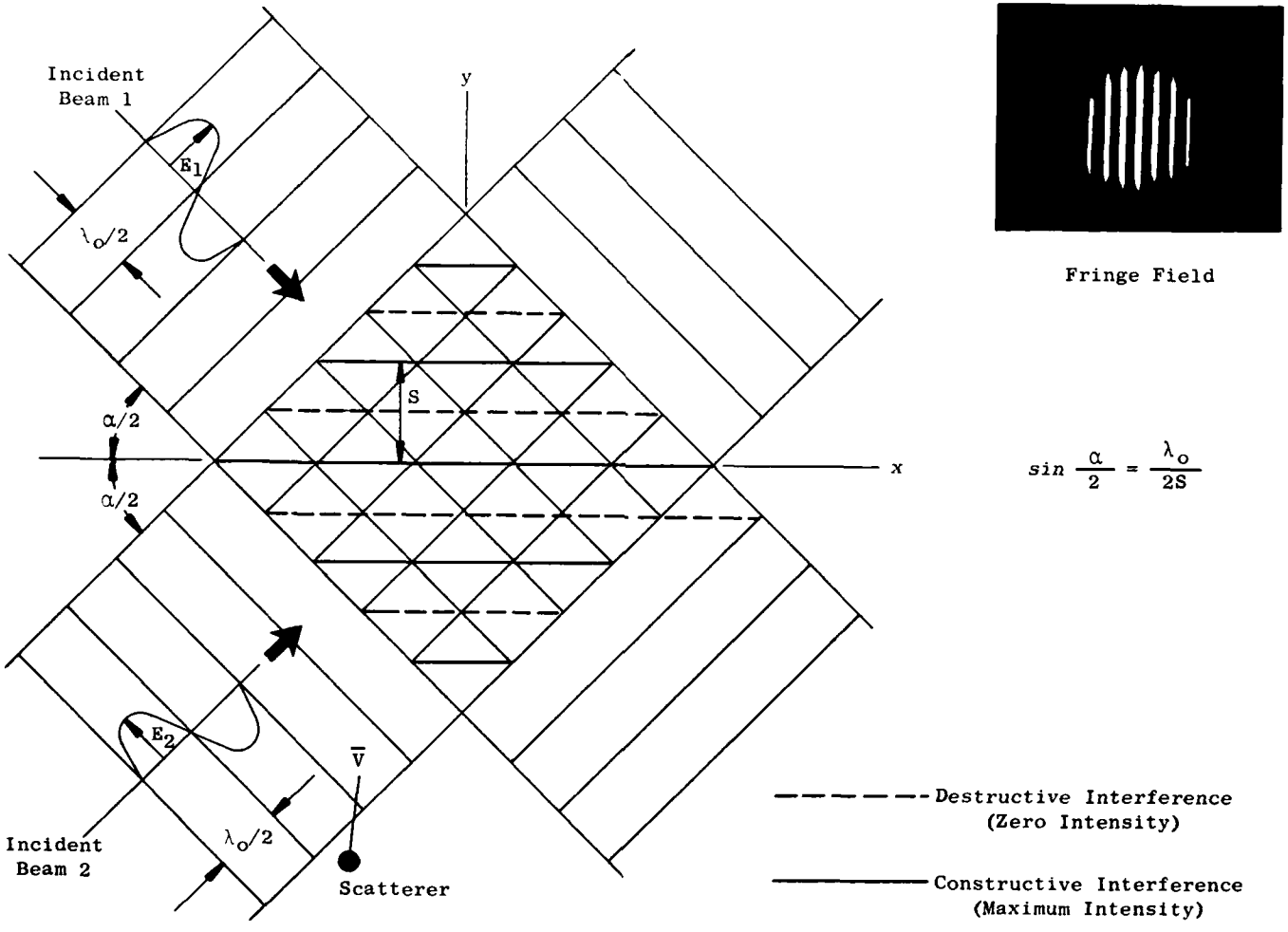

Figure 4-6. Interference Fringes Formed by Two Coherent Crossed Beams.

volume is determined by the optics of the transmitter and the collector lenses and by the size of the laser beam. In most LV arrangements, the beams are focused to spots in order to minimize the scattering volume. Under these conditions, the spot size is then determined by the diffraction limit of the focusing lens.

Consider a beam of parallel, monochromatic light of wavelength λ with uniform intensity, passing through a lens of focal length f. At the focal point of the lens, a diffraction pattern is formed, and the diameter, d, of the central bright spot (called the Airy disc) is given[11] by the relationship:

$$d = 1.22 \lambda f/D \qquad 4\text{-}3$$

where D is the incident beam diameter. This same diffraction limit in the size of the spot at the focus of the transmitter lens determines the scattering volume with a laser beam.

For a laser beam incident on a lens of focal length f_T, the intensity of the laser beam is not uniform but rather Gaussian in character, and the wavefronts are normally not plane, but spherical. Referring to Figure 4-7, when

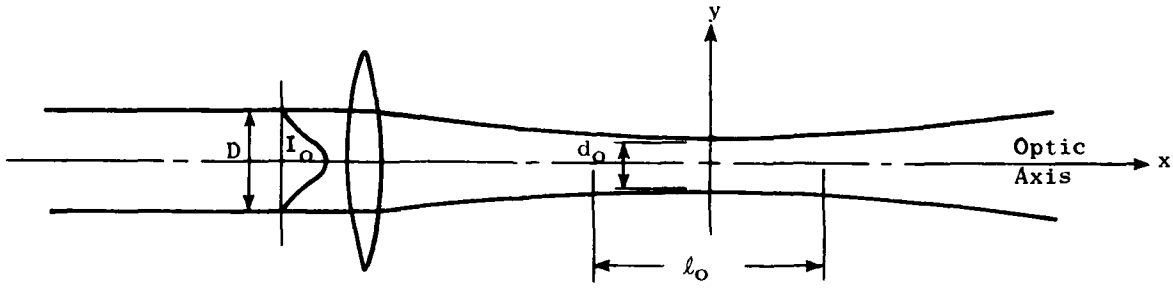

Figure 4-7. Geometry of a Focused Laser Beam.

a beam of this nature (with diameter D at the lens face) is incident on the lens, the intensity in the vicinity of the focal point is given by (see Reference 12):

$$I(u,v) = \frac{I_o}{\pi(1 + u^2)} e^{-v^2/(1 + u^2)}; \qquad 4\text{-}4$$

where

$$u = \frac{\pi x D^2}{2\lambda f_T^2},$$

$$v = \frac{\pi y D}{\lambda f_T},$$

and y and x are coordinates measured perpendicular to and along the optical axis of the beam, respectively, with origin at the focal point of the lens. Thus, the focused beam is seen to be a distorted ellipsoid of revolution with the intensity falling off sharply as a function of x and y. For the intensity to drop to one percent of its incident value, I_o, the size of the spot is:

$$d_o = 1.184\ \lambda f_T/D \text{ and} \qquad 4\text{-}5a$$

$$\ell_o = 7.08\ \lambda(f_T/D)^2. \qquad 4\text{-}5b$$

These two equations give the relative dimensions of the full scattering volume without the use of apertures and stops in the collector optics.

For the differential Doppler method, the two beams intersect at the focal point of the transmitter lens, and the interference fringes are formed only where the beam intersect. Referring to Figure 4-8, when the two beams (of diameter D separated by a distance, b, are focused by the transmitter lens, the width of the spot d_o' is:

$$d_o' = \frac{d_o}{\cos(\alpha/2)}; \qquad 4\text{-}6$$

where α is the angle between the beams, and d_o is calculated by Equation 4-5a. Similarly, neglecting the beam divergence in the vicinity of the focal point, the length of the intersection, ℓ_o', is:

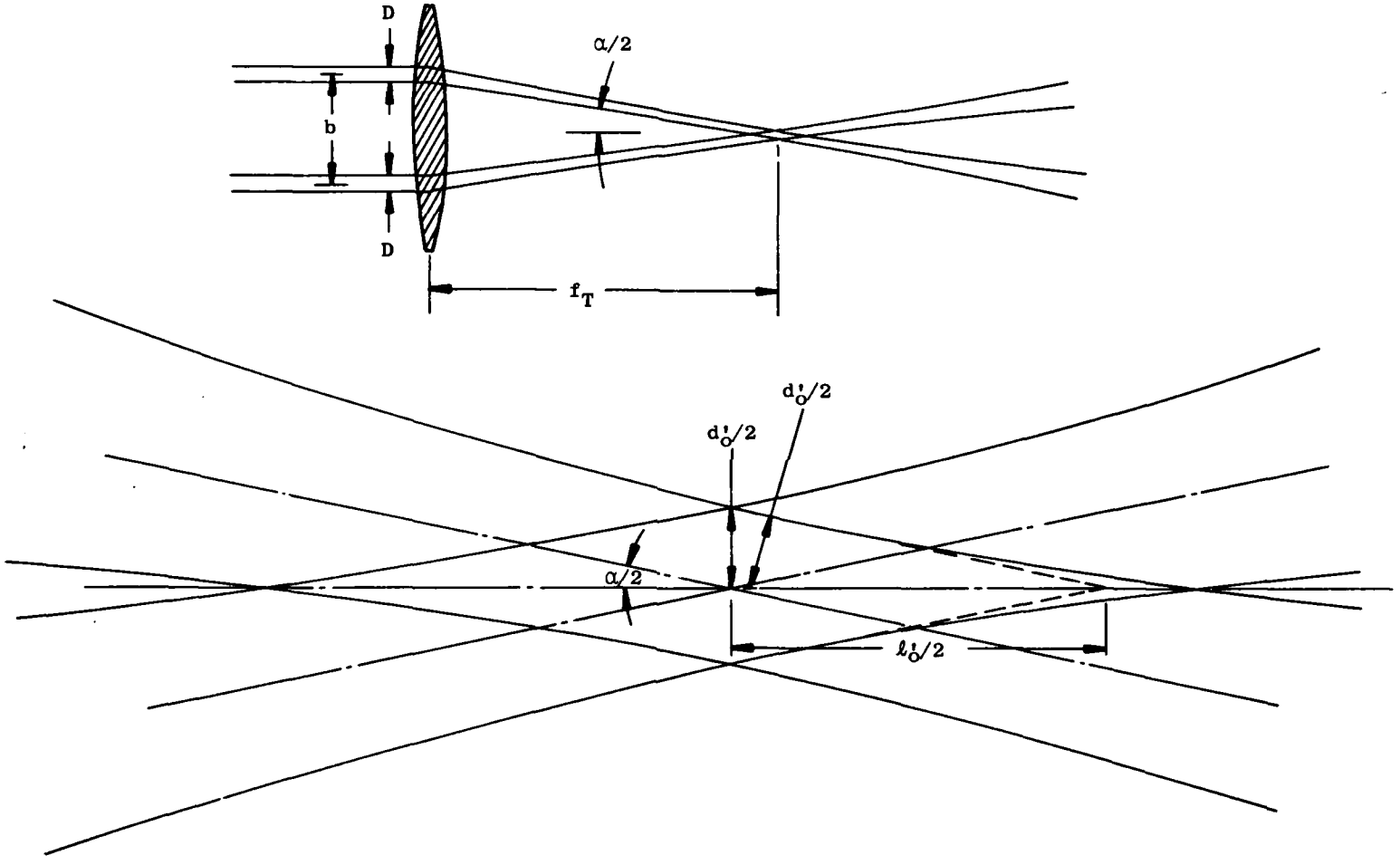

Figure 4-8. Transmission Lens Scattering Spot Size for the Differential Doppler Arrangement.

$$\ell_o' \simeq \frac{d_o}{\sin\ (\alpha/2)} \ . \qquad 4\text{-}7$$

As previously mentioned, stops and apertures in the collector optics are normally used to limit the size of the scattering volume to a "data probe volume," since, generally, the dimension of the scattering volume along the optical axis, ℓ_o or ℓ_o', is too long for good spatial resolution in the flow. A simple means for reducing this dimension by using the collector optics is shown in Figure 4-9, where a narrow slit of height h is placed in the image plane of the collector lens with focal length f_c. With this arrangement, the length of the data probe volume, ℓ, in the focus of the transmitting lens that is seen by a detector placed behind the slit is:

$$\ell \simeq \frac{p}{\sin\ \phi} \ ,$$

where, p is shown in Figure 4-9, and ϕ is the main scattering angle. By use of the lens formula, one can obtain:

$$\ell \simeq (a/f_c - 1)\ h/\sin\ \phi \ . \qquad 4\text{-}8$$

Thus, the length of the scattering volume can be controlled by a judicious choice of the collector optics and the scattering angle.

With respect to limiting spatial resolution, it is possible to further reduce the length of the data probe volume by discriminating the amplitude of the scattered light. Only when the seed particle passes the middle of the scattering volume is the incident light (and therefore the scattered light) at a maximum. On either side of this point, the peak signature amplitude decreases. Furthermore, at either end of the intersection volume the signature becomes dual-peaked, which can be responsible for Doppler dropout where "missing" electronically undiscriminated pulses will improperly add to the average Doppler period. Thus, by amplitude window thresholding (for particles of uniform size) and use of a dropout monitor, the spatial resolution can be increased beyond that generated by the collector optics.

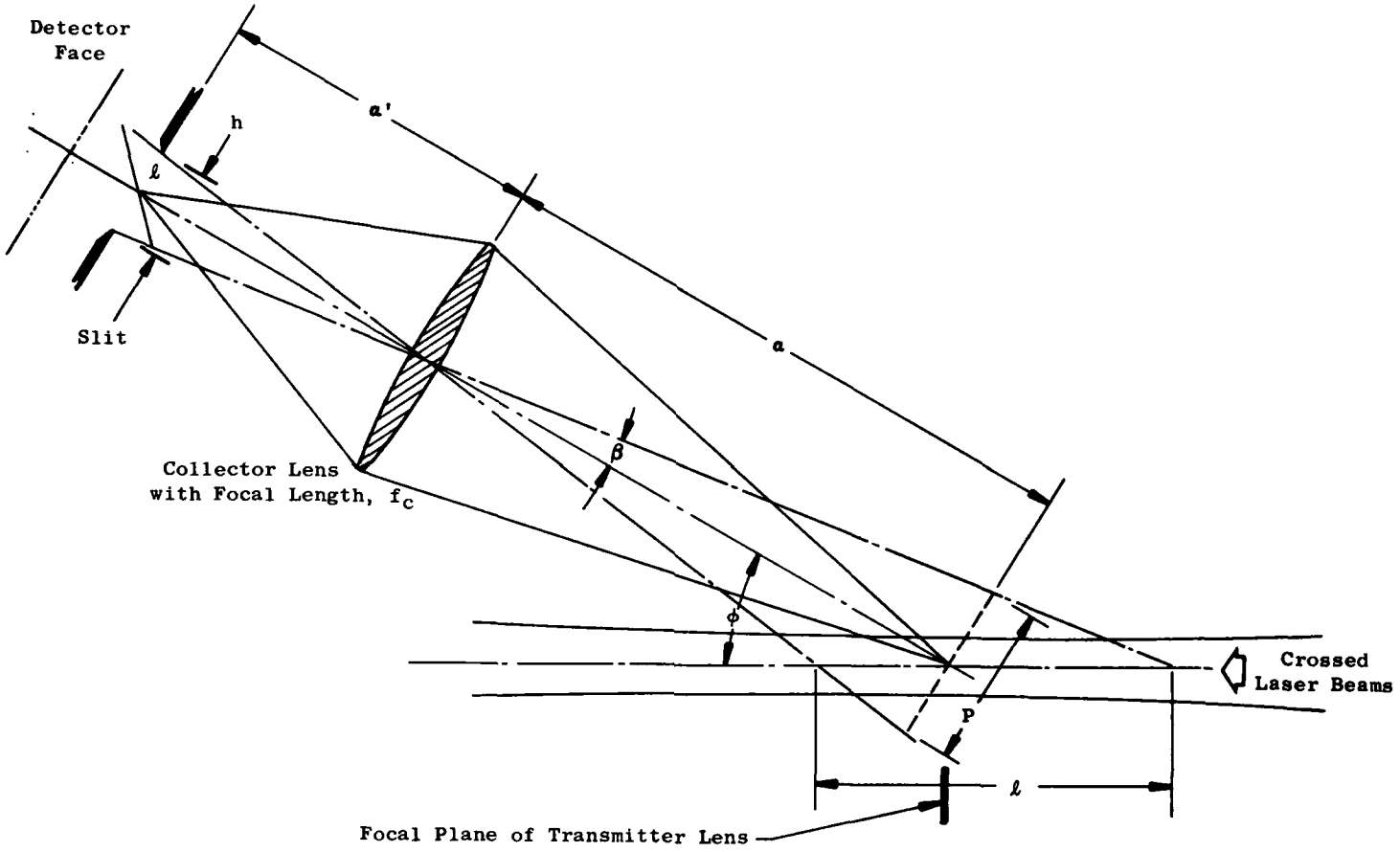

Figure 4-9. Collector Optical Arrangement.

To summarize, the spatial resolution of the LV is determined by both the transmitter and the collector optics as well as by the use of LV signal processor monitors. The width of the spot is normally specified by the diffraction limit of the transmitter lens and is given by Equation 4-5 or 4-6. The spot length is determined by the collector optics containing appropriate apertures and stops to limit the region over which scattered light is collected. Dropout and amplitude threshold windows also can be provided as signal monitors to further reduce the data volume.

4.4 UNIQUE REQUIREMENTS, PROBLEMS AND SOLUTIONS IN THE APPLICATION OF LASER VELOCIMETRY TO JET NOISE DIAGNOSTICS

The laser velocimeter (LV) is used for the purpose of accurately sampling the time history of gas velocity at known points in the nozzle exhaust plumes, and in a known direction. This sequence of velocity samples can be correlated to near-simultaneous samples of velocity at some other plume location, and can also be correlated with near and far-field sound pressure level measurements.

Because these diagnostic LV data must have sample time preserved as well as represent instantaneous and localized velocity vector components, unique requirements are placed on the LV system. Added constraints and problems result when the LV system is expected to work in the non-ideal environment of heated supersonic jet exhausts. The noise level and temperature extremes in the vicinity of an exhaust nozzle (model scale or engine size) may seem incompatible with a precision, laser powered, optical device. This section will attempt to prove the contrary, that each of the application problems, when isolated and fully understood, can be controlled. Thus, the discussion will include: particles as flow tracers, use of laser light, control volume size and optical working distance, signal processing choices, angular acceptance in turbulent flow, and noise and other interfering effects.

4.4.1 The Particle as a Tracer

The clean exhaust jet will not generally scatter the laser light efficiently. An external source is usually required to add tracer particles to the gas. Several constraints are placed on these tracer particles:

1. must be small in size (one micron or less) to avoid "slip" errors in high acceleration fields

2. must be a good light scatterer

3. must survive 2,000° R

4. must be easily dispersed in gas stream

4.4.2 Laser Light Requirements

The light source must be a laser of high angular and temporal stability. A complex set of tradeoffs must be made to determine laser power required. The following parameters or sub-groups of parameters are involved:

1. laser wavelength

2. laser coherence

3. laser beam focusing optics

4. particle size, shape, and scattering optical properties

5. scattering angle selected

6. receiver collector solid angle

7. photodetector quantum efficiency, frequency response and noise properties

8. signal processor bandwidth and noise properties

4.4.3 Control Volume Size and Optical Working Distance

The control volume generally is an ellipsoidal shaped volume, whose dimensions are controlled by choices in the optics (see Section 4.3.2, particularly equations 4-5 and 4-6). The optical working distance is very important in jet plume mapping, as it is important to sample the plume without exposing the LV head to the jet blast itself. Thus the working distance selected will depend on the plume width. The control-volume selected will be based on expected velocity gradients (primarily that found in the small turbulent eddies in the early mixing region of the plume). A tradeoff exists here, because a very small control volume well suited to small eddy mapping may lead to refraction problems. (This is discussed under noise and other interfering effects.)

4.4.4 Types of LV Signal Processors

Various types of LV signal processors may be assessed for their measurement capabilities of the local fluid velocity by deducing the Doppler frequency of scattered light from a seed particle moving at the fluid velocity. These signal processing designs include the following major concepts:

1. Spectrum analyzer
2. Doppler frequency tracker
3. Counter-timer
4. Photon correlator
5. Filter bank

Early in the history of the LV, workers used a spectrum analyzer for processing of the LV signal. Such analyzers, as were and are now available in well equipped labs, employ a slow frequency scanning principle. This is equivalent to turning a narrow band receiver across a frequency range. This type of processor is unsuitable for measuring time dependent flow properties. An alternative approach to the scanning spectrum analyzer is to digitally record each Doppler burst, and, at some later time, analyze on a digital computer. Such a technique was demonstrated by Asher, Scott and Wang[13]. Advances in microcomputers will soon make on-line analysis feasible and cost effective.

4.4.4.1 Doppler Frequency Trackers

Doppler frequency trackers have been in widespread use since the late 1960's[10,14,15]. Commercial equipment is available, for example, from TSI, Inc.[16] and DISA, Inc.[17] Trackers operate by attempting to match the frequency and phase of an internal, controllable oscillator to the incoming Doppler burst. A critical parameter in all trackers is the capture range. Successful tracking can take place only when the incoming Doppler burst frequency is within a certain ratio of the previous burst frequency. This ratio is called the capture range. Usually this range is 0.9 to 1.1. Low seeding density and high turbulence in a mixing jet can cause successive bursts to differ by ratios of 0.3 to 3.0. Consequently, the tracker is generally not usable in jet noise diagnostics.

4.4.4.2 Counter-timer

Counter-timer signal processors use conceptually simple principles, but have features well suited to LV measurements in high turbulence gas flow. The earliest presentation of the concept was by W.B. Jones[18]. Figure 4-2 is a simplified diagram of Jones' arrangement. The high frequency, brief burst from the photomultiplier tube is high pass filtered to remove the gaussion, low frequency envelope (sometimes referred to as a "pedestal"). The signal is then amplified and clipped and enters the preset counter which outputs a single pulse of duration Nt, where t is the burst period and N is the preset number of cycles to be counted. The pulse enters a width to height converter that has output Kt as an amplitude. Thus Kt is proportioned to the transit time of the seed particle through the N fringes. The transit time signal, Kt, may be recorded, or applied to a display oscilloscope, or both.

The counter-timer processor is widely used in low speed/density flow where high precision is needed in the measurement. Advanced developments relating to jet noise diagnostics are described in Section 3.0.

4.4.4.3 Photon Correlation

Photon correlation methods and their application to laser light scattering techniques have been discussed by Pike[19] and by Kalb[20]. The basis of this approach is the detection of individual quanta of light energy (photons) recorded in fixed time intervals. Using appropriate digital processing, the recorded photon "counts" can be shown to represent the autocorrelation function. This signal then contains time-averaged velocity and turbulence intensity information. For this reason, a photon signal processor could only be used in a very inefficient way in jet plume diagnostic velocity measurements. It has been calculated that a velocity spectral analysis using photon correlation would require data collection times in excess of that needed by the counter-timer, for example, by a factor in excess of 100.

4.4.4.4 Filter Bank

Filter bank signal processing for the LV was first reported in 1968 by Rolfe et al.[14] Although showing feasibility of using a set of overlapping

bandpass filters for an efficient spectral analysis, the arrangement was limited in usefulness. The arrangement averaged many Doppler bursts, finally yielding mean velocity and turbulent intensity. Times of arrival of individual bursts were not preserved. The potential for individual burst processing, however, was later pursued at General Electric, and a filter bank processor that is suitable for jet plume time dependent measurements was developed and applied as described in Section 5.0.

4.4.4.5 Summary

The counter-timer and the filter bank were selected by GE to process a velocity sample from just one particle traverse of the LV control volume. The spectrum analyzer, Doppler frequency tracker, and photon correlator were found to be either not capable of or inefficient in handling single particle Doppler burst data.

4.4.5 Angular Acceptance in Turbulent Flow

As the flow turbulence increases, the velocity components show increasing fluctuations. The signal processor must contend with the wide frequency range inherent in this process. In addition, turbulence brings about angular trajectory fluctuations about the jet centerline axis. This illustrated in Figure 4-10, tracer particle trajectories in the control volume. Three illustrative particle trajectories of -60°, 0°, and +60° are shown, where 0° represents the jet axis. Sixteen (16) fringes were placed in the control volume in this example. The 0° particle crosses all 16 fringes, but only 8 fringes are crossed by the -60° and +60° particles. The governing equation of the number of fringes crossed on the probe control volume center is a cosine law, and is illustrated in Figure 4-11. As an example of the signal processing limits, suppose a control volume of only ten (10) fringes was used, and the signal processor required eight (8) good cycles (fringes) of burst signal. In Figure 4-11, the dashed line marked "A" would represent the angular limit line for this case, where only 0.8 of the total fringes are crossed. It may be seen that line A intersects the cosine curve at approximately 37°. Thus, particles beyond ±37° would not be measurable. If it was determined that the angular acceptance of ±37° was not sufficient, then the

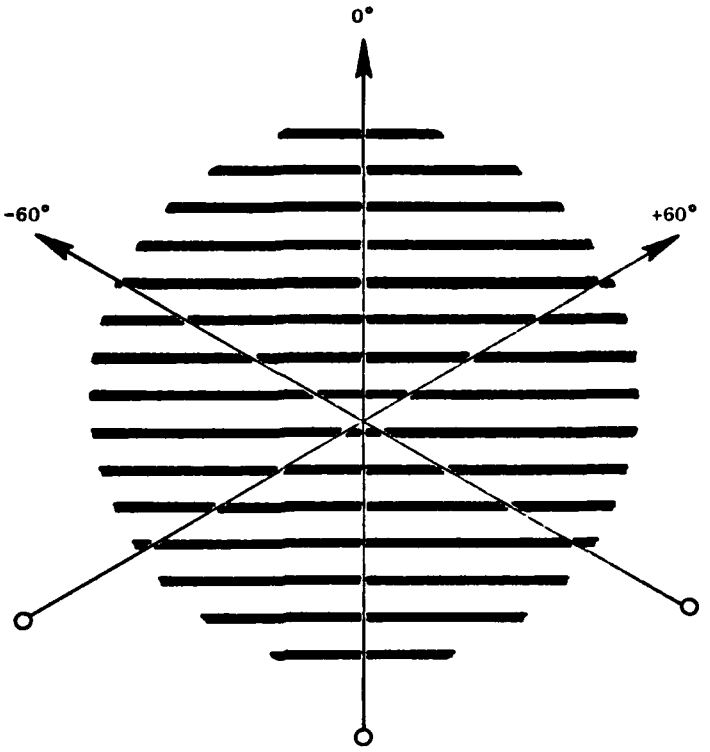

Figure 4-10. Particle Trajectories in Control Volume.

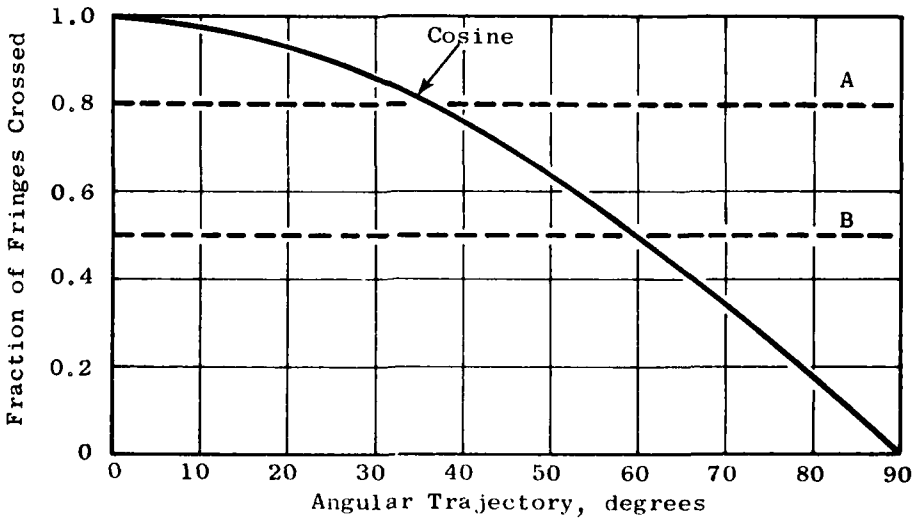

Figure 4-11. Fringes Crossed Vs. Angle of Particle.

ratio of processor cycles required over total fringes in the control volume would have to be decreased. For example, line "B" in Figure 4-11 shows a ±60° angular acceptance when 1/2 of the fringes are crossed.

The examples given are simplified somewhat, in that some particle traverses through the control volume will be off-center and cross fewer fringes than illustrated above.

4.4.6 Noise and Other Interferring Effects

This section outlines the problems of: optical and electrical noise, interference from background light, smoke interference, optical refraction, and environmental protection.

4.4.6.1 Optical and Electrical Noise

Optical and Electrical Noise stems from several sources: A small particle of non-spherical shape may rotate as it passes through the LV control volume, creating intensity modulation in the scattered light collected[21]. The focused and crossed laser beams do not have a perfect sinusoidal light distribution, but have what may be thought of as secondary interference patterns[12]. The photosensor exhibits "shot noise" that stems from the very nature of light: light travels in packets, called photons, that vary in a statistically predictable and sometimes annoying manner - even from a so-called steady light source[22]. The impact of these noise sources is, with a single particle in the control volume, a range of 10 to 30 dB signal to noise ratio on the Doppler burst itself.

The most influential parameter is the scattered light power incident on the photo-detector. Any method used to increase the detected light power will improve the signal to noise ratio.

4.4.6.2 Interference from Background Light

Light received from any source other than the scattered laser light from the particle constitutes an interference source. Therefore, hot particle incandescence, illuminated background from roomlight, sunlight, and even the

laser beams, may degrade the signal. The laser line filter will remove over 99% of unwanted broadband sources. The filter will not remove background laser light. This light may only be excluded by keeping surfaces out of the control volume during data acquisition.

4.4.6.3 Smoke Interference

Smoke interference is related to the background light problem. The laser light scattered from a heavy concentration of smoke particles presents the same interference as a surface in the control volume. In addition, smoke between the control volume and the LV head may attenuate the signal by absorption and scattering.

4.4.6.4 Optical Refraction

Optical refraction is the bending of light rays in the air space between the LV head and the jet, and within the jet. Temperature gradients outside and within the jet plume and static pressure variations within the plume create the optical index gradients which, in turn, cause the refraction. Under severe refraction, the laser beams uncross. The loss of the interference fringes during the uncrossed condition stops the data. Partially uncrossed beams result in shortened Doppler bursts and/or reduced signal strength. The immersion depth of the optical path in the hot jet affects the amount of refraction.

4.4.6.5 Environmental Protection

Environmental protection of the LV head involves several areas. The mechanical mountings of the laser, mirrors, lenses and receiver optics must be designed to withstand temperature changes without undue strain. Use of alloys of equal thermal expansion coefficient, and high thermal conductivity reduce the strain problem. Acoustic noise and vibration effects can be controlled by designing for the highest possible resonant frequency in the LV head and internal optics mountings. Smoke and dust must be prevented from depositing on the optics. Near-air-tight construction, to reduce "breathing", helps. Positive purge with a filtered air source is even better.

5.0 DESCRIPTION OF GENERAL ELECTRIC'S LASER VELOCIMETER

This section presents an up-date on the development and status of General Electric's current arrangement of the real-time diagnostic laser velocimeter systems. The topics covered are:

- Laser velocimeter optical head
- Signal processors
- Seeding arrangements
- Data acquisition and reduction

5.1 LASER VELOCIMETER OPTICAL HEAD

Since 1970, six LV heads have been designed, built and used. Four are currently in use. Table 5-1 summarizes the characteristics of these LV heads. All are of the single component, differential Doppler arrangement (defined in Section 4.0). All except the Model 10-1 are of the backscatter arrangement. The optical working distance varies from 10 inches to 85 inches. The shorter distances are suitable for probing turbomachinery blading. The longer optical working distances have been designed for probing jet exhaust plumes, where no physical part of the head is allowed to contact the high speed exhaust jet. In Table 5-1, the column "Coaxial or Offset" refers to whether the laser beam's bisector has been arranged to be centered inside of the received cone of scattered light ("coaxial") or outside of this cone ("offset"). Note also that view cone requirements vary, and probe volume dimensions are quite different.

The two LV heads used in the cross-correlation measurements (discussed in Section 10.0) are the models 85-1 and 85-2, lines 4 and 6 on Table 5-1. Although outside case dimensions are slightly different, the probe volumes were matched as closely as possible. In two-point velocity correlations, one LV is operated on the 514.5 nm argon-ion laser "green" line. The other head is operated on the 488 nm "blue" line. Each photomultiplier tube is filtered with the appropriate laser line filter. Because of the two colors

Table 5-1. Laser Velocimeters Designed, Built, and Used at General Electric Company's Aircraft Engine Group Measurements and Sensor Development Lab.

Line Number	Model Number	Year First Used	Currently in Use	Back on Forward Scatter	Laser & Power	Optical Working Distance	Coaxial or Offset	View Cone Required	Probe Volume	Rotate For 2-D Meas.
1	10-1	1970	Yes	Forward	Spectra Physics 124A 0.015 Watts Helium Neon	10"	Offset	5° RCVR 2° TRANS	0.005" x 0.070"	No
2	30-1	1971	No	Back	Hughes 3030 Pulsed 6 Watts	30"	Coaxial	11.5° RCVR 2° TRANS	0.030" x 0.150"	Yes
3	40-1	1971	No	Back	Spectra Physics Model 165 1.4 Watts CW	40"	Coaxial	8.6° RCVR 1.4° TRANS	0.020" x 0.500"	No
4	85-1	1972	Yes	Back	Spectra Physics Model 165 1.4 Watts CW	85"	Offset	4° RCVR 1.4° TRANS	0.018" x 0.250"	No
5	25-1	1973	Yes	Back	Spectra Physics Model 164 mod 1.4 Watts CW	25"	Coaxial	11° RCVR 1.9° TRANS	0.012" x 0.160"	Yes
6	85-2	1974	Yes	Back	Spectra Physics Model 165 1.4 Watts CW	85"	Offset	4° RCVR 1.4° TRANS	0.018" x 0.250"	No

used, probe volumes can be moved in close proximity to one another, even overlapping, without interference. The general arrangement of the 85-1 and 85-2 LV heads are shown in Figure 4-3. The argon-ion laser supports a 3X beam expanding telescope. One beamsplitter and three mirrors are used to form the two equal power laser beams of about 0.7 watts each. The beam expander is adjusted so as to focus the laser beams about 90 inches away, to a spot diameter of 0.018 inches. No other lenses or optics are used in the transmitter side of the LV. On the receiver side, a pair of symmetrical, 6-in. diameter, acromatic lenses are used to collect a 4° cone of scattered light and focus through a field stop to the filter and detector. The detector used is a photomultiplier tube, 0.75 inch diameter "S-20" cathode and potted dynode resistors. A wideband preamplifier is located about 10 inches from the detector. Frequency response of the preamplifier is 1 kHz to 150 MHz + 1 db. Voltage gain is 100X. Peak output is ± 1 volt into a 50 Ω transmission line (such as type RG8 cable).

The LV box construction is 1/2 inch thick aircraft aluminum alloy sheet, with a 1/16 inch thick plumber's lead sheet bonded to the inside. The aluminum alloy provides a high mechanical resonant frequency and high thermal conductivity. The lead sheet provides a high mechanical damping. For operation in proximity to scale model exhaust, no additional acoustic protection was found to be necessary.*

5.2 SIGNAL PROCESSORS

Since 1970, six signal processors have been designed, built and used, encompassing five designs. Four are currently in use. Table 5-2 summarizes the characteristics of these processors. The first four lines of the table are models based on the counter-timer technique. The fifth line describes the Mark III signal processor, based on the filter tank technique. A comparative description of these techniques is given in Section 4.0.

* The LV has been used in diagnostic testing of a J79 engine at full and partial power. During such testing a time delay relay tube in the laser powersupply box (about two feet from the LV head) was broken. Wrapping a lead-vinyl acoustic blanket around the laser supply box solved this problem and no further damage to the LV was experienced during engine testing.

Table 5-2. Signal Processors Developed by General Electric for use with the Laser Velocimeters.

Line Number	Processor Type	Model Designation	Currently in Use	Input Frequency Range	Signal Noise (Minimum Input Required)	Features
1	Counter-Timer	Jones - 1970	No	2 to 10 MHz	25 dB	This is first reported signal processor that could make complete velocity sample measurement on one (1) Particle traverse. (Reference 18) Excellent for low to medium density seeding.
2	Counter-Timer Wide Band	Jones - 1970 w Wide Band Input	No	0.1 to 30 MHz	25 dB	As above, but a wide band pedestal remover was designed and added to extend frequency range to 100 to 1 without band switching.
3	Counter-Timer Wide Band w Check Logic	Signal Processor Mark I	Yes (1 each)	0.5 to 40 MHz	25 dB	High Speed Logic, wide band frequency input, and first use of 4 cycle - 8 cycle and 5 cycle - 8 cycle comparative validation technique. (Reference 23) False data greatly reduced.
4	Counter-Timer Wide Band w Extended Check Logic	Signal Processor Mark II	Yes (1 each)	0.5 to 40 MHz	25 dB	First use of complete, all cycle, comparative validation technique. Schottky - TTL logic for highest practical speed. Highest data quality obtainable from a counter-timer. False data are practically eliminated.
5	Filter Bank	Signal Processor Mark III	Yes (1 each)	0.5 to 60 MHz (can be extended)	5 dB	This is the most efficient real time signal processor that is known. Highest data quality obtainable, and from much lower S/N inputs. (Reference 26)

To the counter-timer basic arrangement (line 1, Table 5-2) Mossey added a wide frequency range pedestal remover (line 2), a precision counter-timer-comparator (line 3) and a period-to-velocity converter (see Chapter 5 of Reference 23, and Reference 24). This formed the basis of the Mark I signal processor. Additional refinements were added by Asher (25). The success of the Mark I processor paved the way to development of the more elaborate Mark II processor (line 4). The Mark II processor has an advanced check system. Two of this type of processor are currently in use. The significant advantage of the Mark II is the greatly reduced error rate in the data output stream over any previous processor.

Because of these discretionary features built into the Mark II signal processor, the data output rate drops as the signal to noise ratio (S/N) falls below about 20 db. In order to improve the data output rate under specific low S/N conditions, General Electric developed the Mark III, a completely different type of signal processor, shown on line 5 of Table 5-2.

Both the Mark II and Mark III signal processors have been used in diagnostic and cross-correlation velocity measurements. A detailed operation description of each processor is given below.

5.2.1 Mark II LV Signal Processor

The Mark II LV signal processor is illustrated in Figure 5-1. The amplified Doppler burst signal is applied to the wideband pedestal remover. The square-wave like output is illustrated in Figure 5-1. This output is applied to a four stage binary counter, and also to an under-frequency tester. The binary counter feeds eleven (11) decoders, and each decoder has a unique logical function. Each decoder feeds a time-to-amplitude converter. The first nine (9) decoders are for specific single cycles within the burst. All of these decoders, through their respective time-to-amplitude converters, feed the all-cycle comparator test. In this test, one of the cycle periods is chosen as the reference period. Then, all other periods are compared with this reference. If any periods deviate from the reference by more than the preset fractional value, an "invalidate" signal results. Assuming all tests were "OK", a velocity signal output and a Data "OK" output result. The

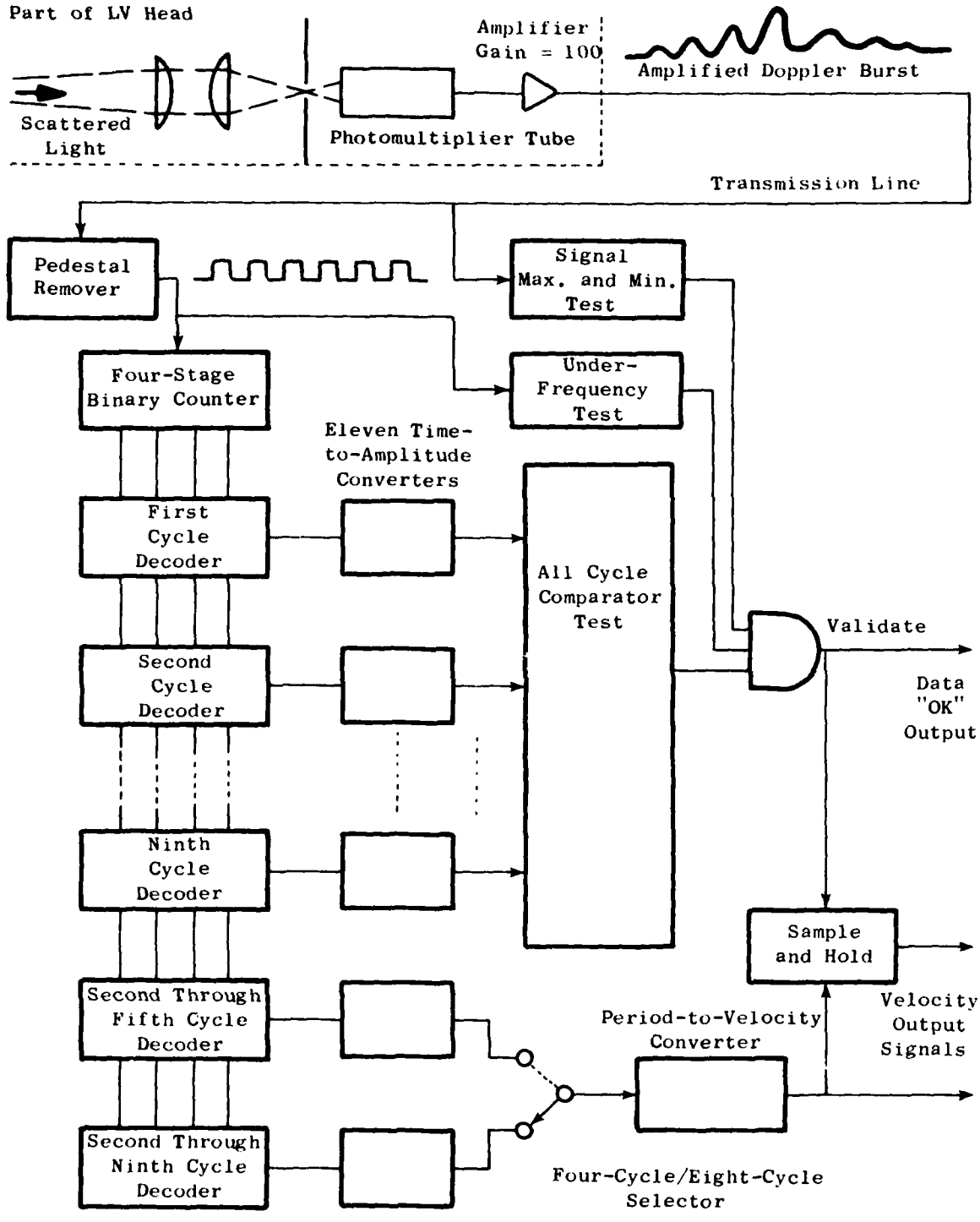

Figure 5-1. Mark II LV Signal Processor.

velocity signal may be selected to be calculated from four (4) cycles of the burst or from eight (8) cycles of the burst, by a manual switch setting. For the LV diagnostic tests performed to date, the nominal setting used for data validation is the eight (8) cycle setting. In addition to the under-frequency and all-cycle tests, a maximum and minimum signal test is done on the amplitude of the burst. This helps to qualify the particle size, since scattered light is dependent to about the fourth power of scatterer size.

This is believed to be the most complete comparative validation technique in existance on a counter-time processor. False data have been practically eliminated.

5.2.2 Mark III LV Signal Processor

The Mark III LV signal processor is illustrated in Figure 5-2. This processor was developed to produce the highest possible data rate under poor signal conditions. The model for the design is the "optimal receiver" - a technique for detecting a signal and estimating its frequency and arrival time. The basis of the receiver is a set of filters, spanning the frequency range of interest, but matched to the expected signal envelope shape. The analysis is given by Whalen in Reference 26. Although the principle has been well known in communications engineering, the application has been largely avoided due to its high cost and complexity. As an example, to obtain a frequency resolution of 1/2% by a conventional filter bank, the filters would be spaced in increments of 1%. For a processor range of 0.5 to 65 MHz, a total of 490 filters would be needed.

In 1972, a technique was conceived that would greatly reduce the number of filters needed for a given resolution. In this technique, instead of choosing the largest output filter, the outputs of all filters with activity over a threshold are used in a calculation program for an arithmetic mean frequency. The Mark III processor uses this innovation, and has a resolution of 1/2% of frequency with only 120 filters to cover the 0.5 to 65 MHz range.

As in the Mark II, the Mark III processor gives a complete data output (velocity and arrival time) for each single particle traverse. The Mark III

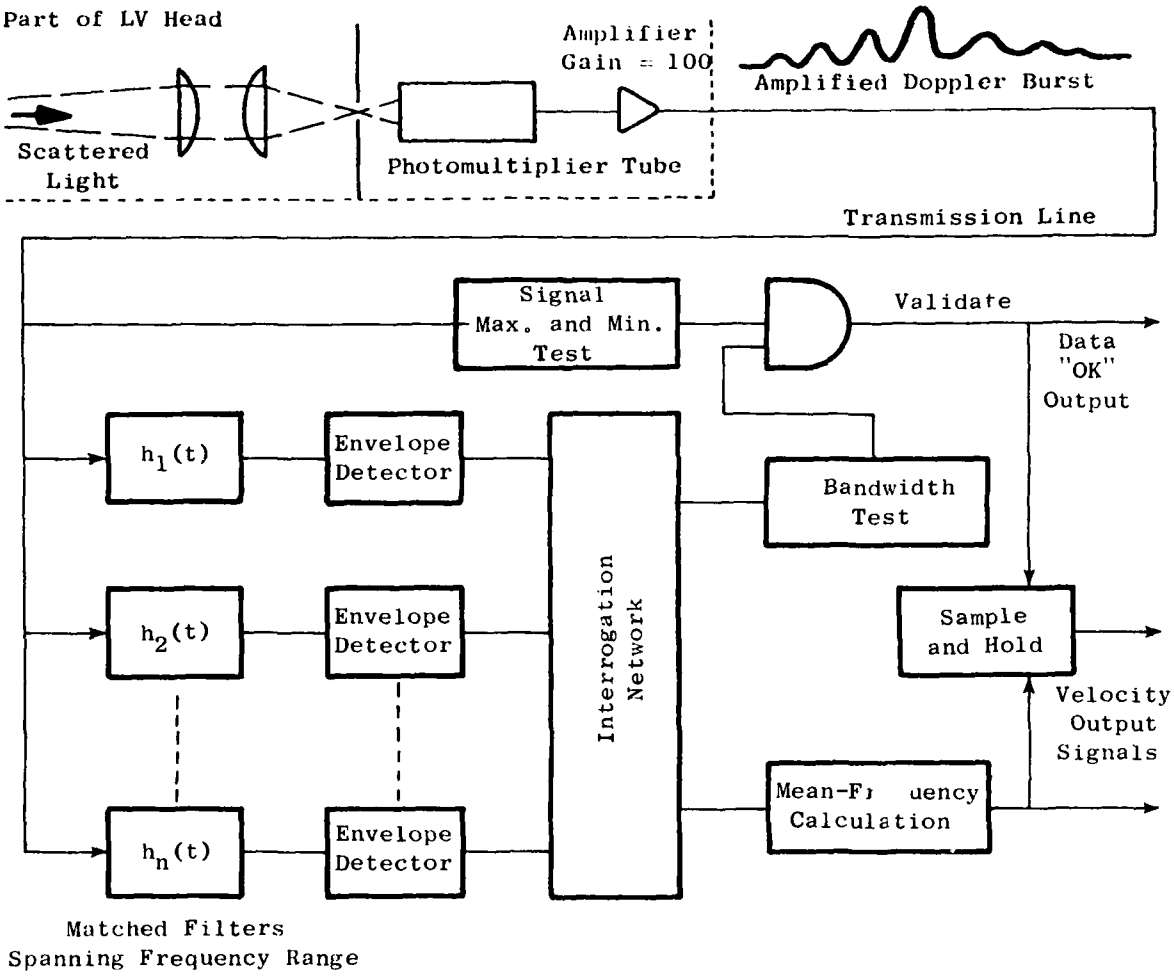

Figure 5-2. Mark III LV Signal Processor.

also has tests that are applied to identify "good" data. In Figure 5-2 a signal is examined for level in a "max-min test". A "bandwidth test" is done to establish the spectral distribution of the signal. For example a very noisy burst will result in a wide bandwidth or excess number of filters having activity. Only if all tests are met, will a DATA "OK" pulse result.

5.3 SEEDING ARRANGEMENTS

For all the scale-model tests performed, an aluminum oxide powder of about 0.7 microns mean diameter was used. Depending on the model tested, seeding is provided to the air entering the combustor of the inner stream flow, the outer stream air (for coannular flow nozzles), and the entrained air. Seed generation is provided by a fluidized bed approach which has a remotely variable rate control. Figure 5-3 is a diagram of the generator, and Figure 5-4 is a photograph of the seed generator and feed and control lines as installed at the General Electric Anechoic Jet Noise Test Facility. The fluidized bed is an ideal device to entrain the particles in the air. The fluidized bed produces an updraft that produces a slow "boiling" action in the bed which allows only the finest particles to be entrained. Large cluster and agglomerates tend to stay behind with this approach. As a result, the entrained seed may be sent through ordinary tubing and pipe, including 90° elbows, tees, and valves over long distances with no clogging or drop-out problems. Generally, a commercial free-flow agent, such as fumed silica, is added to assist feeding and prevent agglomeration.

5.4 DATA ACQUISITION AND REDUCTION

The full sensor system at General Electric's Anechoic Jet Noise Test Facility consists of two laser velocimeters, a network of microphones (both near-field and far-field), two closed circuit television systems (one monitors the LV beams, the other monitors the nozzle under test), and a complete gas and metal temperature, and gas pressure sensor network for scale model nozzle operation. Two minicomputers are used: one for nozzle operation, the other for jet plume diagnostic data acquisition and reduction. This section describes only the jet plume diagnostic data, control, acquisition and reduction. This equipment is shown in schematic form in Figure 5-5.

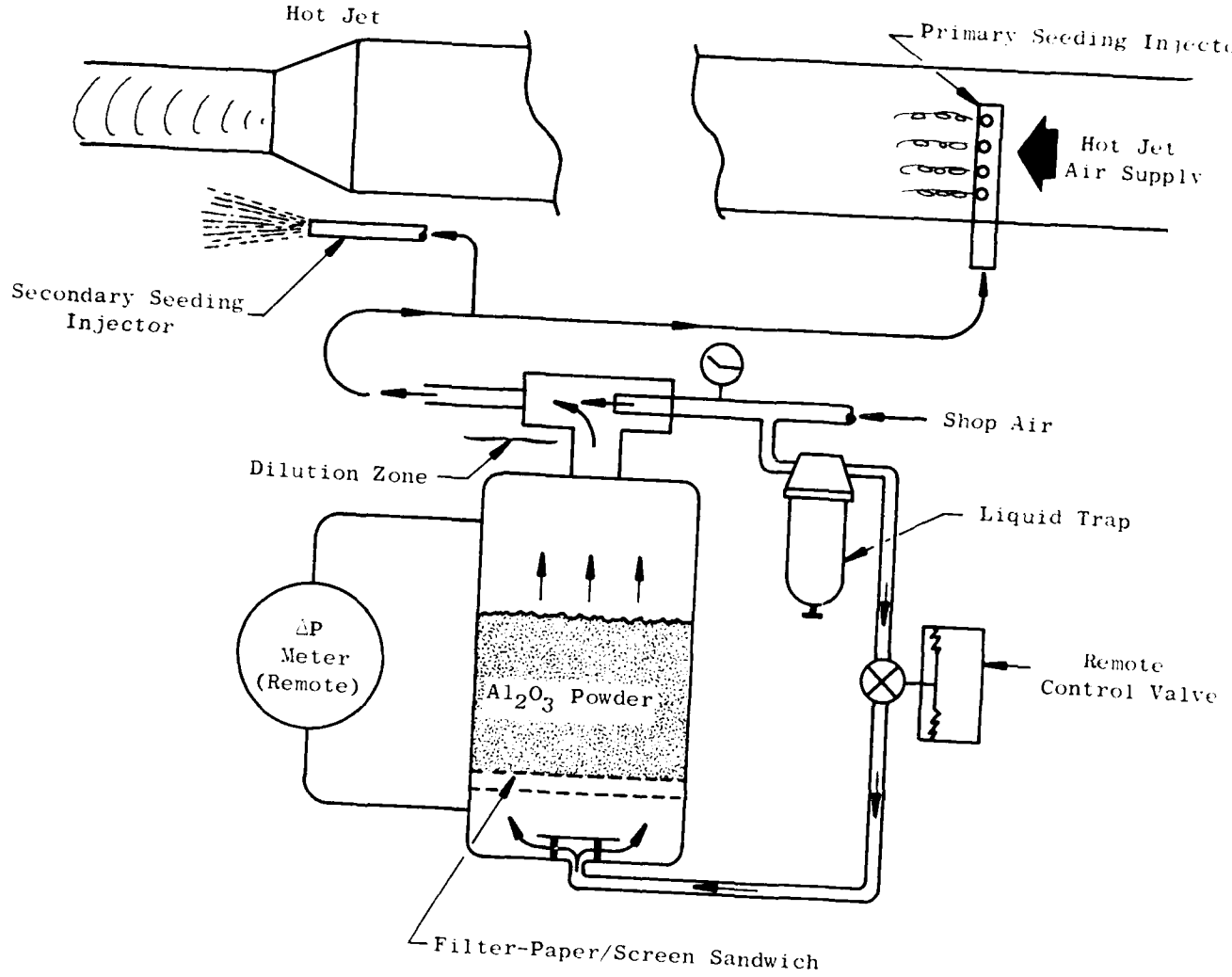

Figure 5-3. Fluidized Bed Powder Feeder and Injectors.

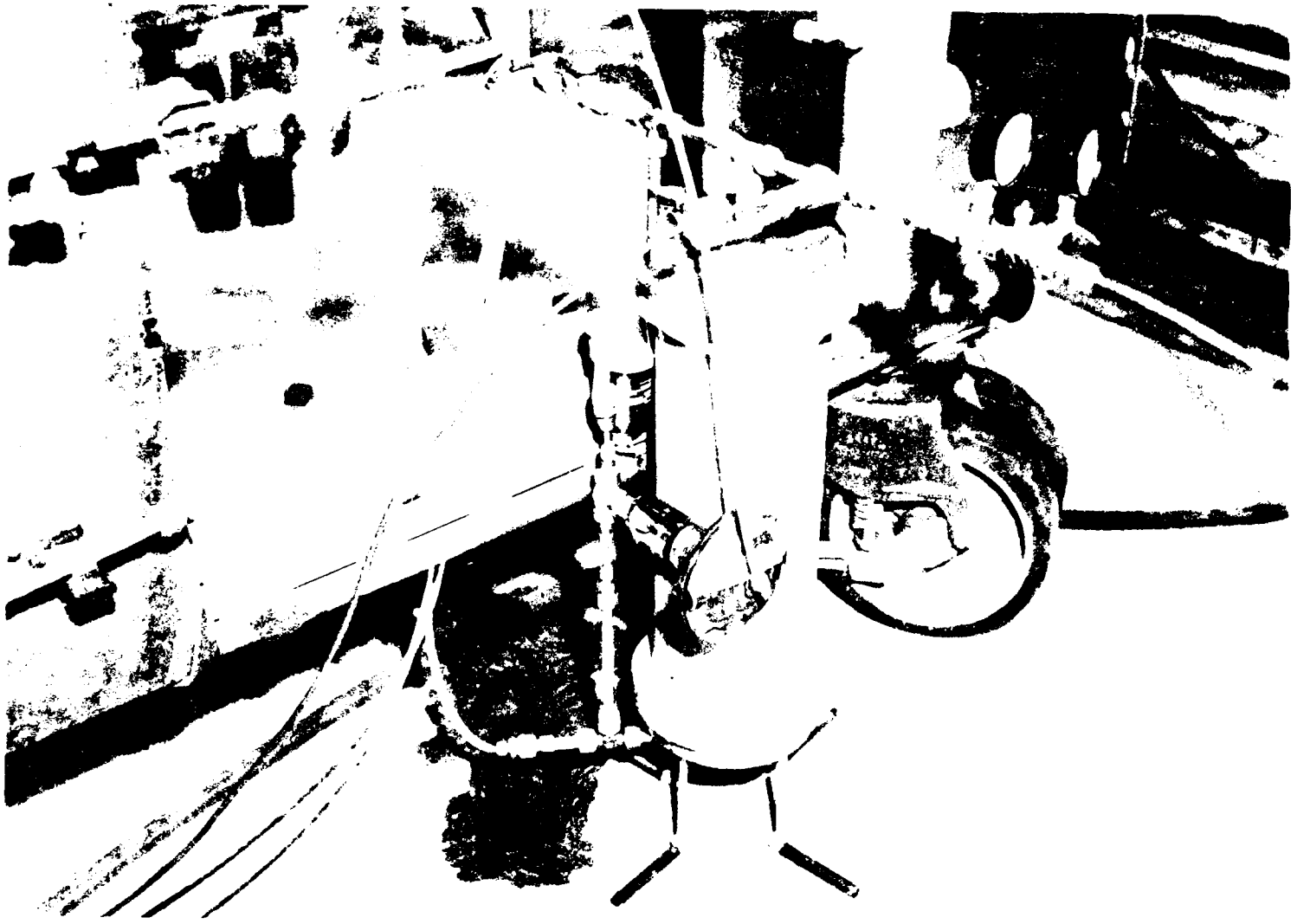

Figure 5-4. View of the Fluidizer Bed Seeder.

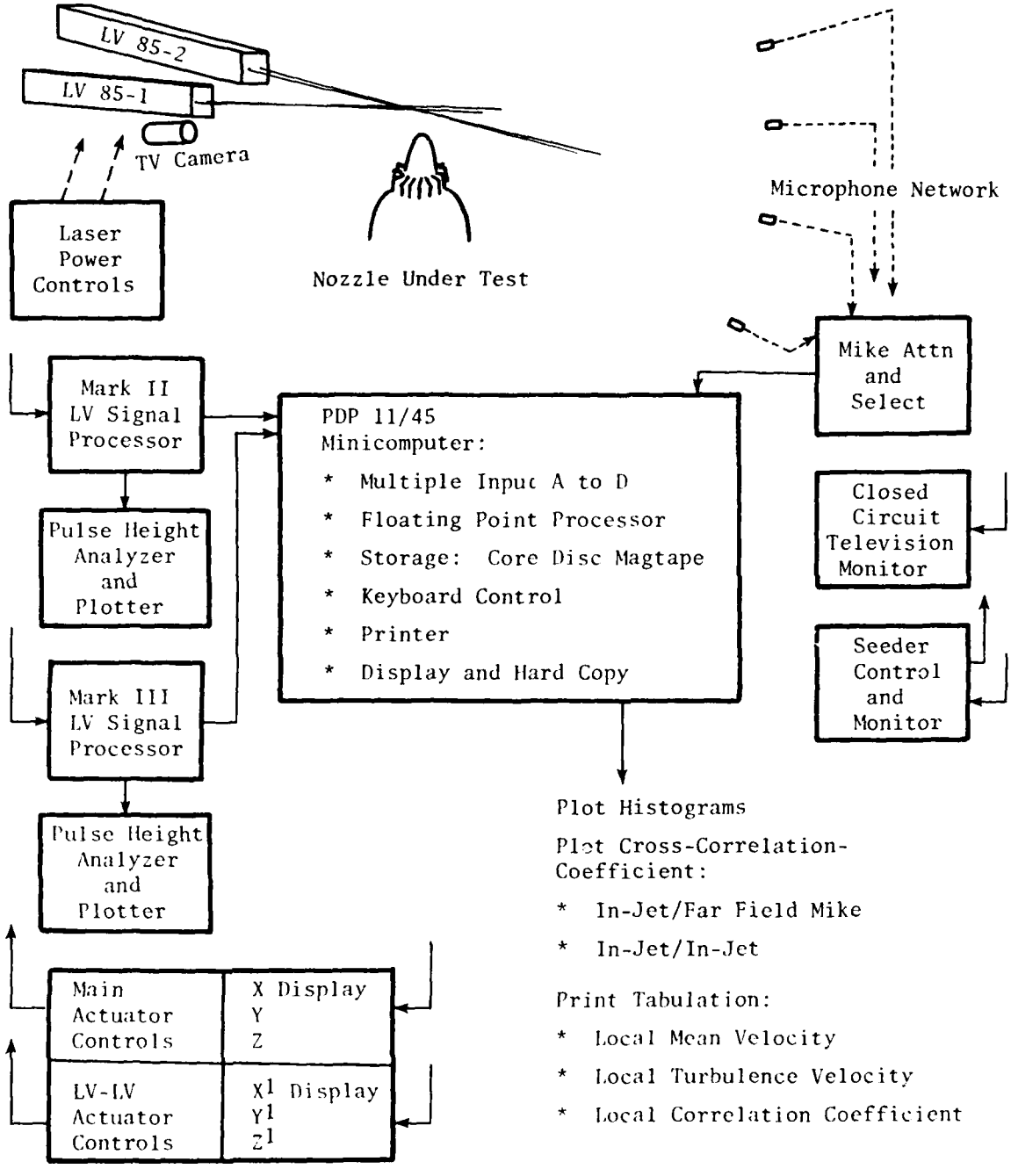

Figure 5-5. Data Acquisition and Reduction.

Individual controls are used for each LV. Each LV has its own original processor assigned. Each processor has its own pulse height analyzer and plotter.

The General Electric LV processor outputs are also directly linked to a PDP 11/45 minicomputer system which is used for the following data reduction and cataloging tasks:

- Log nozzle conditions and plume sensor locations.
- Count and log number of LV data samples per location.
- Plot histogram of velocity samples.
- Plot cross-correlation coefficients (in-jet in-jet and in-jet far-field microphone).
- Calculate and log correlation coefficients, mean and root-mean-square values, confidence intervals, histogram data.

The minicomputer has a multiple input analog to digital converter, floating point processor, core, disc and bulk magnetic tape storage, keyboard control, storage scope display and hard copy unit. The data reductions necessary to control the experiment and confirm that adequate data has been acquired (confidence interval) are performed within seconds of each data collection interval. This allows the engineer to make a decision for or against additional LV samples before actuating the LV system to the next plume location.

All of the above data is provided on-line during test, and is all filed in disk storage. The stored data is used later for data reduction for length and scale of turbulence, convection velocity, spectrum of turbulence and derivatives of cross-correlation functions. The data reduction programs used for on-line data analysis and reduction of the jet's turbulence properties are discussed in Section 7.0 and 8.0.

6.0 THEORETICAL AERO-ACOUSTIC FRAME WORK FOR REAL TIME MEASUREMENTS

The problem of performing meaningful turbulent flow measurements for the purpose of better understanding jet noise continues to be a difficult one for technology and physics in general. Until recently, the prospect of performing real time velocity measurements in realistic jet flows was, practically speaking, impossible. With the advent of today's laser velocimeter, the prospect has changed and moved in a direction of high feasibility. It is only now that the acoustic design engineer has at his disposal the type of advanced instrumentation necessary for performing the type of detailed measurements needed to better understand and postulate more accurate aero-acoustic models.

Jet noise generation and reduction is directly linked to the aerodynamic nature of turbulent jets in the form of what is referred to as the "aerodynamic source team". The definition of this term can be analytically described in terms of direct correlations between the turbulent velocity and the acoustic far-field pressure, or in terms of turbulent structure properties such as turbulent length scale, urbulent convection speed, and turbulence spectra of the moving eddies. The latter turbulence properties can be measured by so-called turbulent velocity two-point cross correlation measurements. Some of the governing equations which are used for describing the aerodynamic nature of jet noise are discussed below.

6.1 GOVERNING EQUATIONS

The generation of aerodynamic noise by free turbulence received its first quantitative formulation by Lighthill.[27,28] The principle quantitative step by Lighthill was his rearrangement of the continuity and momentum equations to yield a wave equation.

For the continuity equation we have:

$$\frac{\partial \rho}{\partial t} + \frac{\partial (\rho u_i)}{\partial x_i} = 0 \qquad (6\text{-}1)$$

From the conservation of momentum

$$\frac{\partial \rho u_i}{\partial t} + \frac{\partial (\rho u_i u_j)}{\partial x_j} = - \frac{\partial p}{\partial x_i} + \frac{\partial \tau_{ij}}{\partial x_j} \tag{6-2}$$

Where τ_{ij} is the viscous stress tensor.

From the above equations the following wave equation can be formed:

$$\frac{\partial^2 \rho}{\partial t^2} - a_o^2 \nabla^2 \rho = \frac{\partial^2 T_{ij}}{\partial x_i \partial x_j} \tag{6-3}$$

where

$$T_{ij} = (\rho u_i u_j - \tau_{ij}) + (p - a_o^2 \rho)\, \delta_{ij},$$

Lighthills stress tensor

a_o = Ambient speed of sound

ρ = Fluid Density

Far from the flow region of the jet itself, the right-hand-side of Equation 6-3 must vanish identically leaving the well-known homogeneous wave equation, which, under homogeneous isentropic conditions, governs linear acoustics in a uniform medium at rest - the implied "acoustic analogy."

The formal transformation of the differential equation presented above into an integral equation may be performed using the Kirchhoff integral. For the pressure perturbation field, one may write:

$$p'(\vec{x},t) = \frac{x_i x_j}{4\pi a_o^2 |\vec{x}|^3} \iiint_{V_o} \left. \frac{\partial^2 T_{ij}}{\partial t^2} \right|_{t-\tau_o} d\vec{y}^3 \tag{6-4}$$

where the coordinate system is defined in the sketch on the following page:

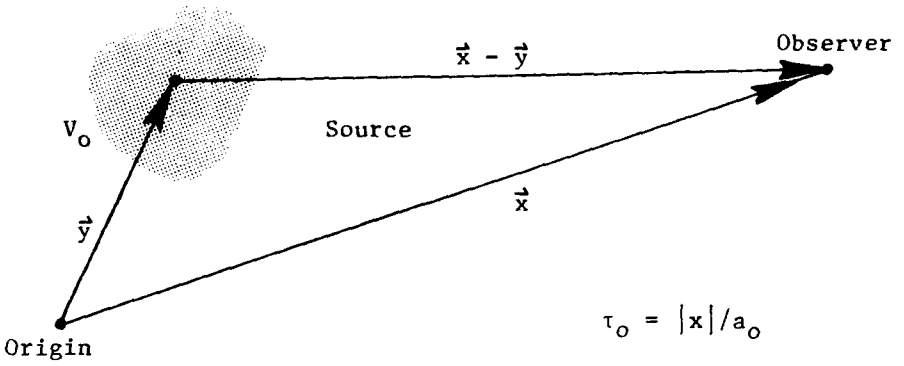

The subject of applying the approximations and extensions to Lighthill's original work are numerous. Some of GE's recent publications are contained in References 7, 23, 29, 30, 31, 32, and 33. However, a team of researchers at the University of Toronto under H.S. Ribner has been performing analysis and measurements to obtain a direct correlation of noise and flow.[34, 35, 36, 37] From the point-of-view of a direct theory experiment verification, and with an objective of learning how to use direct noise source location measurements to help in the design of jet noise suppressors, the work of the Toronto team is unique and attractive. A summary of useful concepts for applying in-jet type measurements to jet noise diagnostics is presented below.

6.2 TYPES OF AERO-ACOUSTIC MODELS FOR JET NOISE DIAGNOSTICS

6.2.1 Indirect Relationships

To obtain estimates for acoustic intensity, a considerable simplification to solving Equation 6-4 results in expressing the Lighthill stress tensor contraction in the Proudman[38] form,

$$x_i x_j \, T_{ij} = |\vec{x}|^2 \, T_{xx}.$$

W.T. Chu[37] has shown that the spectrum of noise per unit volume of turbulence may be estimated using the Proudman approximation:

$$\frac{I(x,f)}{\Delta V_o} = \frac{T_{xx}^2 L_x^3}{16\pi^{5/2} a_o^4 |\vec{x}|^2} \cdot \frac{\omega_t^4 e^{-(\omega_t^2/4\omega_f^2)}}{\omega_f \Theta^4} \qquad (6\text{-}5)$$

where

L_x, ω_f = Typical length scale and frequency of turbulence

ω_t = Radian frequency in the turbulence

$$\Theta = \left[(1-M_c \cos\theta)^2 + \left(\frac{\omega_f^2 L_x^2}{\pi a_o^2}\right)\right]^{1/2}$$

M_c = Convection Mach Number of the Turbulent eddy (V_c/a_o)

$T_{xx} = \rho_o U_x^2$

U_x = The instantaneous velocity component in the x-direction $\bar{U}_x + U'_x(t)$

Thus, from Equation 6-5, note that, if the point properties of the turbulence (L_x, U'_x, $\bar{U}_x$, W_t) can be measured, an estimate of the far-field acoustic radiation per unit volume of jet can be made. Sections 7 and 8 below describe the algorithms necessary to obtain these real-time measurements using the laser velocimeter. Suffice to say here that the mean velocity and turbulent velocity can be determined by a single point measurement. However, to determine the convection speed, length scale of turbulence, and the turbulence spectra of the convecting eddy requires the use of two-point space-time cross correlation measurement technology.

6.2.2 Direct Relationships

In formulating more direct relationships, or correlation between the jet flow and noise, a number of investigators have formulated unique techniques which can be used for various applications (see References 35, 36, 37, 39, 40, and 41). Some of the reported work was formulated for correlations of two pressure signals (References 39, 40, and 41) and others are formulated as a direct cross-correlation between the source velocity field and the acoustic radiation field. In particular, the work of Lee and Ribner[36], and Seiner and Reethof[42] are notable. Basically, however, all the techniques advanced were limited in their demonstration to subsonic ambient jets due to instrumentation limitations. The laser velocimeter does not have the limitations of these older measurement techniques and thus the LV was adapted and developed for the direct causality type measurements.

To obtain a working relationship relating the turbulent jet velocity field to the far-field acoustic pressure field, use of Proudman's form of Lighthill's integral for aerodynamic noise is used again[35]. An illustrative equation is an expression of acoustic intensity at $\vec{x}$ due to a unit volume of turbulence at $\vec{y}$.

$$\frac{I(x,y)}{\Delta V_o} \sim \frac{1}{4\pi a_o^3 r}\left[\frac{\partial^2}{\partial \tau^2} R_{u_x^2\, p'}(x,y,\tau)\right]_{\tau=\tau_o} \tag{6-6}$$

where

$$R_{u_x^2\, p'} = \overline{u_x^2(\vec{y})\, p'(x;\vec{y},\tau)}$$

$$\tau_o = \text{Retarded Time } (x/a_o)$$

$$U_x = \bar{U}_x - u_x'(\tau)$$

Hence, once the value of $R_{u_x^2\, p'}$, and the retarded time τ_o are known, in principle the acoustic intensity of the noise can be determined. Although the concept is simple in principle, carrying out the proper measurement using a

laser velocimeter is quite complicated. The theoretical considerations and computational algorithms used in General Electric's LV system are described in Sections 7.0 and 8.0.

One additional concept which has been introduced into 6-6 is the decomposition into two types of turbulence noise sources. To do this, the instantaneous turbulent velocity field $U_x(y,t)$ can be written as:

$$U_x(y,t) \approx \bar{U}_x + u'_x(y,t)$$

The cross-correlation function $R_{u'^2_x p'}$ can be expressed in terms of two cross-correlations as follows:

$$\begin{aligned} R_{u'^2_x p'} &= E\left\{u'^2_x p'\right\} \\ &= E\left\{(\bar{U}^2_x + 2\,\bar{U}_x\,u'_x + u'^2_x)\,p'\right\} \\ &= \bar{U}^2_x E(p')^0 + 2\bar{U}_x E(u'_x p') + E\,(u'^2_x\,p') \\ &= 2\,\bar{U}_x\,R_{u'_x p'} + R_{u'^2_x p'} \end{aligned} \qquad (6\text{-}7)$$

where $E\{\cdot\}$ denotes statistical expectation.

The first term on the right-hand side of Equation 6-7 may be identified as the shear noise cross-correlation term, while the second term may be identified as a self noise cross-correlation term. Later, the magnitude of these measured terms will be performed and some interesting conclusions will be drawn.

7.0 THEORETICAL CONSIDERATIONS FOR REAL TIME MEASUREMENTS USING THE LASER VELOCIMETER.

The previous sections have established the importance of mean and turbulence velocity measurements, velocity histograms, and time series statistics such as velocity spectrum, and cross correlation functions to the aero-acoustic engineer. This section develops the theory necessary for making these measurements with the laser velocimeter. The reason that special measurement techniques must be developed for the laser velocimeter is that the LV makes discrete measurements randomly in time (measurements are made only when particles arrive at the probe volume). The traditional theories of measurement apply only for continuous signals or for signals sampled in equal spaced time intervals. New theories of measurement are necessary to treat the random time sampling that occurs in laser velocimeter measurements.

Two types of measurements (histograms and correlation functions) can be made from which mean velocity, turbulence velocity, and velocity spectrum measurements can be obtained.

7.1 HISTOGRAM MEASUREMENTS FROM LASER VELOCIMETER DATA

A histogram is an estimate of the first order probability density function of the amplitude of a signal. To obtain a histogram, the range of the input signal, $x(t)$, is divided into classes bounded by values x_i. A counter, k_i, is incremented for each input if $x_i < x(t) < x_{i+1}$. This is done for N independent samples of $x(t)$, such that

$$\hat{P}_i = \frac{ki}{N} \tag{7-1}$$

where $\hat{P}_i$ is an estimate of the probability that a sample of $x(t)$ is between x_i and x_{i+1}. If the true amplitude probability density function, $f(x)$, doesn't vary "very much" in this interval, then

$$f_x = \frac{K_i}{N(x_{i+1} - x_i)} \quad \text{is an estimate of:} \tag{7-2}$$

$$\frac{F(x_{i+1}) - F(x_i)}{(x_{i+1} - x_i)} \simeq f(x_i)$$

If the successive values of x(t) are independent (that is, if sufficient time delay has occurred between samples), the probability distribution which describes the random variable, k_i, is the binomial distribution. If p_i is the true probability that $x_i < x(t) < x_{i+1}$, then

$$P(K_i = k_i) = \binom{N}{K_i} P_i^{K_i} (1 - P_i)^{N-K_i} \tag{7-3}$$

when N independent samples are used to construct the histogram. From this it may be shown that

$$E(K_i) = p_i N; \text{ where } E\{\cdot\} \text{ denotes statistical expectation} \tag{7-4}$$

$$\text{so that} \quad E(\hat{P}_i) = p_i \tag{7-5}$$

and hence the estimate of the probability that x(t) falls in class (x_i, x_{i+1}) is unbiased. For large values of N (in the present case N will always be large enough) $P(K_i)$ is very nearly normal and may be used to put a confidence interval on k_i. Recalling from the theory of Binomial Distributions that

$$VAR(K_i) = P_i(1-P_i)N \tag{7-6}$$

it can be said with β% confidence that the "true" value of K_i is contained in

$$k_i \pm Z_{\frac{\alpha}{2}} \sqrt{P_i(1-P_i)N} \tag{7-7}$$

If p_i is approximated by $\hat{p}_i$, one may then say that the "true" value of K_i is contained in

$$K_i \pm Z_{\frac{\alpha}{2}} \sqrt{K_i \left(1 - \frac{k_i}{N}\right)} \tag{7-8}$$

where $Z_{\frac{\alpha}{2}}$ is related to β as shown in Table 7-1.

Table 7-1. Relationship of $Z_{\frac{\alpha}{2}}$ to β.

β in percent	$Z\ \alpha/2$
90	1.645
95	1.960
98	2.326
99	2.576

The equations stated in this section may be used to estimate the number of points required for a histogram with a given level of precision.

If the fractional error for the i-th class is defined at some level of confidence β% as

$$e_i(\beta) = \frac{\hat{P}_i - P_i}{P_i} \tag{7-9}$$

then using the result of Equations (4) and (8) it may be shown that

$$e_i(\beta) \leq Z_{\frac{\alpha}{2}} \sqrt{\frac{1}{N}} \sqrt{\frac{(1-p_i)}{P_i}} \tag{7-10}$$

where p_i is the probability that a given x(t) falls in the interval (x_i, x_{i+1}). At 95% confidence one can then generate Table 7-2 which shows the total number of data points, N, required to obtain a given error as a function of class interval.

Table 7-2. Data Points Required.

		Percent Error			
		20%	10%	5%	2.5%
.2σ width Class Interval Centered at	μ	1156	4624	18500	74000
	μ + σ	1967	7868	31470	125883
	μ + 2σ	9112	36443	145770	583084
	μ + 3σ	111,222	444,889	1779556	7182240
Number of Points N					

7.1.1 Guide for Obtaining Histograms

When obtaining histograms one should observe the following points:

a. For the histograms to be useful in estimating higher order moments (mean, var, etc.) the classes must be sufficiently fine. Bendat[43] suggests that the class width $\Delta x \leq .2\sigma$ everywhere except at the tails for the means and variances.

b. To have sufficient data for testing, mean computation, etc. the experiment should be planned so that $k_i \geq 5$ for each class. To facilitate this, each tail may be made a class, as shown; all other intervals have widths of 0.2σ.

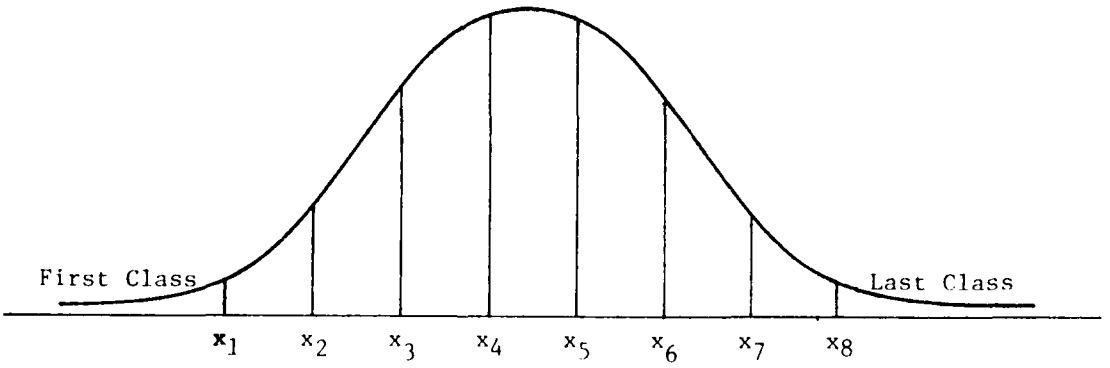

c. If a "histogram analyzer" is used with a countertype laser velocimeter processor with a digital output, a bias error may occur due to the mis-match of quantizing steps between the analyzer and the digital device. For an example of this error, see Reference 44.

d. Use enough data to obtain sufficient accuracy in the histogram, depending on the purpose for which this data will be used where $Z\alpha/2$ is related to β as shown in Table 7-1. Tables 7-2, 7-3 and 7-4 should be useful in determining N before the data is collected.

7.2 STATISTICS DERIVED FROM THE HISTOGRAM

Several useful statistics may be derived directly from the histogram. Among these are the mean (average velocity) and the moments about the mean (central moments). The set of central moments contains the variance and standard deviation (turbulence level), skewness and "Kurtosis" (peakedness).

7.2.1 Mean

Recall that the mean or expected value of a discrete random variable is defined as:

$$\mu_x = E(X) = \sum_{i=1}^{N} x_i \, P(X_i = x_i) \tag{7-14}$$

This may be estimated using the histogram. Recall that

$$\hat{P}_i = \frac{k_i}{N} \tag{7-15}$$

is an estimate of

$P(x_i \leq x(t) < x_{i+1})$, the probability that $x_i < x(t) \leq x_{i+1}$.

Thus if the class intervals are small enough, one may estimate the mean as

$$\bar{x} = \sum_{\substack{\text{all} \\ \text{intervals}}} \left(\frac{x_{i+1} + x_i}{2}\right) \frac{k_i}{N}$$

where $\left(\frac{x_{i+1} + x_i}{2}\right)$ is the value at the center of the class interval.

k_i is the number of counts in that class.

and N is the total number of points in the histogram.

7.2.2 Moments about the Mean

The ℓth moment about the mean is defined as

$$E\{(X - \mu_x)^{\ell}\}$$

After computing $\bar{x}$, one may estimate the ℓth moment about the mean, m_ℓ, as

$$m_\ell = \sum_{\substack{\text{all class} \\ \text{intervals} \\ i}} \left[\frac{x_{i+1} + x_i}{2} - \bar{x}\right]^\ell \frac{k_i}{N} \qquad (7\text{-}16)$$

These estimators are biased, but for large n (as in all GE LV histograms) this bias is negligable[45].

7.2.3 Variance

When $\ell = 2$, Equation 7-16 gives the variance. The square root of this estimates the standard deviation (or turbulence).

7.2.4 Skewness

When $\ell = 3$, one obtains the third moment about the mean. This moment is required to calculate the correlation coefficient between jet velocity squared and acoustic pressure.

If $m_3 = 0$, there is no skewness (the distribution is symmetric:

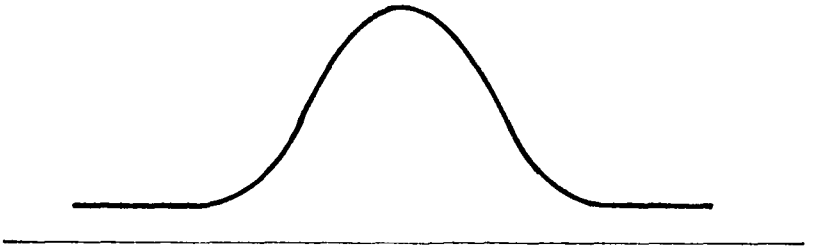

If $m_3 < 0$, the distribution skews to the left:

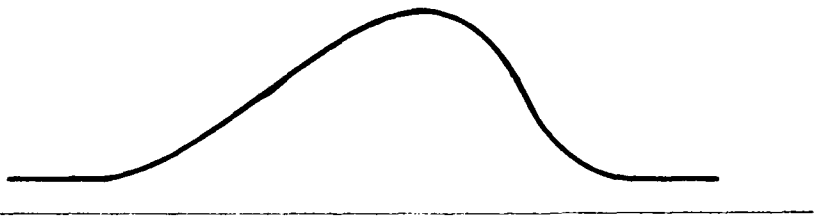

If $m_3 > 0$ the distribution skews to the right:

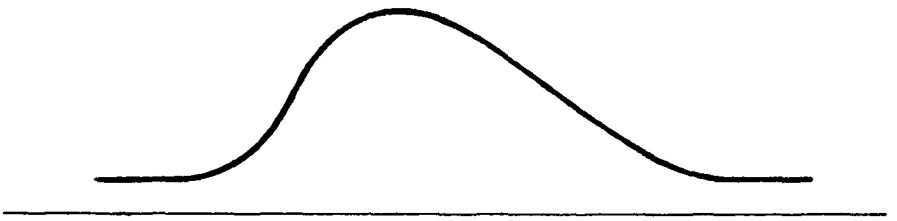

The "Skewness" (α_z in the literature) is normalized so that it is independent of scale and is calculated as

$$\alpha_3 = \frac{m_3}{m_2^{3/2}} \tag{7-17}$$

7.2.5 Kurtosis

When $\ell = 4$, the moment relates to the peakedness of the distribution. This moment is required to calculate the correlation coefficient between jet velocity squared and acoustic pressure. The normalized version of this static is called α_4 and is calculated as

$$\alpha_4 = \frac{m_4}{m_2^2} \tag{7-18}$$

If the distribution is Gaussian,

$$\alpha_4 = 3.0$$

If the distribution is uniform

$$\alpha_4 = 1.8$$

Sometimes α_4 is called the Kurtosis and other times, the Kurtosis is defined so that the Gaussian distribution has zero Kurtosis, i.e.:

$$\alpha_4' = \alpha_4 - 3 \tag{7-19}$$

Both appear as definitions in the literature.

7.3 ERROR IN MEAN AND TURBULENCE MEASUREMENT

The statistical error in the mean and turbulence measurements obtained from the histogram are now investigated. If the histogram is approximately Gaussian in shape, then the sample mean will follow Student's t distribution. If one lets the turbulence level (square root of the sample variance) be s then a 95% confidence statement may be written for the sample mean as:

The true mean is contained in

$$\bar{x} \pm t_{\frac{\alpha}{2} = .025,\ N} \cdot (S/\sqrt{N}) \qquad (7\text{-}20)$$

$$= \bar{x}\ (1 \pm t_{\frac{\alpha}{2} = .025,\ N} \cdot \eta/\sqrt{N})$$

where $\eta = s/\bar{x}$, which is the turbulence ratio.

If the fractional error is defined as:

$$\text{error} = \frac{|\bar{x} - \mu|}{\mu} \qquad (7\text{-}21)$$

then, with 95% confidence, it may be said that

$$\text{error} \leq t_{\frac{\alpha}{2} = .025,\ N} \cdot (\eta/N) \qquad (7\text{-}22)$$

For convenience the error is tabulated in Table 7-3 as a function of N and η for 95% confidence.

Table 7-3. Error Percent in Mean Measurement with 95% Confidence as a Function of N and η

N \ η	.2	.1	.05	.025
10	14.1	7	3.5	1.76
20	9.3	4.7	2.3	1.2
30	7.4	3.7	1.9	.93
40	6.3	3.2	1.6	.8
60	5.0	2.6	1.3	.65
120	3.6	1.8	.9	.45

In a similar manner, one may find the fractional error in the estimate of the turbulence, S. If the histogram is roughly Gaussian,

$$\frac{S^2\ (N - 1)}{\sigma^2} = X^2_{N-1} \tag{7-23}$$

where X^2_{N-1} is a chi-square random variable with N-1 degrees of freedom. Thus, a confidence interval on the true turbulence, S, is then

$$S\sqrt{\frac{N-1}{X^2_{\alpha\ =\ .025,\ N}}} \geq \sigma \geq S\sqrt{\frac{N-1}{X^2_{\alpha\ =\ .975,\ N}}} \tag{7-24}$$

with 95% confidence. The worst fractional error (since the tails of the Chi-square distribution are unsymmetric) is then

$$\text{error} = \frac{|S - \sigma|}{\sigma} \leq \sqrt{\frac{X^2_{\alpha\ =\ .025,\ N-1}}{(N-1)}} - 1 \tag{7-25}$$

The percent error at 95% confidence for various values of N is presented in Table 7-4.

Table 7-4. Fractional Error in Percent for Turbulence Estimate as a Function of N.

N	Error Percent
20	31.5
40	21.8
60	17.8
120	12.6
240	9.12
480	6.45
960	4.56
5000	2.0
25,000	.89

Examination of Tables 7-3 and 7-4 shows that considerably more data must be processed for a turbulence estimate than is needed for a mean velocity estimate of equivalent accuracy. When measuring the skewness or Kurtosis, similar increases in data for equivalent accuracy will be required over the turbulence estimate. Also, the bias due to class interval width will increase and the Bendat rule of .2 will probably have to be tightened. It is difficult to get estimates of skewness and Kurtosis repeatable to less than several percent.

7.4 CORRELATION FUNCTION MEASUREMENT WITH THE LASER VELOCIMETER

The measurement of correlation functions with the velocimeter is important because it extends the usefulness of the tool allowing it to perform measurements of turbulence spectra (obtained by Fourier Transformation of the velocity auto correlation function), turbulence eddy convective Mach number, turbulence length scale, the spectra of turbulence in the moving frame (this information can be obtained from cross correlation between the velocity at two points in the jet), and causality (the Lee-Ribner approach requires the cross correlation between the jet velocity squared and the far field pressure). These measurements require that a special analysis procedure be developed for

the laser velocimeter that accounts for the random sampling. This section presents a method developed at General Electric that has been successfully used to determine the important aerodynamic and acoustic parameters enumerated above.

The procedure is developed in detail for the autocorrelation of the jet velocity, x(t). An explanation is then presented to show how the estimator can be modified for determining the cross correlation of the velocities at two points in the jet and for determining the correlation function between the jet velocity and a continuous signal such as that obtained at the output of a microphone.

The approach considers the assumptions of wide sense stationarity and ergodicity made in all methods of spectrum analysis. Wide sense stationarity prescribes that the values of the autocorrelation function (ACF) are functions of the time between the signal samples and not the times the samples are taken. Hence, the ACF of the signal, x(t), is written as

$$R_{xx}(\tau) = E\{x(+)x(t+\tau)\} \tag{7-26}$$

where $E\{\cdot\}$ denotes expectation. If the signal x(t) is ergodic, one can interpret the expectation as an average over time. Therefore an acceptable estimate of $R_{xx}(\tau)$ for some particular value of τ might be

$$\hat{R}_{xx}(\tau) + \frac{1}{M}\sum_{k=1}^{M} X(t_k)\, X(t_k + \tau) \tag{7-27}$$

where the t_k are M random times at which samples are taken.

Note that Equation 7-27 could be obtained by considering the relationship between the ACF's of the signal before and after sampling[46,47]. If the sampling process is modeled by a signal, x(t), consisting of impulses occurring at the sampling times, then the sampled version of x(t), which is called y(t) can be written

$$y(t) = x(t)\, X(t) \tag{7-28}$$

where

$$S(t) = \sum_{i=-\infty}^{\infty} \mu_o(t-t_i) \tag{7-29}$$

and t_i are the random sampling times. If it is assumed that s(t) and x(t) are independent random processes,

$$R_{yy}(\tau) + R_{xx}(\tau)\ R_{ss}(\tau) \tag{7-30}$$

Then the ACF of x(t) may be estimated by taking the ratio of estimates of the ACF's of the sampled version of the signal, y(t), and of the sampling signal, s(t). It has been shown (43,44) that the ACF of s(t) is directly related to the inter-arrival probability density functions of the sampling process. These are determined by measuring the time intervals between samples. Substitution of the traditional estimators into the ratio gives Equation 7-27. The derivation of Equation 7-27 sketched above requires that

$$R_{ss}(\tau) \neq 0 \tag{7-31}$$

for all τ of interest. This requirement is equivalent to stating that there must be a finite probability that samples are taken τ time units apart; otherwise no products can be accumulated. This derivation also requires that s(t) and y(t) be stationary processes; a condition which is not really necessary.

Finally, apart from the requirement stated in Equation 7-31, no assumptions are made on the statistics of the sampling process. The ability to construct the ACF of the sampled process is not affected by the mean sampling rate. There is no "Nyquist Criterion" as exists in traditional sampled data spectrum analysis.

It is shown below that the ACF reconstruction technique proposed in Equation 7-27 yields an acceptable estimate of $R_{xx}(\tau)$.

In particular, it will be shown that it has the following properties:

1. It is unbiased.

2. It has finite variance.

3. The variance goes to zero as the number of samples in the estimate goes to infinity, i.e., the estimate converges in the mean.

Thus the estimate satisfies the conditions necessary to be called consistent.

It is easy to show that $\hat{R}_{xx}(\tau)$ will be an unbiased estimate of $R_{xx}(\tau)$ since

$$E\{\hat{R}_{xx}(\tau)\} = \frac{1}{M} \sum_{k=1}^{M} E\{X(t_k)X(t_k+\tau)\} = R_{xx}(\tau) \tag{7-32}$$

One may now derive the variance of the ACF estimate given in Equation 7-27 by first writing:

$$E\{\hat{R}^2_{xx}(\tau)\} = \frac{1}{M^2} \sum_{i=1}^{M} \sum_{j=1}^{M} E\{X(t_i)X(t_j)X(t_i+\tau)X(t_j+\tau)\}$$

$$= \frac{1}{M^2} \sum_{i=1}^{M} E\{X^2(t_i)X^2(t_j)\}$$

$$+ \frac{1}{M^2} \sum_{\substack{i=1 \\ i\neq j}}^{M} \sum_{j=1}^{M} E\{X(t_i)X(t_j)X(t_i+\tau)X(t_j+\tau)\} \tag{7-33}$$

where the expectation is over x(t); and t_i and t_j given samples at $t_i+\tau$ and $t_j+\tau$.

If it is assumed that x(t) is jointly normal and zero mean, the result for the expected product of four normal variables can be used to simplify the summations. With

$$E\{X(t)X(t+\tau)\} = R_{xx}(\tau)$$

one has:

$$E\{\hat{R}^2_{xx}(\tau)\} = \frac{R^2_{xx}(0)+2R^2_{xx}(\tau)}{M} + E_{(t_i-t_j)}\left\{\frac{1}{M^2}\sum_{i=1}^{M}\sum_{j=1}^{M}\left[R^2_{xx}(\tau) + R_{xx}(t_i-t_j+\tau)R_{xx}(t_i-t_j-\tau)\right]\right\} \tag{7-34}$$

where the expectation is over (t_i-t_j) given samples at $t_i+\tau$ and $t_j+\tau$. The first term in the summation gives us $(1-1/M)R_{xx}^2(\tau)$. Combining this with the term outside the summation, and subtracting the square of the expected value of the estimate yields

$$VAR\{\hat{R}_{xx}(\tau)\} = \frac{R^2_{xx}(0)+2R^2_{xx}(\tau)}{M} + E_{(t_i-t_j)}\left\{\frac{2}{M}\sum_{i=2}^{M}\sum_{j=1}^{i-1}\left[R^2_{xx}(t_i-t_j)+R_{xx}(t_i-t_j+\tau)R_{xx}(t_i-t_j-\tau)\right]\right\} \tag{7-35}$$

This is a general result for the variance of the estimator. Written in this form, the first term represents its variance if all of the product pairs in the estimate are independent. The second term represents the increase in the variance due to redundant information in the product pairs. Therefore, if the samples are taken far enough apart so that

$$R_{xx}(t_j-t_j) \tilde{=} 0 \text{ all } t_i \neq t_j \tag{7-36}$$

the variance of the estimate is

$$VAR\{\hat{R}_{xx}(\tau)\} = \frac{R^2_{xx}(0)+R^2_{xx}(\tau)}{M} \tag{7-37}$$

This result may still be a good approximation to the true variance if the mean arrival rate of product pairs (generally much less than the mean

sampling rate) is less than the reciprocal of the length of the correlation function of x(t).

While Equation 7-35 gives a generic result for the variance of the AFC estimate, it is of little use in performing "engineering" calculations of the error in laser velocimeter correlation functions. However, experiments at General Electric have shown that the particle arrivals closely follow a Poisson probability distribution. Assuming a Poisson distribution allows considerable simplification of Equation 7-35 and provides some simple rules for estimating errors in correlation measurements.

Obtaining the result for the Poisson sampling case is simplified by the fact that the subset of samples at times t_i, with a sample in $[t_i+\tau-\Delta/2, t_i+\tau+\Delta/2]$, is also a Poisson process. The mean arrival rate for product pairs can be shown to be

$$\lambda' = \lambda^2\Delta \tag{7-38}$$

where Δ is the "time grid width" representing the amount of deviation allowed in selection of products lag τ apart, and λ is the mean rate of the original Poisson process. The reason for the time grid width, Δ, is that the probability of taking two samples <u>exactly</u> τ apart is zero. Thus in any practical realization of Equation 7-27 one must lump together those samples which occur $\tau-\frac{\Delta}{2}<\tau<\tau+\frac{\Delta}{2}$ apart. Averaging product pairs at close to the same lag value results in the addition of a "time" grid jitter error to the estimate. Fortunately it may be shown that this error may be made negligibly small if Δ is small enough[44].

To simplify the derivation of the bound, one can assume with no loss of generality that the t_i's in Equation 7-35 are ordered so that

$$t_i > t_j \text{ when } i>j$$

One may then write Equation 7-35 in terms of the inter-arrival density functions of the Poisson process. These are

$$f_k(t) = \frac{(\Delta\lambda^2)^k t^{k-1} e^{-(\Delta\lambda^2)t}}{(k-1)!}\ \mu_{-1}(t) \tag{7-39}$$

Thus Equation 7-35 becomes

$$\mathrm{VAR}\{\hat{R}_{xx}(\tau)\} = \frac{R_{xx}^2(0)+R_{xx}^2(\tau)}{M}$$

$$+\frac{2}{M}\sum_{k=1}^{M-1}(M-k)\int_0^\infty [R_{xx}^2(\mu)+R_{xx}(\mu+\tau)R_{xx}(\mu-\tau)] \tag{7-40}$$

$$\frac{(\Delta\lambda^2)\mu^{k-1}}{(k-1)!}\ e^{-(\Delta\lambda^2)\mu}d\mu$$

Since the integrals in the summation are all positive, one may write an upper bound on this result as

$$\mathrm{VAR}\{\hat{R}_{xx}(\tau)\} < \frac{R_{xx}^2(0)+R_{xx}^2(\tau)}{M}$$

$$+\frac{2}{M}\int_0^\infty [R_{xx}^2(\mu)+R_{xx}(\mu+\tau)\ R_{xx}(\mu-\tau)] \tag{7-41}$$

$$\Delta\lambda^2\sum_{k=1}^{M-1}\frac{(\lambda^2\Delta)^{k-1}\mu^{k-1}e^{-\lambda^2\Delta\mu}}{(k-1)!}\,d\mu$$

By extending the summation to infinity, an identity is obtained for $\lambda^2\Delta\mu$. Employing Schwarz's Inequality, it can be shown that

$$\int_{-\infty}^{\infty} R_{xx}(\mu+\tau)R_{xx}(\mu-\tau) \leq \int_{-\infty}^{\infty} R_{xx}^2(\mu)d\mu \tag{7-42}$$

Therefore the upper bond may be written:

$$\mathrm{VAR}\{\hat{R}_{xx}(\tau)\} < \frac{R_{xx}^2(0)+R_{xx}^2(\tau)}{M} + \frac{2\lambda^2\Delta}{M}\int_{-\infty}^{\infty} R_{xx}^2(\tau)d\tau \tag{7-43}$$

This is the upper bound for the variance of the ACF estimate in Equation 7-27 when the sampling is the Poisson process.

Consider the significance of the two terms in Equation 7-43. Note that the first term is independent of λ and that the second term depends on λ^2. Thus for the low mean sampling rates, the first term dominates and the variance is the same as for the case where all product pairs in the sum are independent. Now if λ becomes very large so that the second term dominates,

$$\mathrm{VAR}\{\hat{R}^2_{xx}(\tau)\} \cong \frac{2\lambda^2\Delta}{M} \int_{-\infty}^{\infty} R^2_{xx}(\mu)d\mu \tag{7-44}$$

If T_L is defined as the length of time over which the observations are taken, then $T_L = M/\lambda^2\Delta$ and

$$\mathrm{VAR}\{\hat{R}^2_{xx}(\tau)\} \cong \frac{2}{T_L} \int_{-\infty}^{\infty} R^2_{xx}(\tau)d\tau \tag{7-45}$$

If the mean arrival rate is very large, successive samples are highly correlated and the variance is reduced as the observation time increases. In either case the variance goes to zero as the amount of data processed increases so that the estimate is always consistant.

Usually, the laser velocimeter's mean particle arrival rate is less than 10,000 particles/second. For most jet flows, it can be shown that the first term of the variance equation dominates the second. Thus for engineering purposes, the variance of the AFC estimate can be approximated by

$$\mathrm{VAR}\{\hat{R}_{xx}(\tau)\} \cong \frac{R^2_{xx}(0)+R^2_{xx}(\tau)}{M} \tag{7-46}$$

This can be used to construct confidence limits on the estimate if $R_{xx}(\tau)$ is assumed to be roughly Gaussian. With this assumption, a 98% confidence statement can be written as

$$\hat{R}_{xx}(\tau) - 2.33\sqrt{\frac{\hat{R}^2_{xx}(0)+\hat{R}^2_{xx}(\tau)}{M}} \leq R_{xx}(\tau) \leq \hat{R}_{xx}(\tau) + 2.33\sqrt{\frac{\hat{R}^2_{xx}(0)+\hat{R}^2_{xx}(\tau)}{M}} \tag{7-47}$$

The estimation procedure given in Equation 7-46 can be extended so that the cross correlation between the outputs of two laser velocimeters can be determined. This is done by simply accumulating cross product pairs:

$$\hat{R}_{xy}(\tau) = \frac{1}{M}\sum_{k=1}^{M} X(t_k)y(t_k+\tau) \tag{7-48}$$

The procedure can also be used to cross correlate the output of a laser velocimeter with a continuous signal. In this case, let $y(t_k+\tau)$ represent the continuous signal that is physically sampled (using a sample and hold circuit and an A/D converter) at time $t_k+\tau$. For a particular value of τ, a delay circuit can be used to cause the occurrence of this sample when a particle arrives at the probe volume at t_k.

The procedures described above have been used successfully at General Electric to determine the auto correlation function at a single point in a jet, the cross correlation function between two points in a jet and the cross-correlation between the jet velocity and the jet velocity squared and a far field microphone signal.

7.5 MEASUREMENT OF EDDY CONVECTION VELOCITY

Cross-correlation data obtained between the outputs of two laser velocimeters can be used to determine the velocity of turbulent eddies in a jet. To do this, a set of several correlation functions are obtained with the laser velocimeter probe volumes at different spacings, ξ_i. For the i^{th} correlation function, the lag value corresponding to the peak in the correlation function, τ_i is determined. Thus

τ_i is the value where

$$R_{xy}(\tau) \text{ is maximum} \tag{7-49}$$

Physically, τ_i is interpreted as the time required for the eddy to travel from the first laser velocimeter to the second. Since the eddy has traveled the probe volume separation distance in this time interval, an estimate of the eddy convection velocity is

$$\hat{V}_i = \frac{\xi_i}{\tau_i} \tag{7-50}$$

An improved estimate of eddy velocity is obtained by considering a series of such measurements. If the points (τ_i, ξ_i) were plotted for a set of N such measurements on a piece of graph paper, the eddy convection velocity, V_c, would be slope of the best line that could be drawn through the points. Thus when determining V_c from a set of correlation functions, the standard linear regression formulas can be employed:

$$\bar{\tau} = \frac{1}{N} \sum_{i=1}^{N} \tau_i \tag{7-51}$$

and

$$\hat{V}_c = \frac{\sum_{i=1}^{N} (\tau_i - \bar{\tau}) \xi_i}{\sum_{i=1}^{N} (\tau_i - \bar{\tau})^2} \tag{7-52}$$

The convective mach number can be estimated by dividing $\hat{V}_c$ by the appropriate jet velocity.

7.6 DETERMINATION OF TURBULENCE LENGTH SCALE

Turbulence length scale can also be determined from a set of velocity cross correlation measurements obtained at different separation distances. The procedure used is given in Hinze[48]. Defining the ensemble of correlation functions as

$$R_{xy}(\tau_j \xi_i) \tag{7-53}$$

where τ is the time lag and ξ_i is the separation distance, one can form the longitudinal correlation coefficient

$$f(\xi_i) = \frac{R_{xy}(0,\xi_i)}{\sqrt{R_{xx}(0)R_{yy}(0)}} \tag{7-54}$$

by evaluating each correlation function obtained at $\tau=0$. The integral length scale is then given from

$$L_x = \int_0^\infty f(\xi)d\xi \tag{7-55}$$

This integral is approximated by fitting a curve of the form

$$f^1(\xi) = a_1 \exp\left(\frac{-|\xi-a_2|^{a_3}}{a_4}\right)\cos(a_5\xi) \tag{7-56}$$

to the data points $f(\xi_i)$ using the Conjugate Gradient[49] procedure. The function, $f^1(\xi)$, is then numerically integrated using the Simpson's rule procedure. Gaussian Quadrature integration could also be employed to directly obtain L_x from the $f(\xi_i)$.

7.7 DETERMINATION OF LAGRANGIAN TIME CORRELATION

A series of two-point velocity correlations at different separation distances, ξ_i, can also be used to determine the time correlation function of an eddy in the moving reference frame. Since the separation distance, ξ_i,

and the lag in the moving frame t_i are related by the convective eddy velocity, it is true that the peak values of the cross-correlation functions represent respective values of the moving frame eddy correlation function. With $R_L(t)$ defined as this LaGrangian correlation function,

$$R_L(t_i) = \text{MAX}\{R_{xy}(\tau, \xi_i)\}$$

where t_i = the value of τ where the maximum occurs.

The spectrum of the eddy in the moving frame can be determined by taking the Fourier transform of the above.

AD-A094 296 GENERAL ELECTRIC CO CINCINNATI OH AIRCRAFT ENGINE GROUP F/G 20/1
HIGH VELOCITY JET NOISE SOURCE LOCATION AND REDUCTION, TASK 3, --ETC(U)
DEC 78 P R KNOTT, P F SCOTT, P W MOSSEY DOT-OS-30034
UNCLASSIFIED R78AE6627-VOL-4 FAA-RD-76-79-3-4 NL

2 OF 2
AD A094296

END
DATE FILMED
3-81
DTIC

8.0 DESCRIPTION OF GENERAL ELECTRIC'S COMPUTATIONAL ALGORITHMS

Two computer programs have been designed to perform the collection and correlation of the test data. The program INJET/INJET handles data from two laser velocimeters (LV1 and LV2); and as the name implies, it is used to correlate velocity data from two points in the jet stream. The second program, INJET/FARFLD, operates on data from a single velocimeter (LV1) and data from a far field pressure transducer (P2).

Both programs employ a data collection and summation module written in assembly language for efficiency with regard to execution time. The input data are quantized to 32 levels, and a technique called quantized product factoring is used to defer the multiplication process until a point in the data processing when real time computations are not required.

Prior to the start of the data summation portion of both programs, an estimate is made of the mean and variance of each input. This is done by reading 128 samples, summing each input and summing the square of each input in double precision integer form. The mean is used as a reference or DC level for all subsequent data inputs and calculations. The variance is found from $\Sigma V^2/128 - \bar{V}^2$ and is used in determining the cell size to be used for quantizing. A cell size equal to $3/16\sqrt{\text{variance}}$ assumes that 32 levels will encompass 99% of the total input range for a normal distribution.

Although the two programs are similar in structure, the details of the data collection and summation differ. For clarity, the two programs will be discussed separately.

8.1 QUANTIZED PRODUCT FACTORING

Quantized product factoring might best be described by the following:

The normal expression for the sum of products is:

$$\sum_{i=1}^{m} x_i y_i$$

If the variables x and y are quantized to N levels, there are N finite values that the quantized variables, X and Y, can take on. This means that the product can now be factored, and further that the quantized values can be used as an index or pointer into a vector. The quantized factored form of the sum of products is

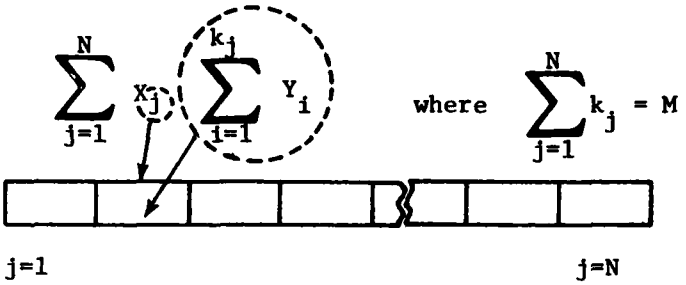

Quantized factorization means that summations may be used instead of multiplications during that portion of the data processing which is being done in real time.

8.2 INJET/INJET DATA COLLECTION

All velocity data is collected using an interrupt technique. When a velocity data point is obtained, that is, the LV circuitry has indicated that the A/D conversion is complete, an interrupt is generated in the computer. Four words are read from the digital input device in response to each interrupt, T1, V1, T2 and V2 in that order. T1 and T2 are the external clock times at the start of the A/D conversion, V1 and V2 are the A/D output values. Since either LV can generate the interrupt, the sign of the velocity word causing the interrupt is forced to a 1 to indicate valid data.

Input data for each LV is stored on stacks of 1024 words each. This allows room for 512 time and velocity pairs. A counter keeps track of the remaining room on each stack, and a pointer locates the next open location on each stack. When these pointers reach the bottom of the stack, they are reset to the top of the stack as long as the counter indicates space available.

The time value is placed on the data stack directly. The velocity value put on the stack is a quantized velocity relative to the mean or DC level, i.e., Q1 = (V1 - $\overline{V1}$)/CS1 where CS1 is the cell size for LV1.

This data input process goes on independent of the correlation process which will free locations on the data stacks as the data is used, with the oldest data being processed first.

8.3 VELOCITY CORRELATION AND HISTOGRAM ALGORITHMS

The correlation process is a pairing of each data point on one stack with all data points on the other stack whose time differnce (ΔT) satisfies some predefined criteria. A total of 512 lag values ($\Delta T = T_2 - T_1$) was chosen, resulting in a range for ΔT of $-256 \leq \Delta T \leq +255$.

A rectangular array, 32 columns by 512 rows, is used to sum the results of the pairing process. The ΔT value is used as a row pointer, since each row corresponds to a specific lag value from -256 to +255. Each column corresponds to a quantizing level from -16 to +15. When a pair of data points is found which meets the ΔT criteria, one quantized velocity (say Q1) is used as a column pointer, ΔT as the row pointer, and Q2 is added into the specified array element. This is using the quantized factorization technique described previously. Histograms for each velocity are formed by using the paired Q values as pointers into vectors 32 elements long and incrementing the corresponding elements. The number of occurrences of each lag value is generated in a similar manner by using ΔT as a pointer into a 512 element vector and incrementing the indicated element.

When data points on one stack do not pair with any points on the other stack, the locations they occupy become available for input again. This pairing and summing process is continued until some predetermined number of data points has been processed, usually 20,000 to 30,000 points; then, all data input and processing is halted. This is done to prevent an overflow from occurring in the summing array.

Another interrupt is used to detect the overflow of the external clock. When the clock overflows, data input is temporarily halted until all the data

currently on the data stacks have been correlated, then the data input and processing is resumed again. This is done because the time information becomes ambiguous after a clock overflow unless a double precision clock counter is used.

8.4 DATA COMPRESSION AND INTERMEDIATE DISPLAYS

When the required number of data points has been examined and processing halted, the summing array is compressed to a double precision vector. This is done by multiplying each column of the array by its corresponding quantized velocity value and summing across the columns. In this manner, the more time consuming multiplication process is done at a point where execution time is not critical. The double precision vector now contains the sum of the quantized product pairs for each lag vlaue (ΔT).

New estimates of the mean, variance and cell size are calculated for each velocity from the histogram data. The histogram data are then normalized and displayed on a scope for operator monitoring.

The current cross-correlation contribution is calculated from the double precision sum of the product pairs and the previous mean and cell sizes. The total run correlation coefficient is then updated along with the total mean and variance values. A normalized correlation coefficient is then calculated and displayed on the scope. The number of data points in each histogram along with the total number of data points processed in the run is also displayed on the scope.

A new DC level is calculated using the latest value of the mean, all buffers are cleared and the data collection and summing process is resumed again.

This processing of data, in groups of 20,000 to 30,000 points, is repeated until a total of approximately 300,000 points have been sampled, and then the run is terminated. Although the segmented processing is required to prevent overflows in the summing buffer, it also allows the quality of the data collection to be monitored at intervals during the run. This means that bad data can be detected earlier and the run aborted, rather than at the end of a complete run.

8.5 INJET/FARFLD DATA COLLECTION

Pressure data are obtained on an interrupt basis from a separate A/D converter that is part of the 11/45 computer system. The conversions are initiated by signals from the external clock that is part of the laser velocimeter circuitry. When the conversions are complete, an A/D interrupt is generated. The external clock rate is divided by 4 so that the pressure interrupts will occur at a 20 KHz rate. The 11/45 clock is set up to generate a clock interrupt when the external clock overflows. A software clock is used internally in the program and is incremented every time a pressure interrupt is serviced.

Velocity data are obtained through the same digital input device that is used for the INJET/INJET program, except that only one velocimeter is used. A device flag is set rather than generating an interrupt when a new sample of velocity and time is ready.

The down stream separation between the velocimeter and the microphone is converted to a delay time in clock count units using the speed of sound in the test cell and the clock frequency. This value is reduced by 256 counts so that a time window for correlation is centered at the mircophone.

When each velocity and time pair is read, the velocity is placed on a delay stack, and the time value, increased by the delay counts, is placed on a start time stack. A delay stack counter is decremented to show one less space is available on the delay stack. When the software clock matches the start time, the corresponding velocity value is removed from the delay stack, 512 counts are added to the start time to form a stop time, and this value is placed on a stop time stack. The velocity is then paired with the next 512 pressure values as they are read in the pressure interrupt routing.

8.6 VELOCITY-PESSURE CORRELATION AND HISTORGRAM GENERATION

The correlation of each velocity-pressure pair is done entirely in the pressure interrupt routine. The quantized factoring technique is utilzed to defer the actual multiplication operation. A quantized velocity, Q1, is formed as indicated in Section 8.2 and is used as a column pointer into the summing array.

The summation is done entirely within the pressure interrupt routine. In response to each pressure interrupt, the A/D value is read and a quantized pressure, Q2, is formed in a manner similar to the velocity quantizing. In this case, no subtraction of a DC level is made; since, by definition, the DC pressure level is zero.

Implied in the definition of the time window and, therefore, the start and stop times is that, at the start time $\Delta t = -256$ clock counts and at the stop time $\Delta t = +255$ clock counts. Therefore, when a velocity value is "started", Δt can be thought of as pointing to the first row in the summing array. The quantized pressure Q2 can, therefore, be summed into the first element of the column pointed to by the quantized velocity Q1.

Since each pressure interrupt will occur one clock count later, the next Q2 value will be summed into the next element of the same column which corresponds to $\Delta t = -255$. This summing process is continued until the clock time matches the stop time for this velocity value or 512 clock counts later. The pressure interrupt routine is coded to handle four of these summing and auto-indexing sequences, which are referred to as accumulators. Therefore, four different velocity values can be paired with the same pressure value. Twelve velocities may be waiting on the delay stack.

When a velocity is "started", it is removed from the delay stack and the delay stack counter is incremented to indicate an available location for a new velocity. A check is made to see if an accumulator is available. If all accumulators are in use, the velocity value is discarded. However, if an accumulator is available, the quantized velocity, Q1, is used to increment the velocity histogram as described in Section 8.3, the stop time is calculated and stored on the stop stack, and the processing counter is incremented. This is the counter that is used to halt processing when 20,000 or 30,000 points have been processed. The accumulator chosen is loaded with the Q1 value and enabled so that during the next 512 pressure interrupts it will be active.

When the clock value matches a stop time, the corresponding accumulator is turned off and the last quantized pressure value is used to increment the pressure histogram.

External clock overflows generate an interrupt which causes the software clock to be reset to zero. To prevent this from happening while any accumulator is running, a velocity value will never be put on a delay stack if the delay time plus the accumulated time will exceed the remaining time in the current clock cycle.

8.7 DATA COMPRESSION AND DISPLAY

The compression of the summing array to a double precision vector containing $\Sigma Q1*ZQ2$ is accomplished as described in Section 8.4 for the INJET/INJET program. An additional step is introduced so that the sum of $Q1^2*Q2$ is formed for each lag value.

The remainder of the calculations and display generations is essentially identical to the procedure described for the INJET/INJET program.

9.0 EXPERIMENTAL ARRANGEMENTS USED FOR LASER VELOCIMETER MEASUREMENTS - GENERAL ELECTRIC ANECHOIC JET NOISE FACILITY

This section contains a brief sketch of the physical experimental arrangement of General Electric Laser Velocimeter system as configured for the Anechoic Jet Noise Test Facility.

The nozzle under test and two LV systems are similar to what is shown in Figures 9-1 and 9-2. The laser beams are highlighted above the nozzle by nature of the seeding. In the right of Figure 9-1 the two-velocimeter package may be seen mounted on its main-three-axis (X-Y-Z) actuator. The LV to the right is installed on an independently operated sub-three-axis (X'-Y'-Z') actuator that controls the spacing of the twin LV measurement control columns. Control and data acquisition consoles are shown in the photographs of Figures 9-3 and 9-4. The minicomputer is in the three low cabinets to the right in Figure 9-3. The keyboard input and printer is at the far right. The Mark II signal processor is in the left-hand cabinet, and the Mark III processor is on the lower shelf of the cart. This photograph was taken before equipment locations were finalized. The console of Figure 9-4 is mainly for nozzle operation, with the exception of the right-hand cabinet, that houses the LV actuator controls.

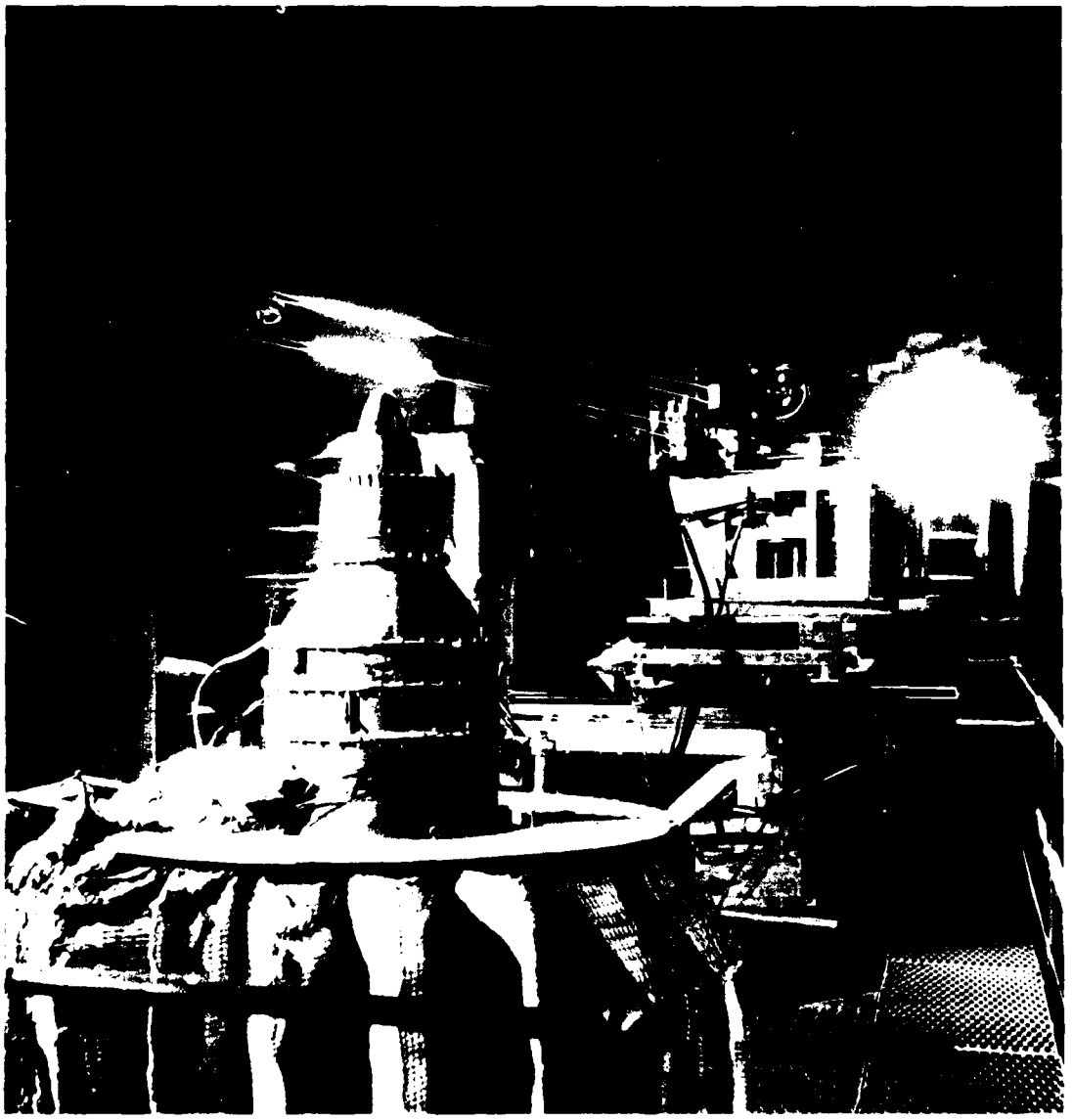

Figure 9-1. Dual Laser Velocimeter in Operation in the GE Anechoic Jet Noise Facility.

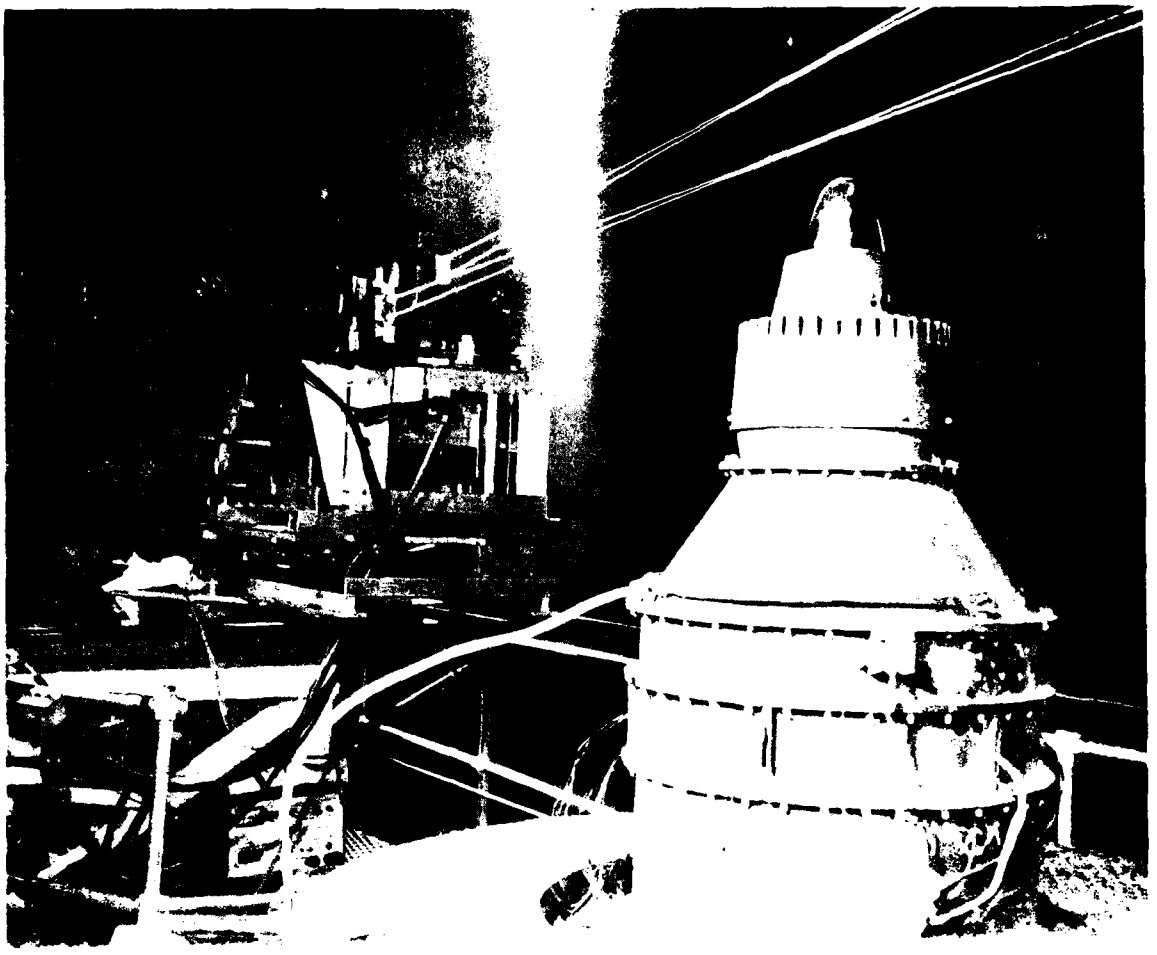

Figure 9-2. Dual Laser Velocimeter - Closeup View.

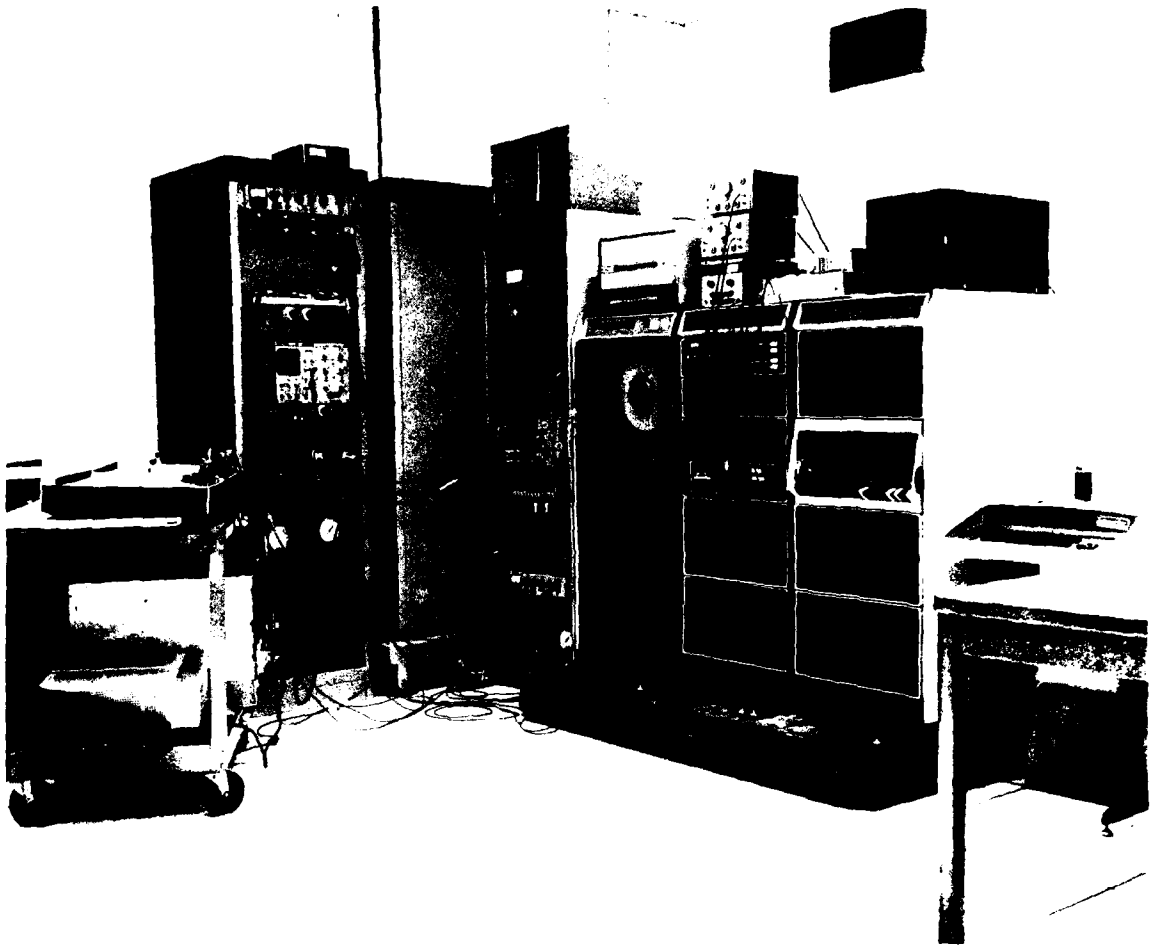

Figure 9-3. LV Control and Data Acquisition Consoles, GE Anechoic Jet Noise Facility.

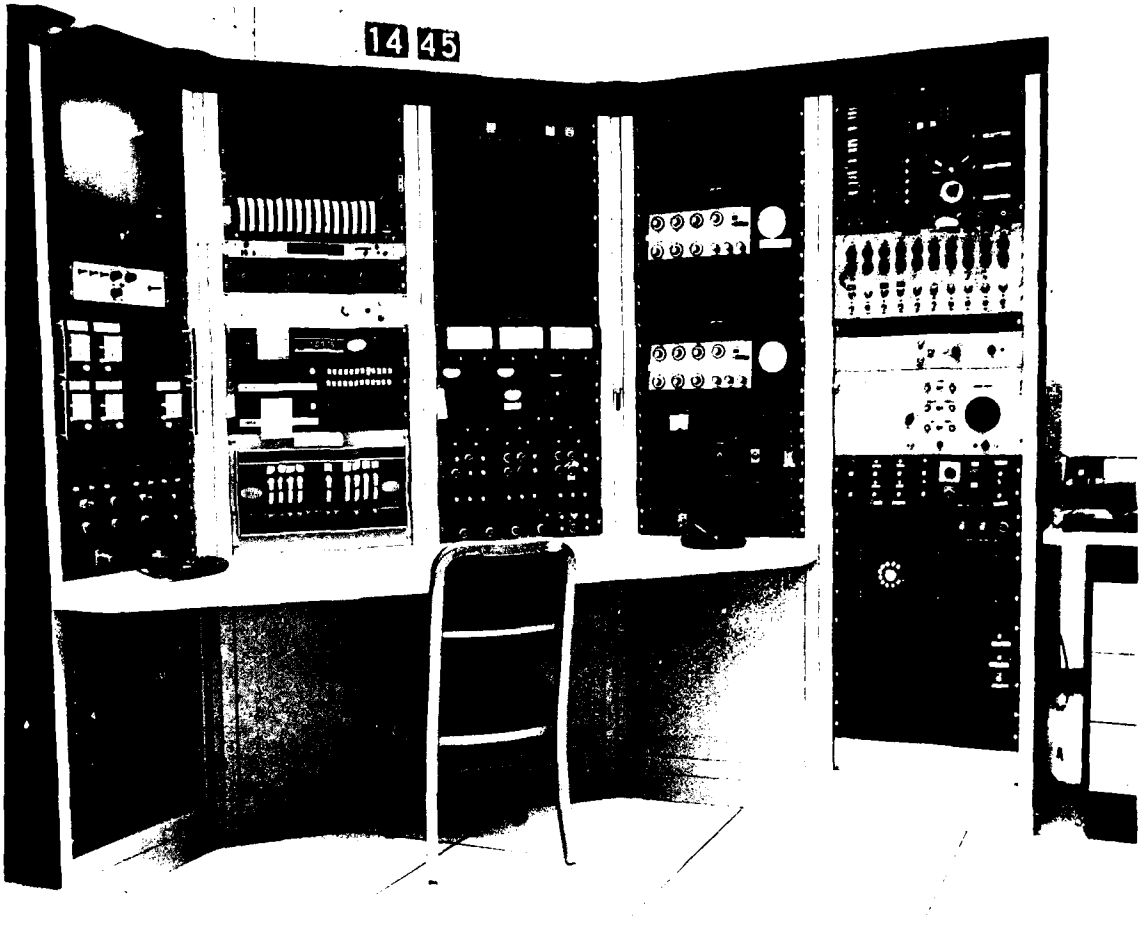

Figure 9-4. Nozzle Control Console, GE Anechoic Jet Noise Facility.

10.0 RESULTS OF MEASUREMENTS

The General Electric Laser Velocimeter system has undergone a series of electronic and automated data processing developments over the last several years. For example, within the last two years, new improvements in signal processing and data processing techniques have increased data taking capability by a factor of 90 for two-point, space-time type of measurements. Sections 3.0 through 8.0 describe many of the existing improvements and techniques necessary for performing advanced real-time measurements. References 30, 31, 50 and 51 provide some of the reference material in which has been demonstrated unique LV diagnostic capability for heated high velocity exhaust jets.

The first item discussed in this section is a summary of some highlights of previously acquired mean velocity and turbulent velocity measurements performed on heated supersonic jets and of turbulence spectra measurements. Secondly, results are presented of more recently obtained two-point, space-time, in-jet measurements; and in-jet to far-field cross-correlation measurements performed on a conic nozzle and a coannular plug nozzle.

10.1 MODEL SCALE MEAN VELOCITY AND TURBULENT VELOCITY MEASUREMENTS

The laser velocimeter measurements reported herein were made in General Electric's Jet Noise Acoustic Test Facility. Two nozzles were used in the tests: a converging-diverging nozzle producing shock-free supersonic flow, and a conical nozzle used for subsonic tests and shock structure measurements. The exit diameter of both nozzles was 6 inches.

The velocity measurements were obtained as probability density distributions and the data were reduced by using statistical techniques discussed in Sections 7.0 and 8.0 to compute the mean values and standard deviations (mean velocity and turbulent velocity), respectively. Typical mean and turbulent laser velocimeter (LV) measurements for an ambient subsonic jet are compared with hot film/hot wire measurements in Figures 10-1, a and b. LV measurements of mean velocity and turbulent velocity were then obtained for the high-temperature (1500° R), fully-expanded supersonic (M_j = 1.5) convergent-divergent

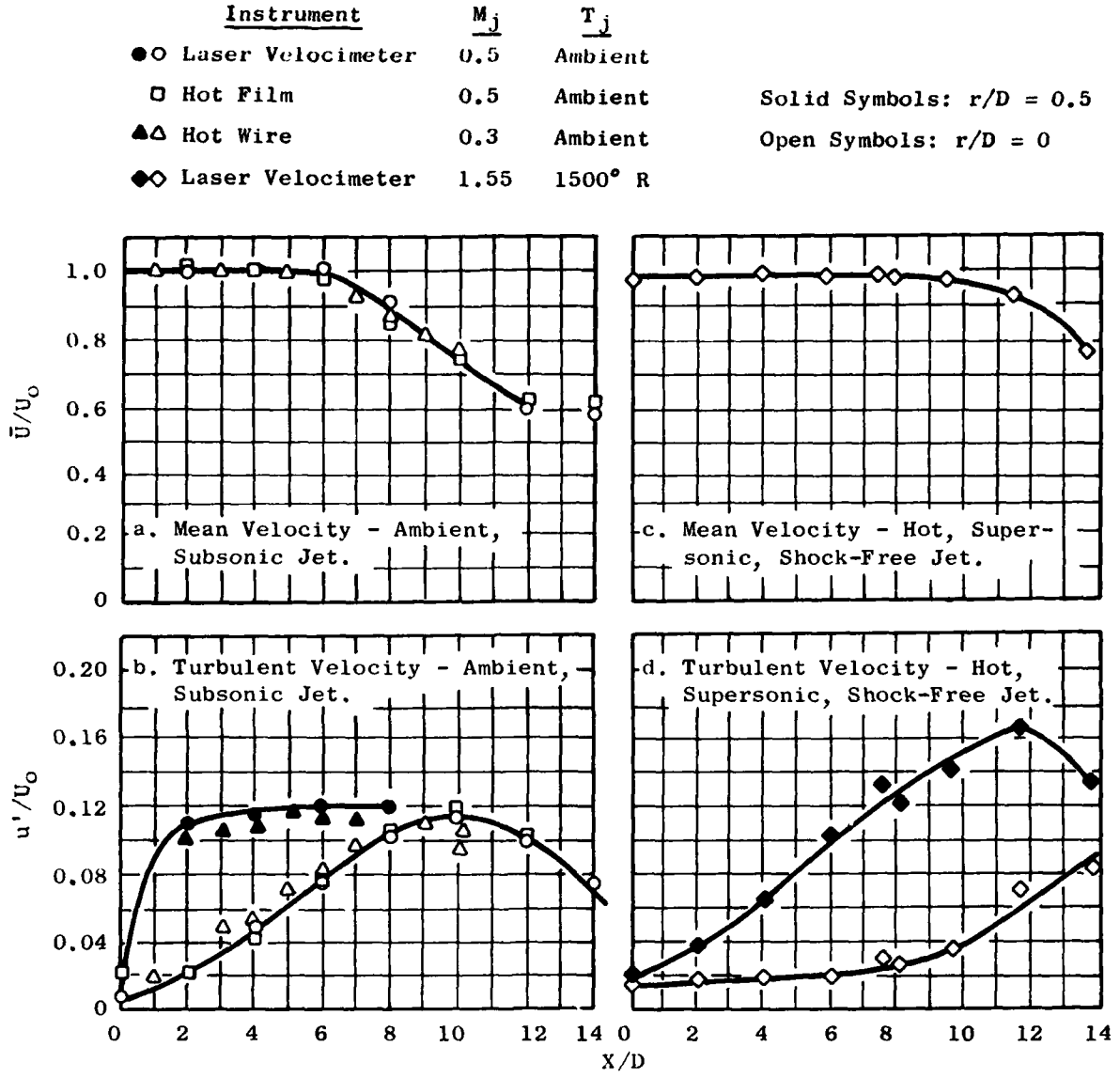

Figure 10-1. Normalized Mean Axial Velocity and Normalized Turbulent Velocity for Subsonic (Conical Nozzle) Jet and Supersonic (Convergent/ Divergent Nozzle), Shock-Free Jet.

nozzle. The results of these measurements are presented in Figures 10-1c and d. In Figures 10-1a and c, the existence of the entended potential core for the supersonic jet is evident. The differences in turbulence distributions between the subsonic and supersonic jet can be observed by comparing Figures 10-1b and d.

Further experimental measurements were obtained using the converging-diverging shock-free nozzle flow and the shocked conic nozzle flow. For both cases, the exit Mach number of the jet was 1.55 and the total temperature was 1500° R. Radial profiles of mean axial velocities were obtained for various axial locations, X, in the jets of both nozzles. The results, presented in Figures 10-2a and b, are plotted using the parameter, η, which collapses all of the data onto one curve and clearly defines the jet boundary and the shear layer at $r = r_o$. For the conic nozzle case, Figure 10-2b, the under-expansion in the jet boundary is apparent as the value of the normalized mean velocity becomes greater than 1.0 in the expansion region near the jet exit plane (X/D = 2).

Radial profiles of normalized turbulence velocity for the converging-diverging nozzle are shown in Figure 10-2c as a function of the same variable, η, (used in the previous figures) and was again used here to collapse all the profiles onto one curve. The peak turbulence (maximum shear) is clearly observed to occur at the jet boundary, $r = r_o$.

To complement the above conic nozzle measurements, a series of LV measurements was also made to define the conic nozzle shock structure. Figure 10-3 shows the measured axial mean velocity and turbulent velocity distributions along the centerline of the jet. The expansion and contraction of the axial velocity in the shock-flow region are clearly shown. For reference purposes, predicted velocity is also shown. The amplification of turbulent velocity due to the shock is also evident.

10.2 TURBULENCE SPECTRA

To construct turbulence spectra from the discontinuous output of the LV presents a difficulty not encountered with continous type instrumentation. Conventional point spectra estimate techniques assume that all values of the

a. Mean Velocity; C/D Nozzle, Shock-Free Data, M_j = 1.55, T_T = 1500° R.

b. Mean Velocity; Conical Nozzle, Shocked Data, M_j = 1.55, T_T = 1500° R.

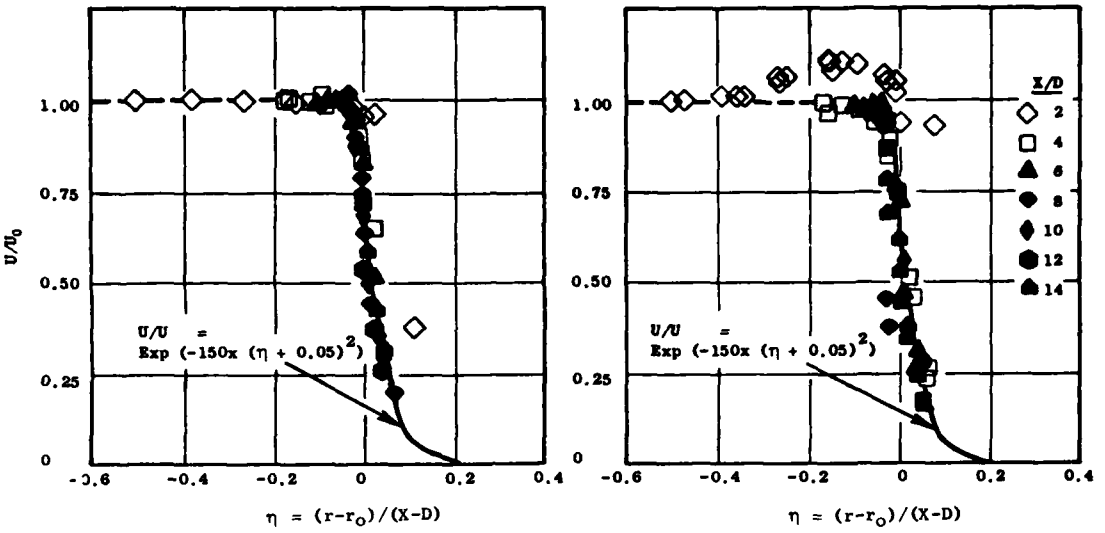

c. Turbulence Velocity; C/D Nozzle, Shock-Free Data, M_j = 1.55, T_T = 1500° R.

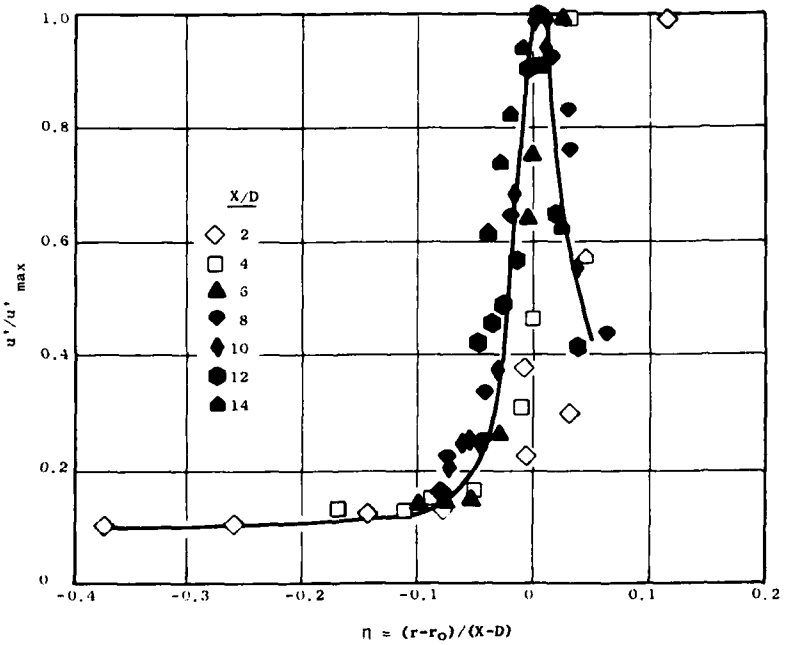

Figure 10-2. LV Measured Radial Profiles of Normalized Mean Velocity and Normalized Turbulent Velocity.

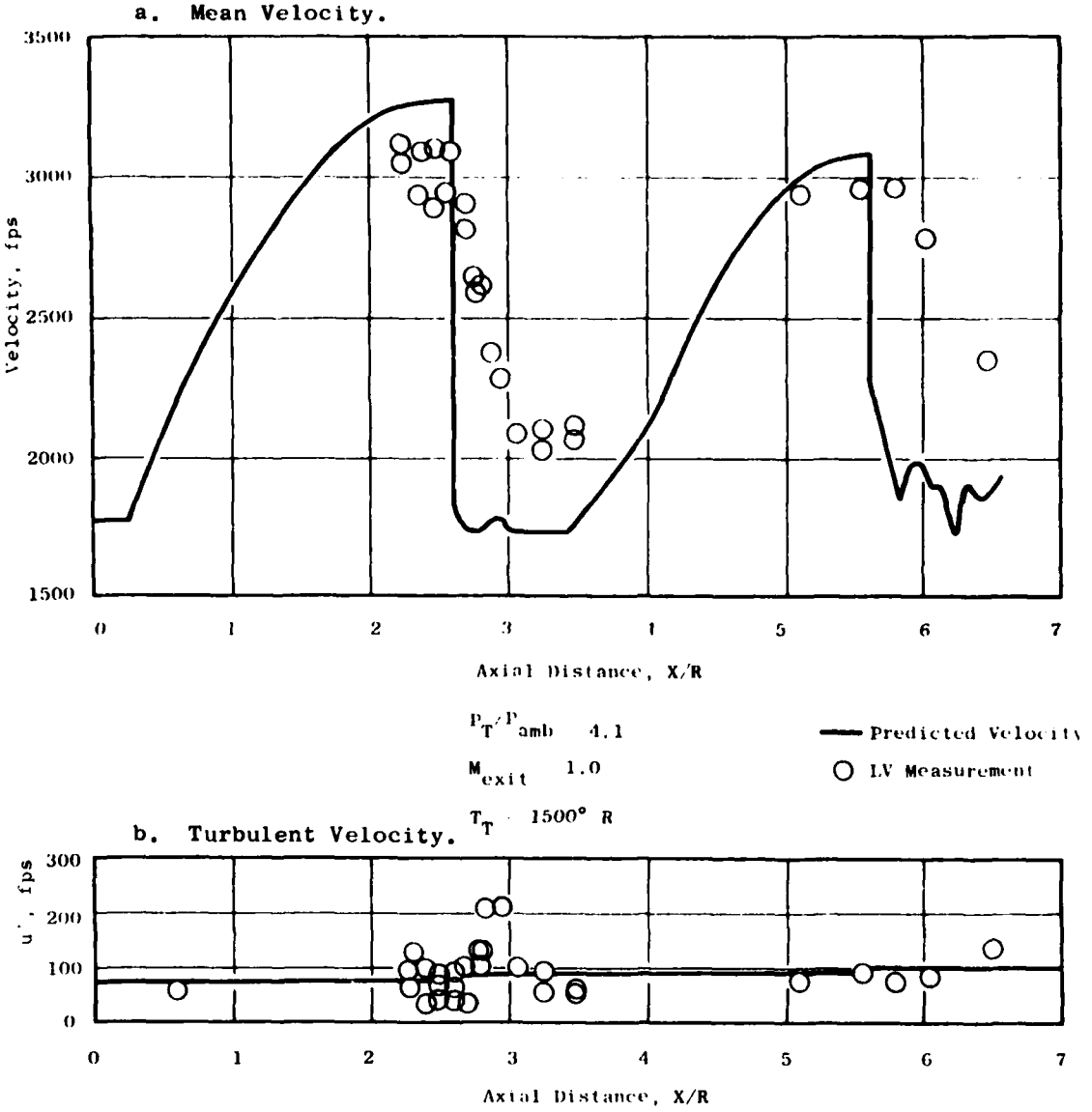

Figure 10-3. LV Measured Mean Velocity and Turbulence Intensity on Center-Line for a High Velocity, High Temperature Jet.

input signal are known in the analysis interval. Such knowledge is not available at the LV output. To overcome this problem, it was necessary to construct the autocorrelation function of the velocity signal, then obtain the spectrum as its Fourier transform. Sections 7.0 and 8.0 describe the theoretical and computational considerations for these types of measurements. Figure 10-4a shows a comparison of the LV reconstructed spectra with that using a hot film for a subsonic jet. Figure 10-4b shows the LV measured turbulent spectra for a sonic (M_j = 1.0) heated (total temperature of 1500° R) jet. These results were quite encouraging in regard to the real-time measurement studies. These results gave more confidence to pursue cross-correlation type real-time studies.

10.3 TWO-POINT, SPACE-TIME, IN-JET, CROSS-CORRELATION MEASUREMENTS

In order to develop the technology of using the laser velocimeter for performing advanced type turbulence measurements, a combination of signal processing development, theoretical analysis, computer software data processing techniques and laser velocimeter actuation equipment development was necessary. Sections 3.0 through 9.0 describe the extent of development necessary. The measurement of two-point cross correlations with a non-contact-type measuring device such as a laser velocimeter has never been performed before. The full accomplishment of such techniques will enable the measurement and location for an exhaust jet's aerodynamic noise source and will eventually lead to a new diagnostic device for evaluating and better designing exhaust nozzle suppression devices.

Discussed below are results of a series of two-point, space-time, in-jet type measurements in a conic nozzle and a coannular plug nozzle. The resultant measurements could be used in the aero-acoustic indirect models described in Section 6.0.

10.3.1 Conic Nozzle Measurements

Although all the computational schemes and algorithms for performing the two-point, space-time, cross-correlation measurements are covered in detail in Sections 7.0 and 8.0, it is instructive to briefly review the concepts here. Sketches shown in Figures 10-5a and b serve the purpose for the following

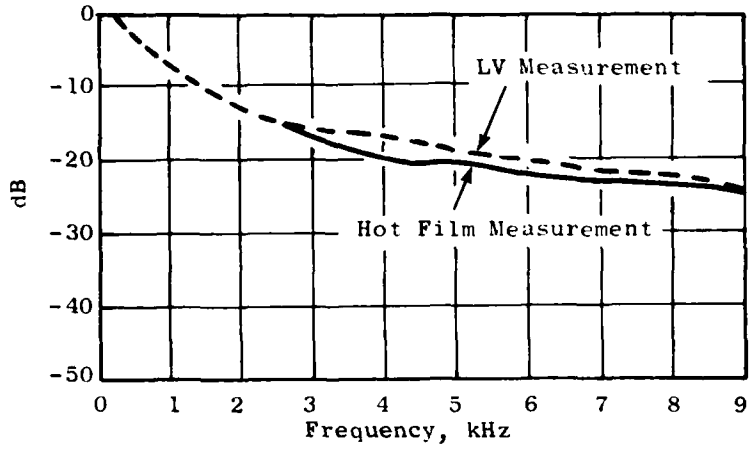

a. Comparison of Laser Velocimeter and Hot Film Turbulence Spectra.

M_j = 0.5, X/D = 6, r/r_o = 1

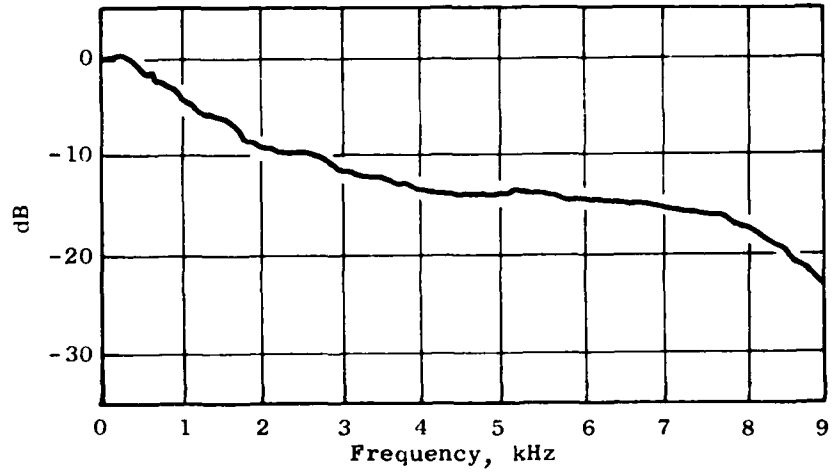

b. Measured Laser Velocimeter Turbulent Spectrum for a Hot, Sonic Jet.

M_j = 1.0, T_8 = 1500° R, X/D = 10, r/r_o = 0

Figure 10-4. LV Measured Axial Turbulent Velocity Spectra for Ambient and Heated Jets.

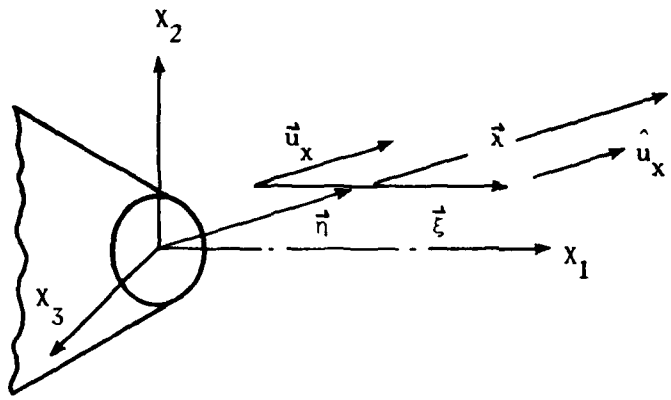

a. Coordinate System

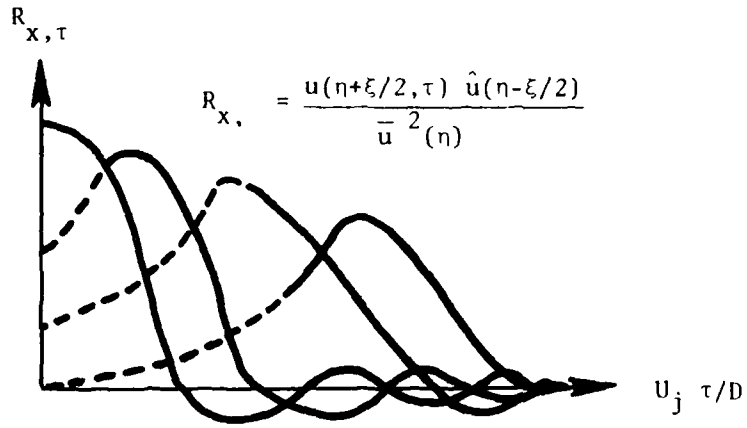

(1) $L_x, (\eta) = \int_{-\infty}^{\infty} R_{x,\tau}(\eta,\xi,0)\ d\xi$: Turbulent Length Scale

(2) Curve of ξ Vs. τ at $\frac{\partial R_{x,\tau}(\eta,\xi,\tau)}{\partial \xi_1} = 0$: Defines Convection Velocity

(3) $\int_{-\infty}^{\infty} R_{\tau,c}\ e^{i\omega\tau}\ d\tau$

b. Turbulent Properties Defined by In-Jet Two-Part Space-Correlation

Figure 10-5. Sketches Illustrating the Coordinate System and Turbulent Properties Defined by Two-Point Space-Time Cross Correlation Measurements.

discussion of results. Shown in Figure 10-5b are the concepts necessary to compute the turbulent length scale, L_x, the convection velocity, V_c, and the spectra of the moving eddy turbulence. Measurements of the turbulent structure properties were performed in General Electric Anechoic Jet Noise Test Facility described in Section 9.0. Figures 9-1 and 9-2 are photographs of the two-laser velocimeter system built for the following measurements.

For the conic nozzle measurements, two nozzle conditions were tested: Subsonic (M_j = 0.5) ambient, and sonic (M_j = 1.0) heated (T_T = 1600° R). Figure 10-6 shows a sample of six two-point, space-time, cross correlations for the subsonic ambient conic nozzle. The axial spacings for this test were ξ/D = 0, 0.25, 0.45, 0.6, 0.85 and 1.0; where ξ is the axial separation distance between the two LV control volumes, and D is the diameter of the conic nozzle (D = 4.64 inches). The ordinate on each scale is the normalized cross-correlation function, R_{xt}, while the abscissa is the normalized time scale, $\tau V_j/D$ (where τ is the time, V_j the ideal exhaust velocity). From such a series of cross-correlation measurements, the convective speed and length scale can be determined as illustrated in Figure 10-5b. Table 10-1 summarizes the results of the conic nozzle measurements.

To illustrate the computation of the convection velocity, V_c, Figure 10-7 was constructed from the test results shown on Figure 10-6. These results show that, at an axial location of 4 diameters at τ/D = 0.25, the convection velocity, V_c, is 0.723 V_j for both the ambient subsonic jet and the sonic treated jet. Summarized in Figures 10-8a and b is the LV measured axial variation of the turbulent length scale and the radial variation of convection velocity for the measurements taken. The test results shown in Figure 10-8a show that the turbulent length scales for the subsonic unheated and the sonic heated jet are much the same. There is, however, a noticeable radial variation of length scale, but it is not large. Also, the classically quoted value, L_X/D = 0.12 X/D, is at variance with the above-measured length scales, as well as some University of Toronto hot wire measurements. Instead of L_X/D = 0.12 X/D, perhaps a more representative equation would be L_X/D = 0.03 X/D.

The radial variation of convection velocity for the subsonic unheated and the sonic heated jet measurements are summarized in Figure 10-8b. These

Table 10-1. Summary of Turbulent Properties Measured on a Conical Nozzle.

a. Subsonic Ambient Conical Nozzle Test Results (M_j = 0.5; Total Temperature = 519° R)

X/D	r/D	$\bar{V}$, fps	$U'/\bar{V}$	V_c/V_j	Lx/D	Lx, in.
4	0	531.4	0.043	0.75	0.057	0.26
	0.25	516.3	0.11	0.723	0.091	0.42
	0.5	152	0.471	0.414	0.172	0.8
8	0	485.3	0.132	0.809	0.211	0.98
	0.25	390.0	0.215	0.580	0.223	1.03
14	0	304.9	0.195	0.487	0.396	1.84

b. Sonic Heated Conical Nozzle Test Results ($M_j \simeq 1.0$; Total Temperature ≈ 1600° R)

X/D	r/D	$\bar{V}$	$U'/\bar{V}$	V_c/V_j	Lx/D	Lx, in.
4	0	1739.7	0.048	0.74	0.0428	0.2
	0.25	1511.2	0.10	0.797	0.0934	0.43

where:
- X = Axial location measured from the jet centerline
- r = Radial location measured from the jet centerline
- V_c = Measured turbulent convective speed
- $\bar{V}$ = Measured local mean velocity
- V_j = Ideally expanded jet velocity
- U' = Measured axial turbulent velocity
- $U'/\bar{V}$ = Local turbulence intensity

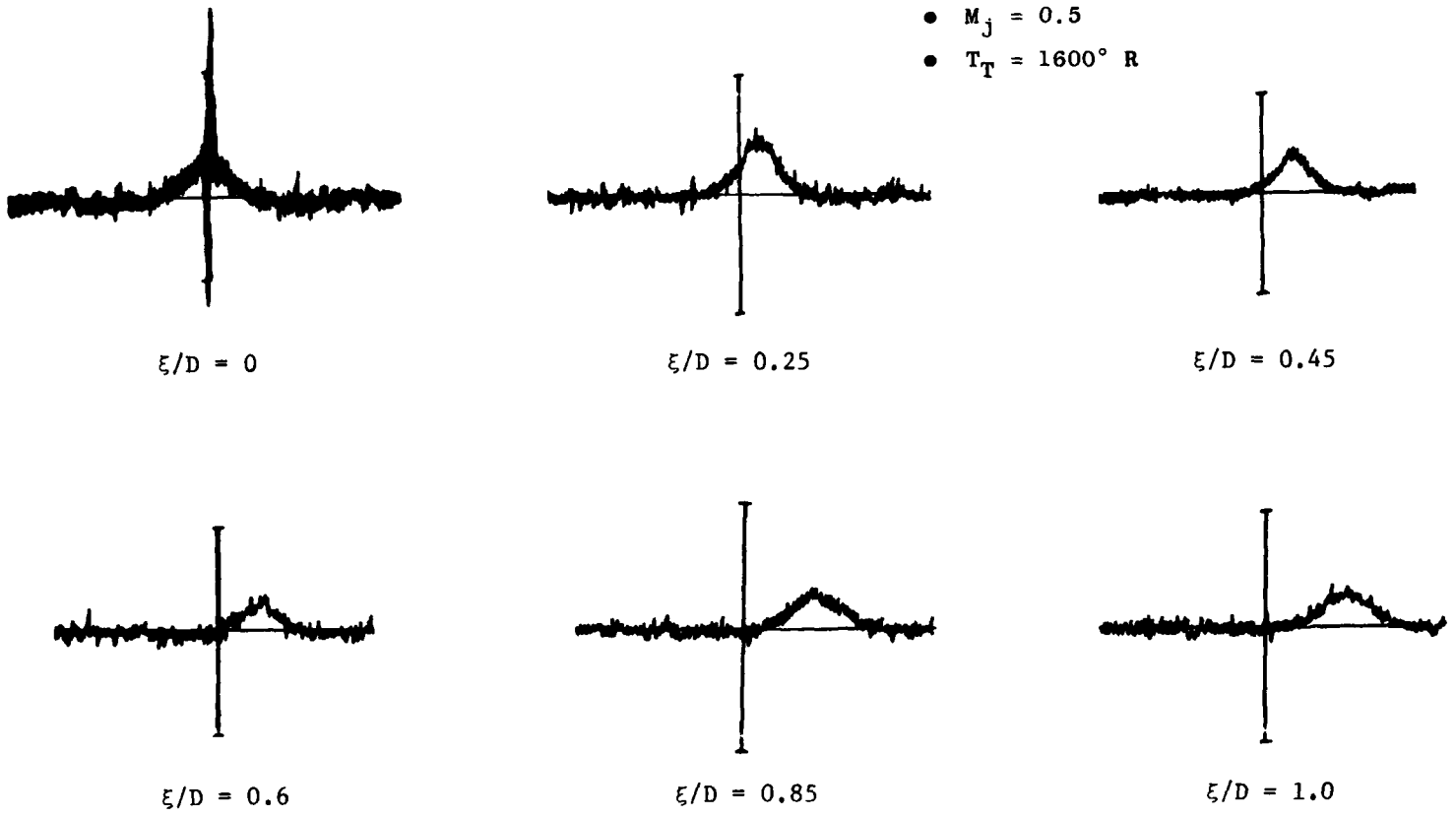

Figure 10-6. LV Measured Two-Point Cross Correlation for a Range of Axial Separation Distances for a Conical Nozzle.

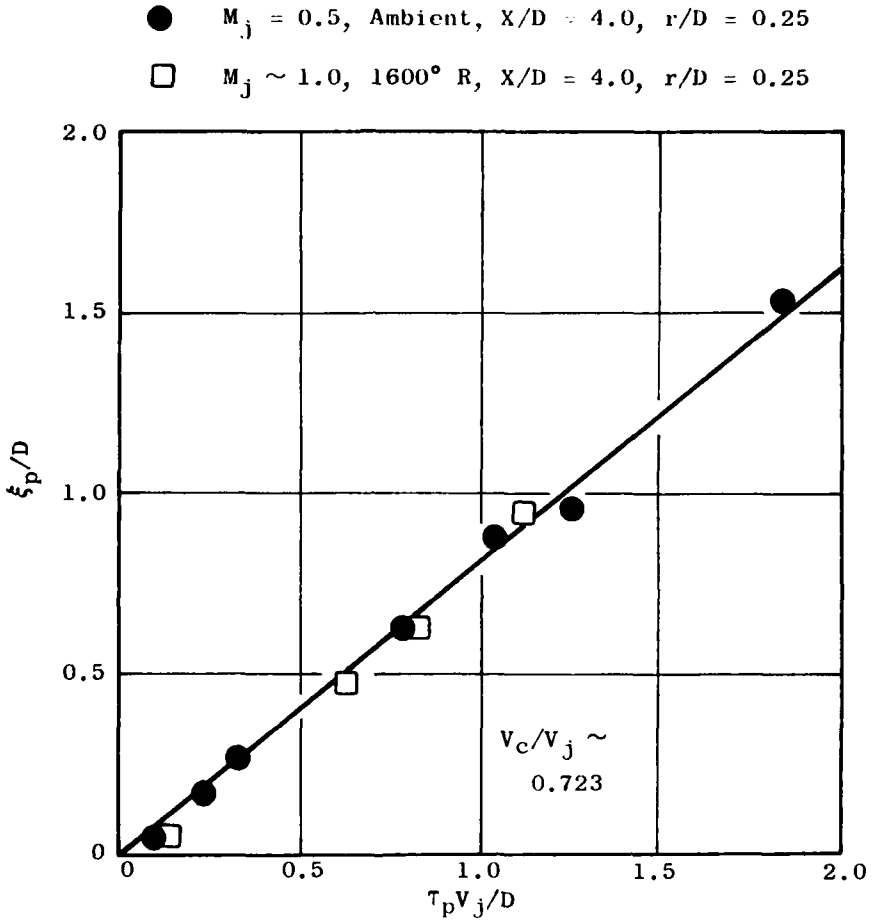

Figure 10-7. Illustration of Method for Determining Convective Results of the Two-Point Space-Time Cross Correlations.

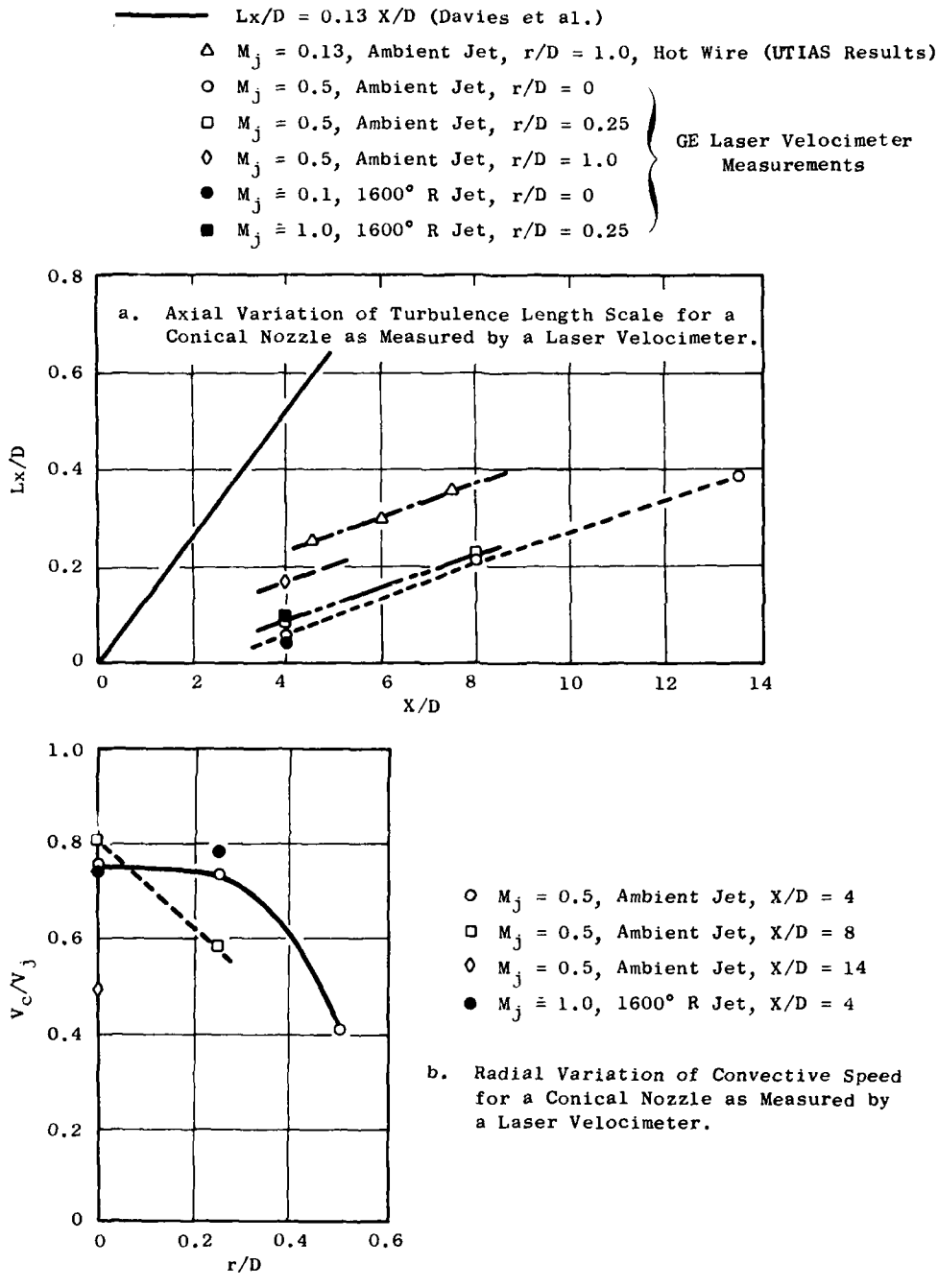

Figure 10-8. LV Turbulent Structure Measurements for a Conical Nozzle.

results show that unheated and heated convective speeds are similar in value, but there does exist an axial and radial variation in value throughout the exhaust jet.

10.3.2 Coannular Plug Nozzle Test Results*

A second series of two-point, space-time measurements were performed on a second nozzle to explore the type of phenomenon and problems that are encountered with nozzle systems that are different than the simple conic nozzle. The second nozzle selected was a coannular plug nozzle configuration illustrated in Figure 10-9. Also shown on Figure 10-9 are the two nozzle test conditions for which the cross-correlation measurements were performed. The coannular plug nozzle tested was a high radius ratio ($R_r^o = 0.85$), low area ratio ($A_r^i = 0.33$) nozzle tested acoustically under Contract NAS3-19777. This particular nozzle has been found to exhibit favorable jet acoustic reduction characteristics relative to a conic nozzle at an equivalent specific thrust. The test conditions chosen were such that, for the first test point, the outer and inner streams were slightly less than critical; for the second test point, the inner stream was maintained at the same conditions as for test point 1, but the outer stream was raised to a super critical pressure ratio. Table 10-2 summarizes the results of all the two-point, space-time measurements taken for this test series.

For this coannular plug nozzle, in-jet, cross-correlations were generally taken at three radial locations for each axial station**. The locations were chosen so as to take measurements at the nozzle exhaust centerline, at the peak velocity location and at a radial location where the local mean velocity

---

* Note that there was a year lapse in time between the conic nozzle measurements (performed in August 1976), and the coannular plug nozzle measurements (performed in August 1977). During that interval, improvements in the data acquisition and process were made. Data acquisition and reduction were improved by a factor of 90.

** Note that at each measurement station (x,r), several axial and separations of the two LVs are required in order to form the manifold of cross-correlations depicted in Figure 10-5b. In general, the separation distances used were $\varepsilon/Deq = 0.04, 0.22, 0.39, 0.57, 0.74, 0.92, 1.09, 1.27$. Thus, for each location, approximately seven cross-correlation measurements were made.

a. Sketch of Coannular Plug Nozzle.

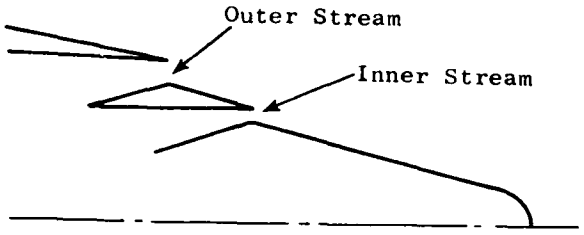

- Test Nozzle from NAS3-19777
- The Outer Stream Nozzle Radius Ratio, $R_r^o = 0.85$
- Inner Stream to Outer Stream Area Ratio, $A_r^i = 0.33$
- Outer Stream Annulus Height, $h^o = 0.675$ inches
- Inner Stream Annulus Height, $h^i = 0.311$ inches
- Outer Stream Area, $A^o = 18.049$ in.^{2}
- Total Area, $A_T = 23.927$ in.^{2}
- Equivalent Diameter, $D_{eq} = 5.519$ inches

b. Nozzle Test Conditions.

Point	P_r^o	T_T^o, ° R	V_j^o, fps	$\dot{W}^o$, lb/sec	P_r^i	T_T^i, ° R	V_j^i, fps	$\dot{W}^o$, lb/sec	$\dot{W}_T$, lb/sec	V_j^{mix}, fps
1	1.8	1650	1758	6.1	1.8	850	1250	2.7	8.8	1602
2	2.7	1650	2216	8.4	1.8	850	1250	2.7	11.1	1981

Where: V_j^{mix} = Mixed Stream Velocity: $V_j^{mix} = (V_j^o \dot{W}^o + V_j^i \dot{W}^i)/\dot{W}_T$

V_j = Ideally Expanded Jet Velocity

$\dot{W}$ = Weight Flow

P_r = Reservoir to Ambient Pressure Ratio

T_T = Total Temperature

o (Superscript) = Outer Stream Property

i (Superscript) = Inner Stream Property

Figure 10-9. Coannular Plug Nozzle and Test Conditions for LV Measured Cross Correlations.

Table 10-2. Summary of Turbulent Structure Properties Measured on a Coannular Plug Nozzle.

a. Test Point 1 (P_r^o = 1.8, T_T^o = 1650° R, V_j^o = 1758 fps, p_r^i = 1.8, T_T^i = 850° R, V_j^i = 1250 fps, V_j^{mix} = 1602 fps)

X/Deq	r/Deq	$\bar{U}$, fps	U', fps	V_c, fps	Lx, in.	V_c/V_j^{mix}	Lx/Deq
1.81	0.460	1760.0	96.84	1587.6	0.0495	0.991	0.0089
2.54	0.172	1225.2	63.71	1227.1	0.0288	0.766	0.00522
	0.241	1370.9	116.53	1297.6	0.1765	0.810	0.03199
	0.378	1758.9	91.46	1754.2	0.1715	1.095	0.03107
4.71	0	1098.3	121.9	901.9	0.2098	0.563	0.038
	0.329	1606.3	168.66	1510.7	0.3512	0.943	0.0636
	0.546	1082.3	284.6	858.7	0.5817	0.536	0.1054
8.15	0	1228.0	136.3	1115.0	1.0089	0.696	0.1828
	0.409	1117.8	271.6	842.6	1.1728	0.526	0.2125
	0.567	879.5	226.03	765.8	1.5775	0.478	0.2822
9.97	0.181	1145.7	221.1	954.8	1.3886	0.596	0.2516
	0.444	1025.8	245.2	746.5	1.4421	0.466	0.2613
	0.631	816.0	246.4	730.5	1.7545	0.456	0.3179

b. Test Point 2 (P_r^o = 2.7, T_T^o = 1650° R, V_j^o = 2216 fps, p_r^i = 1.8, T_T^i = 850° R, V_j^i = 1250 fps, V_j^{mix} = 1981 fps)

X/Deq	r/Deq	$\bar{U}$, fps	U', fps	V_c, fps	Lx, in.	V_c/V_j^{mix}	Lx/Deq
2.54	0	608.4	119.8	1010.0	0.212	0.510	0.03845
	0.529	1419.6	359.0	1010.0	0.128	0.510	0.02313
	0.572	981.9	387.0	1021.0	0.283	0.515	0.05135
4.71	0	1038.8	133.9	1295.0	0.294	0.654	0.05334
	0.399	2024.1	151.8	2009.0	0.272	1.014	0.04924
	0.546	1704.2	313.6	1088.0	0.687	0.549	0.1245
8.15	0	1255.8	251.2	1338.0	0.4649	0.675	0.08423
	0.314	1456.2	262.1	1403.0	0.9774	0.708	0.1771
	0.634	856.11	290.3	1887.0	1.5105	0.445	0.2737
9.97	0	1265.3	270.8	1271.0	1.2423	0.642	0.2251

was approximately 70% of the peak velocity. Figure 10-10 illustrates the typical mean velocity profiles for test point 1. Illustrated in this figure is the inverted velocity distribution (high velocity on the outside stream and lower velocity on the inside stream) typical of this type of test nozzle. Also shown on this figure are the approximate locations for the cross-correlation measurements.

Choosing the proper normalization or similitude parameters for the coannular plug nozzle is not as easily done as for the conic nozzle. For the coannular plug nozzle, there are two flow streams issuing through annular gaps. For the turbulent length scale, the outer stream annulus height, h^o, was chosen as the length scale characteristic dimension. For the convection velocity, V_c, normalization, the ideal outer stream velocity V_j^o was used for locations X/Deq < 5, r/Deq ≠ 0; at r/Deq ~ 0, the inner stream velocity, V_j, was the normalizing velocity used at X/Deq < 5; and the specific thrust, V_j^{mix}, was the normalizing velocity used when X/Deq < 5. Figures 10-11 and 10-12 summarize the in-jet, cross-correlation turbulence structure measurements taken to date.

Figure 10-11 illustrates the axial variation of the LV measured turbulent length scale for the coannular plug nozzle at three streamlike locations: region of peak velocity, 70% of Local $\bar{U}_{max}$, and along the centerline of the nozzle.

The physical picture which emerges from these measurements is the length scale of the convecting eddies are smallest along the centerline, largest at the 70% $\bar{U}_{max}$ stream line and intermediate in length along the $\bar{U}_{max}$ stream line.

Figures 10-12a and b illustrate the convective speeds for the two coannular plug nozzle test conditions. The physical picture illustrated by these results is not clear. In general, it might be postulated that the larger eddies moving at the 70% $\bar{U}_{max}$ stream lines are convecting at the slowest speed (V_c ~ 0.4 → 0.66 V_j^{CH}, while the smaller eddies moving along the centerline and at $\bar{U}_{max}$ are moving along at a faster rate relative to the chosen characteristic velocity (V_c ~ 0.4 → 1.0 V_j^{CH}), with the higher convection speeds occurring closer to the nozzle (X/Deq < 5). One conclusion which can

Test Point 1: $P_r^o = 1.8$, $T_T^o = 1650°$ R, $V_j^o = 1758$ fps, $P_r^i = 1.8$, $T_T^i = 850°$ R, $V_j^i = 1250$ fps,

$D_{eq} = 5.519$ in.

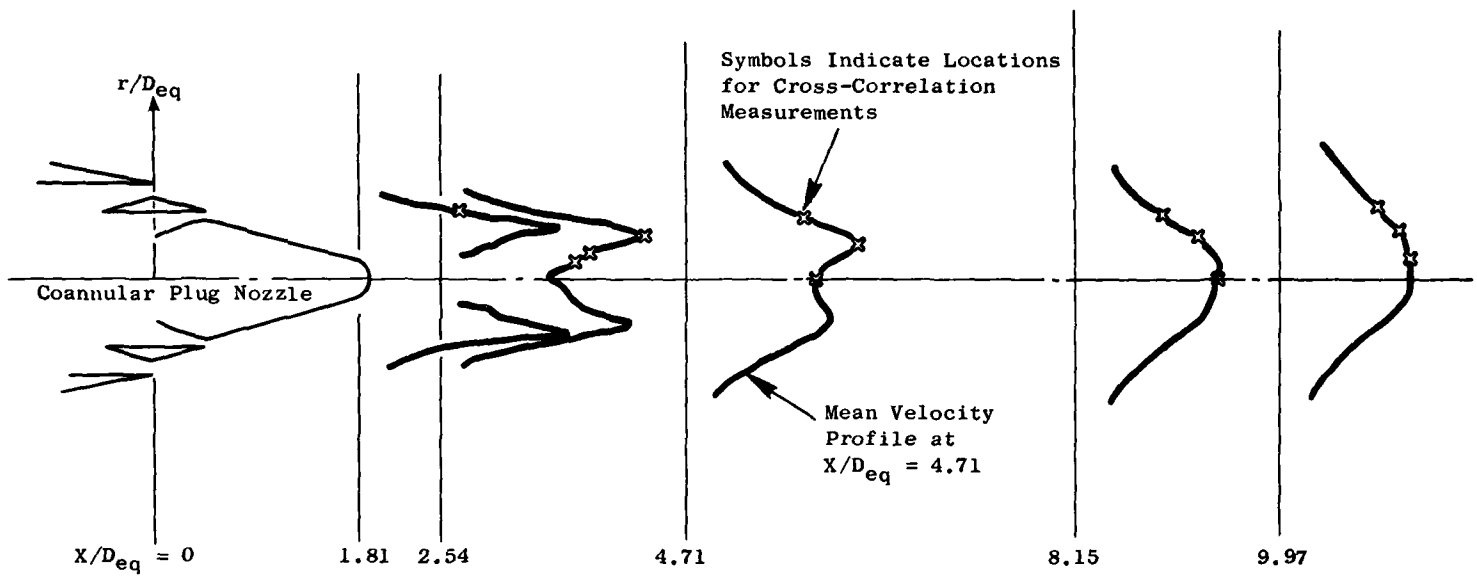

Figure 10-10. LV Measured Mean Velocity Flow Field for Test Point 1 In-Jet Cross Correlations.

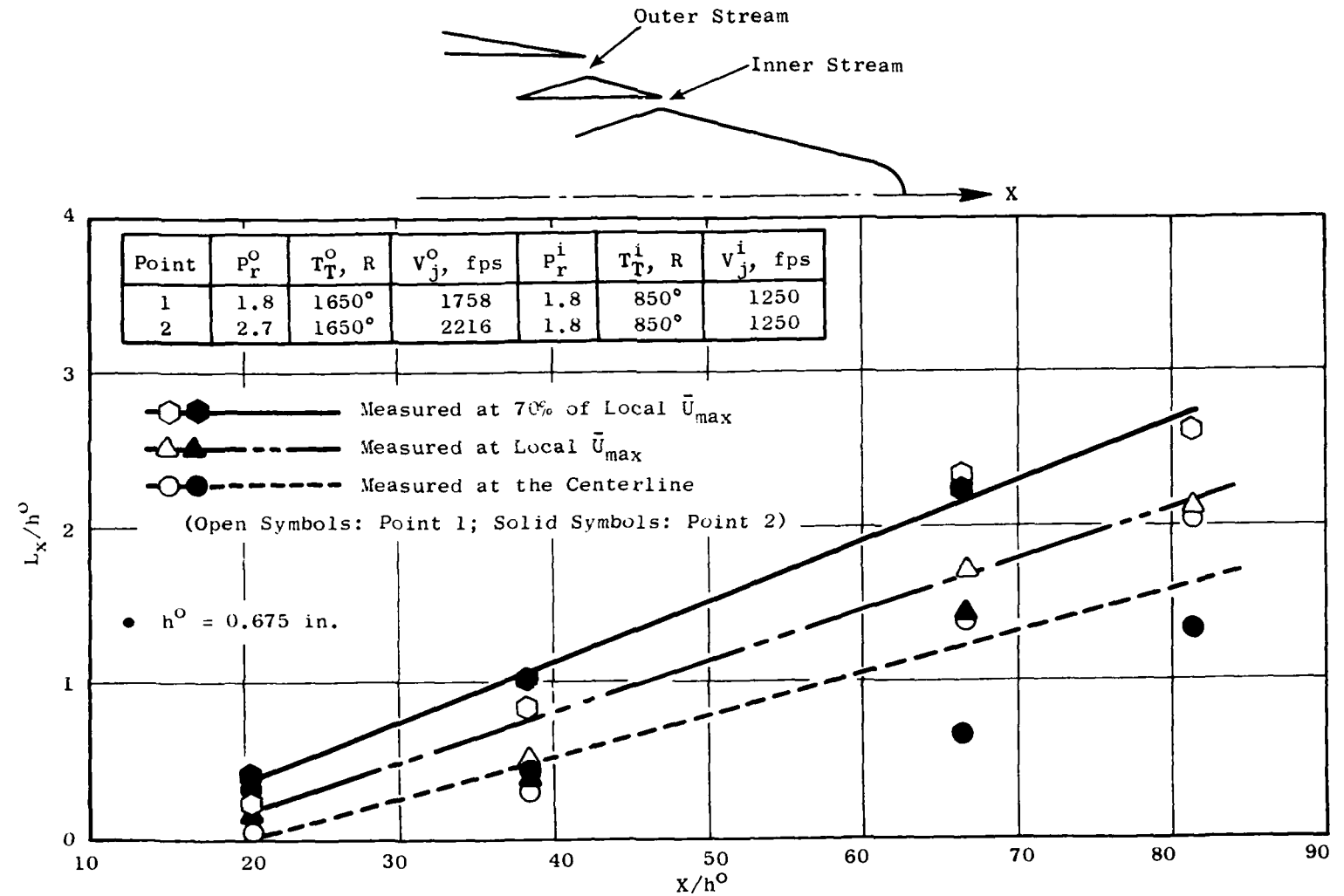

Figure 10-11. Axial Variation of LV Measured Turbulent Length Scale for a Coannular Plug Nozzle.

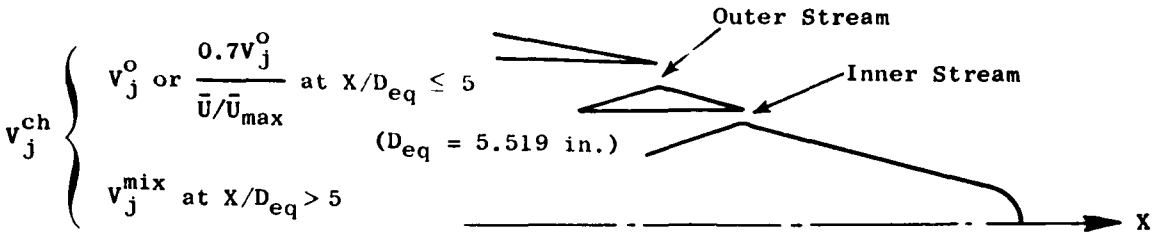

Point	P_r^o	T_T^o, R	V_j^o, fps	P_r^i	T_T^i, R	V_j^i, fps
1	1.8	1650°	1758	1.8	850°	1250
2	2.7	1650°	2216	1.8	850°	1250

Measured at 70% of Local $\bar{U}_{max}$

Measured at Local $\bar{U}_{max}$

Measured at the Centerline

(Open Symbols: Point 1; Solid Symbols: Point 2)

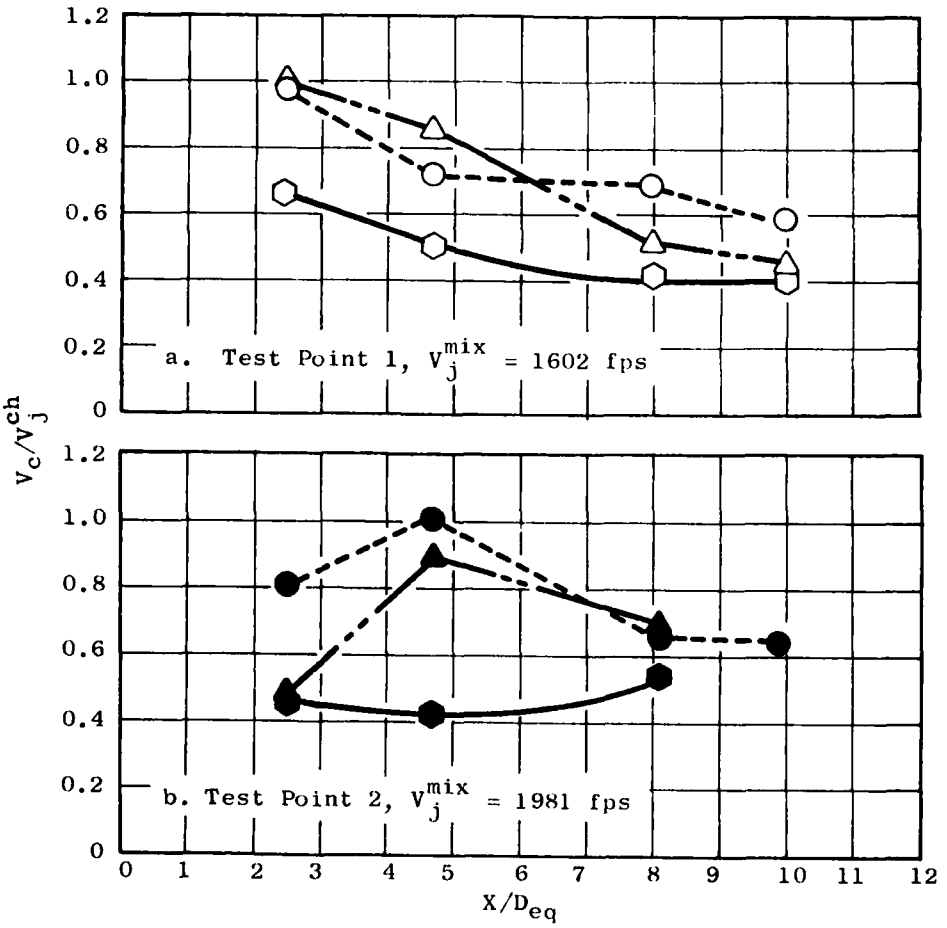

Figure 10-12. Variation of LV Measured Convection Velocity for a Coannular Plug Nozzle at High Velocity and Temperature Conditions.

be drawn, by comparing the conic nozzle data shown on Figure 10-9b to that of the coannular plug nozzle with inverted velocity profiles, is that the convection speeds downstream of the nozzle (X/Deq > 5) are higher for the conic nozzle than for the coannular plug nozzle. Acoustically, this implies that the low frequency jet noise has equivalently less convection amplification and fluid shielding (both phenomena are strong functions of convection velocity).

The relative turbulent length scales between the conic nozzle and the coannular plug nozzle are roughly the same for equivalent X/D (compare tables of Lx in Tables 10-1 and 10-2). Smaller eddies are close to the nozzle and larger eddies are downstream (high frequency noise close to nozzle exit and lower frequency noise downstream).

10.4 TWO-POINT, SPACE-TIME, IN-JET TO FAR-FIELD, CROSS-CORRELATION MEASUREMENTS

During the same test period in which the two-point, space-time, in-jet/in-jet measurements were performed on the coannular plug nozzle, a series of in-jet velocity to far-field acoustic cross-correlations was also performed with the LV system. The primary purposes of this series of experiments were to:

1. Identify any strongly correlated regions of the jet in a qualitative manner.

2. Evaluate the use of this technique as a potential diagnostic tool.

The general test arrangement for the laser velocimeter was the same as used for the in-jet/in-jet measurements described above (and described in Section 9.0), but for these measurements only one laser was used. The microphone used during the experiments was usually the microphone at 20° to the jet axis*. A sketch of the test arrangement in the Anechoic Facility is shown on Figure 10-13.

*Note that to perform the in-jet to far-field acoustic correlations precisely, the velocity vector in the direction of the microphone (as described in Section 6.0) is required. For the current measurements, the LV control volume was set to measure only the axial velocity component. For the purpose of these experiments, this alignment variation with respect to θ_i = 20° was not considered serious and the results obtained are considered to be representative.

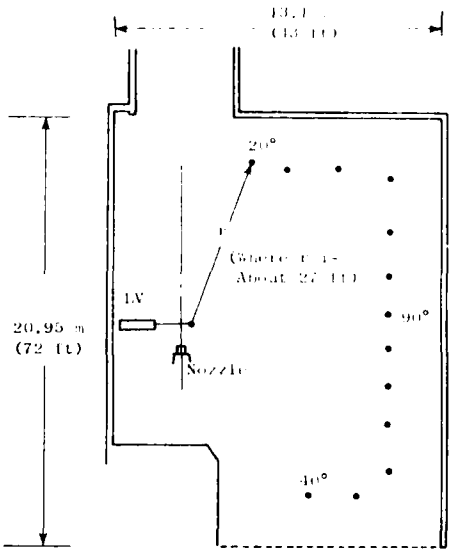

a. Sketch of LV In-Jet Velocity to Far-Field Acoustic Microphone Measurement Test Setup in the GE Jet Noise Anechoic Test Facility.

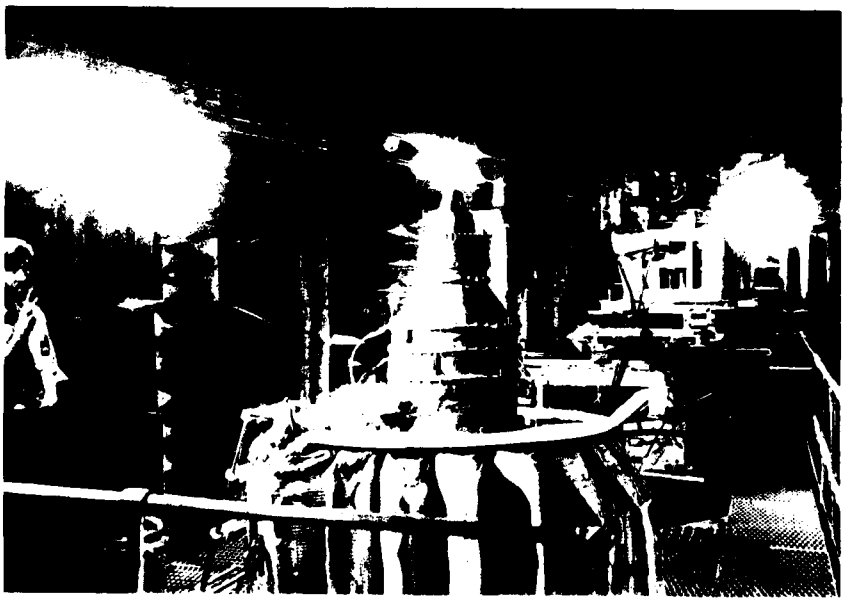

b. Photograph of the General Electric Two-Laser System in the GE Anechoic Jet Noise Test Facility.

Figure 10-13. General Test Arrangement for In-Jet to Far-Field Acoustic Cross-Correlation Measurements.

The test conditions for performing the in-jet turbulent velocity to far-field acoustic cross-correlation measurements with the laser velocimeter were the same test conditions as set for the in-jet/in-jet velocity cross-correlation measurements described above (Section 10-3, see Figure 10-9):

Point	P_r^o	T_T^o, ° R	V_j^o, fps	P_r^i	T_T^i, ° R	V_j^i, fps
1	1.8	1650	1758	1.8	850	1250
2	2.7	1650	2216	1.8	850	1250

That is, the test conditions were for a high velocity and high temperature coannular plug nozzle with inverted velocity and temperature flow streams. A summary of some of the major results is contained in Table 10-3.

Contained in Table 10-3 are the maximum values of the normalizer total cross correlation coefficient, R_{up}'; the shear portion, R_{shear}; and the self-portion, R_{self}, of the total correlation function; the peak frequency, fp, of the power spectrum of R_T, and the maximum of the second derivative of R_T (near $\tau = \tau_0$). This laser velocimeter measured data are for axial and radial point locations that were nearly the same as were taken for the turbulent structure measurements discussed in Section 10.3 above. Figure 10-14 illustrates the measurement locations on the laser velocimeter measured mean velocity flow profiles for test point 2.

An example of a series of the LV to far-field acoustic cross-correlation measurements is shown in Figures 10-15a through g. The data shown in Figure 10-15 are for test point 1 at X/Deq = 9.97, r/Deq = 0 (the Appendix shows the radial distribution of cross-correlations also found for this case). Figures 10-15a and b show the cross-correlation functions for the shear and the self-noise portions of the total cross-correlation function. Figures 10-15c and d shown the total cross-correlation function and the second derivative of the total cross-correlation functions. Figures 10-15e and f are the laser velocimeter measured power spectra of the total cross-correlation function and the second derivative of the total cross-correlation function.

Table 10-3. Summary of In-Jet LV to Far-Field Acoustic Cross-Correlation Measurements for a Coannular Plug Nozzle.

a. Test Point 1 (P_r^o = 1.8, T_T^o = 1650°R, V_j^o = 1758 fps, P_r^i = 1.8, T_T^i = 850°R, V_j^i = 1250 fps, V_j^{mix} = 1602 fps)

X/Deq	r/Deq	θ_I	R_{Total}	R_{Shear}	R_{self}	f_p, kHz	D^2_{max}, $\frac{\mu\ bar - ft^2}{sec^4}$
1.812	.58	160	.015	.015	.001	--	--
2.537	.172	160	.05	.05	.001	.92	1.8×10^{14}
	.241	160	.046	.046	.001	.92	3.8×10^{14}
	.379	160	.052	.052	--	.833	-3.4×10^{14}
4.71	0	160	.155	.148	.011	.667	3.1×10^{14}
	.329	160	.103	.104	.001	.667	1.4×10^{15}
	.546	160	.042	.038	.006	.500	-5.7×10^{14}
8.154	0	160	.222	.223	.003	.583	3.8×10^{14}
	.408	160	.081	.078	.003	.333	3.4×10^{14}
	.567	160	.045	.043	.006	.583	1.4×10^{14}
9.96	.181	160	.140	.141	.003	.317	1.3×10^{14}
	.444	160	.078	.076	.002	.317	1.1×10^{14}
	.631	160	.050	.045	.006	.500	2.4×10^{14}
11.78	0	160	.153	.150	.004	.250	2.2×10^{14}

b. Test Point 2 (P_r^o = 2.7, T_T^o = 1650°R, V_j^o = 2216 fps, P_r^i = 1.8, T_T^i = 850°R, V_j^i = 1250 fps, V_j^{mix} = 1981 fps)

X/Deq	r/Deq	θ_I	T_{Total}	R_{shear}	R_{self}	f_p, kHz	D^2_{max}, $\frac{\mu\ bar - ft^2}{sec^4}$
2.54	0	160	.028	.026	.002	--	--
	.415	160	.024	.025	.001	1	3.6×10^{14}
	.529	160	.039	.038	.002	1.33	-6.0×10^{14}
	.573	160	.027	.027	.002	1.0	-3.6×10^{14}
4.71	0	160	.090	.091	.001	.875	-1.1×10^{15}
	.406	160	.129	.132	.004	1.08	-7.2×10^{15}
	.573	160	.065	.066	.005	1.00	-2.6×10^{15}
8.15	0	160	.161	.161	.004	.708	-1.2×10^{15}
	.314	160	.176	.181	.006	.667	8.9×10^{14}
	.634	160	.092	.086	.009	.667	5.8×10^{14}
	.743	160	.013	.013	.003	--	
9.97	0	160	.261	.272	.010	.500	3.2×10^{15}
	.246	160	.238	.250	.012	.375	-2.7×10^{15}
	.246	130	.064	.066	.003	.375	-4.6×10^{14}
	.661	160	.065	.058	.007	.417	1.2×10^{15}
11.78	0	160	.195	.197	.006	.325	9.1×10^{14}

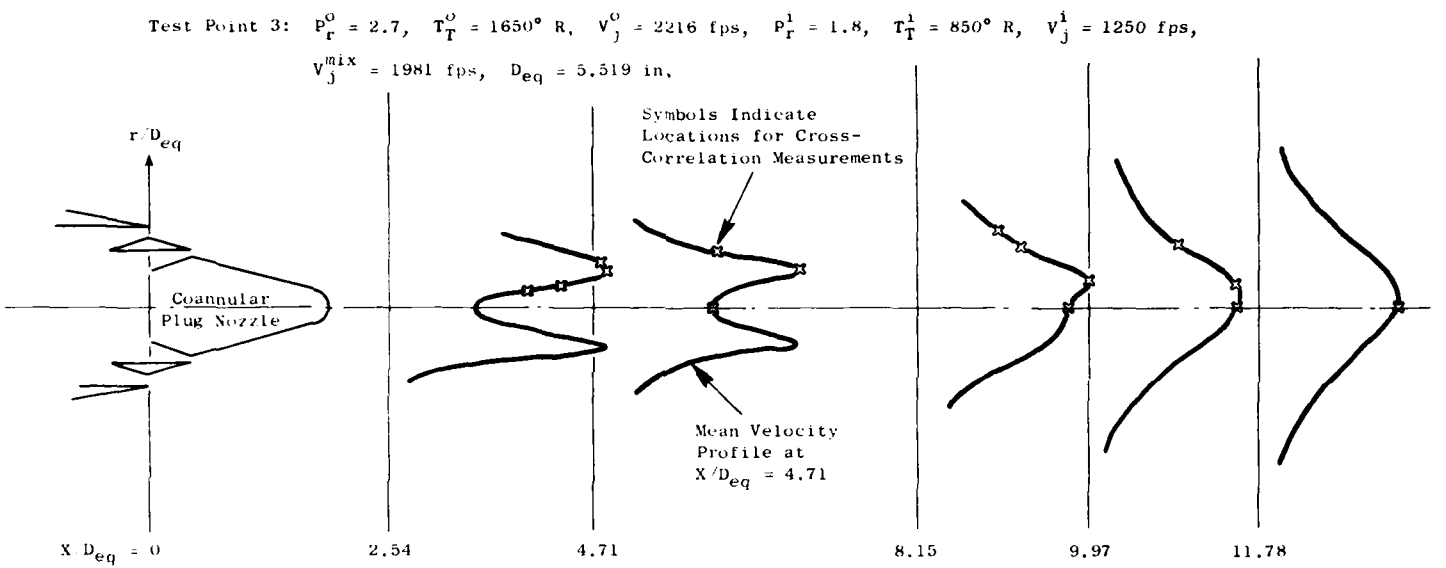

Figure 10-14. LV Measured Mean Velocity Flow Field for Test Point 3; In-Jet Cross Correlations.

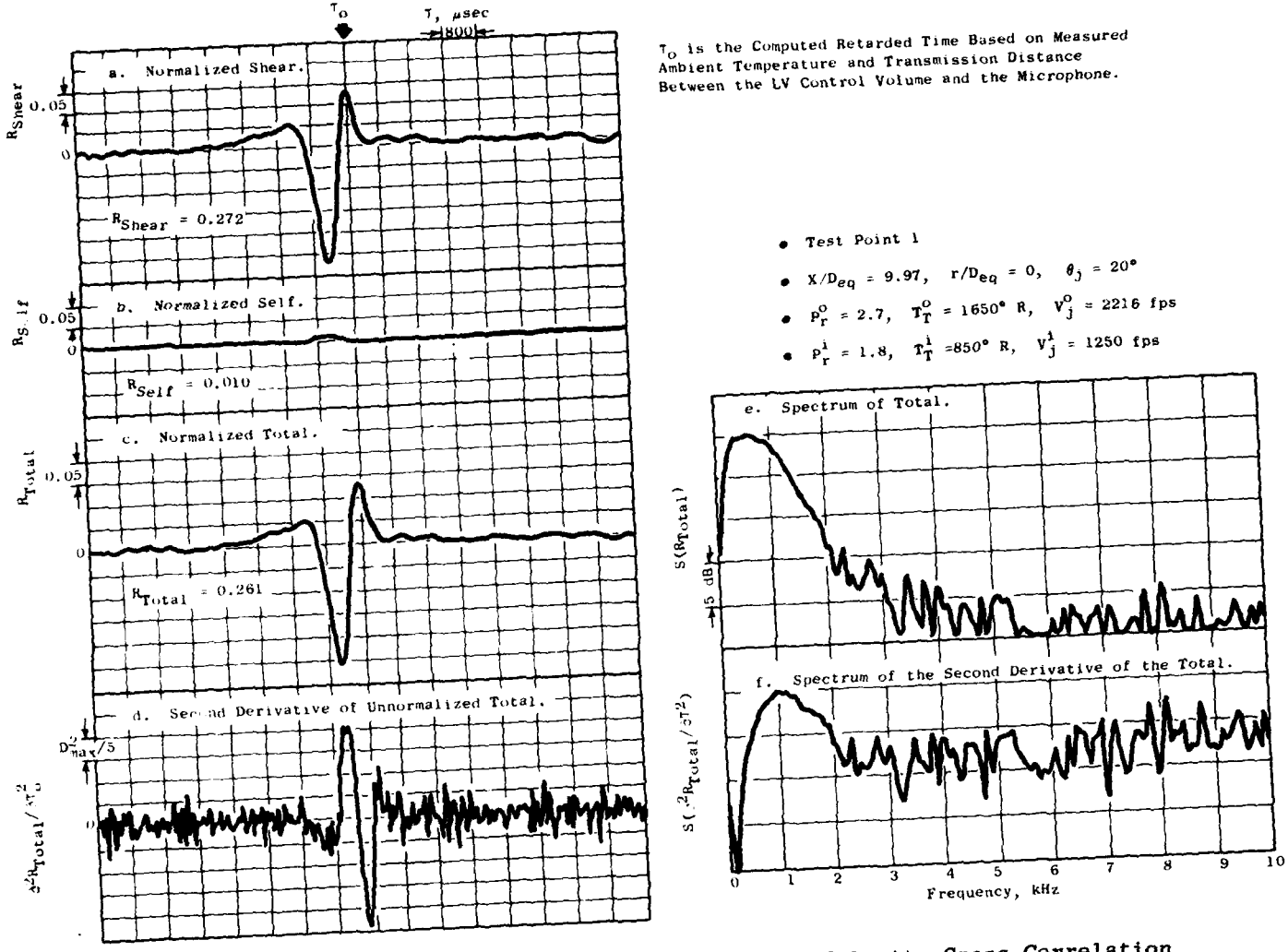

Figure 10-15. Laser Velocimeter Measured In-Jet Velocity Cross Correlation with Far-Field Acoustic Measurements for a Coannular Plug Nozzle.

The results of Figure 10-15 illustrate features which exemplify most of the measurements taken for this test series. The values of the measured in-jet velocity to far-field acoustic normalized cross-correlations are of significant magnitude (for this illustrative case $R_{Total} = 0.261$) and the actual measured correlation function shape is precise enough to ensure that "real" regions of strong correlations are being measured between the laser and the acoustic microphone. Figures 10-15a, b, c also show that the shear portion (that is, the mean/turbulence velocity interaction field) dominates the measured total cross-correlation function. The preeminence of the shear cross-correlation was found to be true for 100% of the measurements performed. Figure 10-15d shows the second derivative measurements. This figure illustrates that the new statistical estimator procedures developed (see Sections 7.0 and 8.0) together with the improvements of the laser processor, were successful*. The LV measured spectra of the total normalized cross-correlation function and its second derivative are shown in Figures 10-15e and f. These spectra results show that for the current measurement the dominant frequency is in the lower frequency end of the spectrum and is fairly clear in the region of importance. For R_{Total} the spectrum is quite good up to 3 kHz; thereafter, the results are more than 25 dB down from the peak. For the spectrum of the second derivative, after 15 dB down from the peak, the results indicate further improvement could be made to define the higher frequency region.

Figures 10-16a, b and c summarize some of the additional results obtained from this series of measurements. Figure 10-16a shows the axial variation of the maximum value of the total in-jet velocity to far-field acoustic pressure (at $\theta_{jet} = 20°$) for the coannular plug nozzle for the two test conditions tested; the results are for the centerline measurements only**. The values of R_{Total} show a range between 0.029 to 0.261, depending on axial location; with the maximum occurring between 8-10 Deq. For test point 2 (the higher velocity coannular plug nozzle test case), Figure 10-16b illustrates that R_{shear} is generally 20 times greater than R_{self} for all of the measurements.

---

*These new results are an up-date to previous results reported in Vols I and II of Reference 31.

**Peak values of R_{Total} were found along the centerline. See Table 10-3 for values at other radial locations. Also see the Appendix.

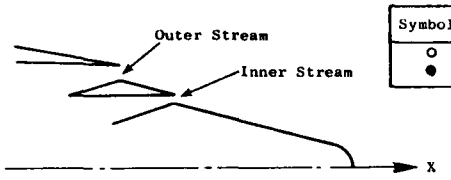

Symbol	Point	P_r^o	T_T^o, R	V_j^o, fps	P_r^i	T_T^i, R	V_j^i, fps	V_j^{mix}, fps	D_{eq}, in.
○	1	1.8	1650°	1758	1.8	850°	1250	1602	5.519
●	2	2.7	1650°	2216	1.8	850°	1250	1981	5.519

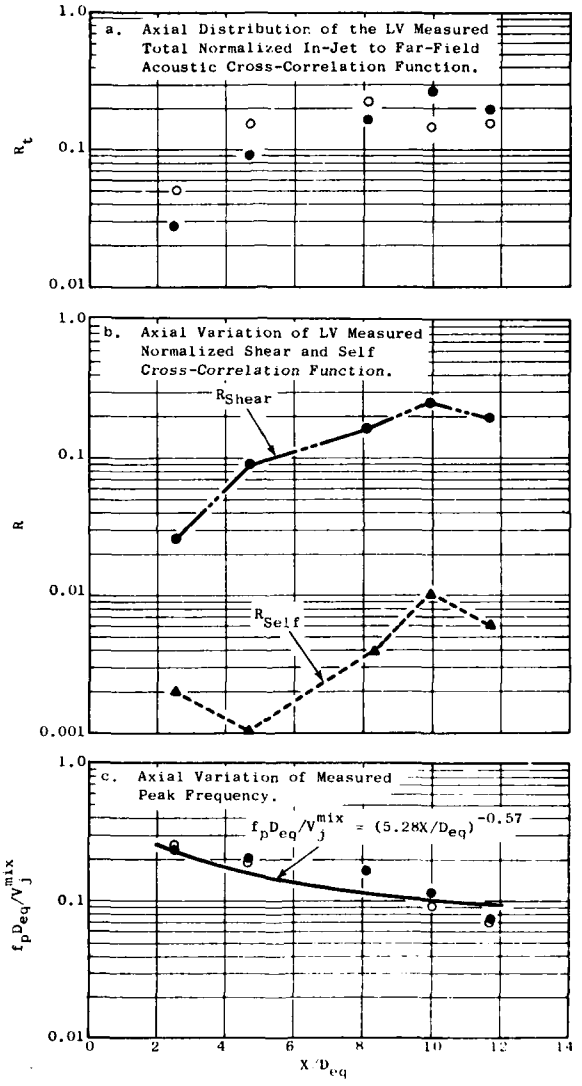

Figure 10-16. Laser Velocimeter In-Jet to Far-Field Measurements for a High Velocity and Temperature Coannular Plug Nozzle.

Figure 10-16c illustrates the axial variation of the peak frequency for both nozzle conditions tested. These results show that the measured peak frequency of the Fourier-Transform of R_{Total} decreases with increasing axial location (higher frequency close to the nozzle, lower frequency further downstream). The rate of decrease in frequency is somewhat slower than what would be expected from a conic nozzle. For illustrative purposes, it was found that:

$$\frac{f \cdot Deq}{V_j^{mix}} = (5.28\ X/Deq)^{-0.57}$$

is somewhat representative of the measured findings.

As an example of LV measured acoustic intensity per unit volume, Section 6.0 showed that the quantity to be evaluated was:

$$I/\Delta V = \frac{1}{a_o^3 r} \frac{\partial^2 R_u{}^2 p'}{\partial \tau^2}\bigg|_{\tau=\tau_o}$$

A measure of this quality* is illustrated using results from test case 2 at X/Deq = 9.97, r/Deq = 0. The maximum value of $\partial^2 R_u{}^2 p'/\partial \tau^2$ was found to be 3.2×10^{15} μbar-ft^2/sec^4. The distance from the measurement station to the acoustic microphone was 24.27 feet. Thus, the computed acoustic intensity level at $f_p \sim 500$ Hz is found to be ~ 110 dB at $\theta_j = 20°$. Measurements of acoustic intensity for this nozzle at the same V_j^{mix} (Reference 52) was found to be 114.8 dB at $f_{1/3} = 500$ Hz. The computed value of 110 dB from the LV measurements is considered to be quite representative since, in fact, it is expected that the 500 Hz spectrum is composed of noise elements from several jet volume sources.

*The value used to approximate $\partial^2 R_u{}^2 p'/\partial \tau^2|_{\tau=\tau_o}$ was the value of $\partial^2 R_u{}^2 p'/\partial \tau^2$ at the τ which $R_u{}^2 p'$ was measured as a maximum. This quantity is called D^2_{max} in Table 10-3 and is also shown on the cross-correlation figures. The results have shown that the τ for which $R_u{}^2 p'$ is a maximum always occurred slightly prior to the calculated τ_o. The reason the computed τ_o value itself was not used was because the real retarded time for these test cases are known to be less than the simple $\tau_o = r/a_o$. The reason this is true is that part of the sound transmission path is through the heated portion of the jet. During that period the sound is transmitted faster (due to the jet's higher temperature) than the ambient speed of sound. Thus the actual retarded time should be expected to be somewhat less than the r/a_o calculation.

The results illustrated above have shown that the laser velocimeter techniques developed over the past several years can be useful as a diagnostic tool for better understanding realistic jet nozzle turbulent and acoustic features at typical engine velocity and temperature conditions. The results have illustrated that important aerodynamic source term results, such as turbulent length scale, convection velocity, turbulent and mean velocity, can be measured for complex nozzle flow fields and that cross-correlation measurements between the point velocity field and the far-field acoustic radiation field have shown strong regions of correlation heretofore not measured. These results are considered to be quite encouraging for future investigations in nozzle noise and aerostructure characteristics of high velocity and temperature jets.

Some additional remarks regarding the cross-correlation function should be noted. As shown in Figure 10-15c the measured normalized cross-correlation function is somewhat symmetrical with a negative peak. This shape was not always the same for all measurements. For certain locations, the cross-correlation coefficient was symmetric with a positive peak. An example of this type of correlation function is given in the Appendix (X/Deq = 9.97, r/Deq = 0.246). The reason for such a contrasting difference between the two cross-correlation functions is expected to be related to some physical flow phenomenon which needs further evaluation and explanation.

11.0 CONCLUDING REMARKS AND RECOMMENDATIONS

11.1 CONCLUDING REMARKS

The studies and discussions contained in this report include a number of unique and modern concepts for laser velocimeter signal processing and data handling and reduction associated with performing real-time velocity and cross-correlation measurements in realistic jet exhaust nozzle flows. The introduction of the filter bank approach for LV signal processing and the use of quantized product factoring in the LV data handling cycle have enabled a time improvement of a factor of 90 in LV data acquisition in the most severe type of velocity and temperature conditions.

A series of two-point space-time velocity measurements for determining a jet's turbulent length scale and convection speed was successfully performed for a baseline conic nozzle and for an inverted velocity and temperature flow coannular plug nozzle. Experiments were performed in jet exhausts of 2200 fps and 1650° R. Additionally, a series of in-jet velocity to far-field acoustic cross-correlation measurements was performed on a coannular plug nozzle at sonic and supersonic heated flow conditions. Measurements of this type have not been previously performed. The results of the studies performed to date indicate that the LV technology is at hand to begin systematic aerodynamic and acoustic noise source type experiments for high temperature subsonic and supersonic exhaust jets.

Some of the results obtained from the recent cross-correlation measurements are:

- For a simple conic nozzle, there exists a radial and axial variation of turbulent length scale and convection speed throughout the jet.
- For the conic nozzle, it was found that not a great difference between ambient and heated jet flow existed for length scale and convection speed.
- For the inverted flow, coannular plug nozzle tested, an axial and radial variation of length scale and convection speed also was found. The physical picture that emerges is that the smaller

turbulent eddies of the exhaust plume are convecting along the center line, the larger eddies are at a 70% $\bar{U}_{max}$ stream-line on the outside of the jet, and intermediate size eddies are convecting along of the $\bar{U}_{max}$ stream line.

- The convection velocities for the coannular plug nozzle were found to be highest close to the nozzle and to gradually decay in speed with increasing axial location. The centerline and $\bar{U}_{max}$ streamline eddies convected the fastest, with the slower convecting eddies located at the 70% $\bar{U}_{max}$ streamline. Typical convection speeds ranged as $V_c = 0.4 - 1.0$ $V_{characteristics}$.

- Regions of strong correlation were measured on the coannular plug nozzle where the LV velocity signal was cross-correlated with an acoustic microphone. Normalized cross-correlations of 0.26 were obtained.

- For all tests performed, the shear turbulence aeroacoustic correlation function dominated. The shear cross-correlation coefficient was at least a factor of 20 greater than the self-turbulence aeroacoustic cross-correlation function.

- The peak frequence of the cross-correlation function varied as

$$\frac{f_p D_{eq}}{V_j^{mix}} = (5.28\ X/D_{eq})^{-0.57}$$

Thus, the classic notion of high frequency noise generation occurring close to the coannular plug nozzle and low frequency noise occurring downstream was verified.

11.2 RECOMMENDATIONS FOR FUTURE WORK

1. The development of the laser velocimeter as a viable, economical jet noise diagnostic tool has been demonstrated. It is recommended that a series of systematic and detailed measurements be performed to better define the turbulent structure of jets, convection speed and scale of turbulence. The initial nozzles recommended for study are: 1) the conic nozzle, 2) coaxial coplanar, 3) coannular plug nozzle. Experiments should be performed at subsonic and supersonic conditions. In addition, in-jet velocity to far-field acoustic pressure cross-correlation measurements on the above three nozzles should be performed to quantify the regions of strong correlation for these nozzles. Further extension of the methods developed here to partial coherence techniques is also recommended.

2. Application of some of the more modern theoretical acoustic modeling techniques toward additional definition and clarification of the aerodynamic source terms should be performed.

3. Although great strides have been made in the improvements of the LV processor and LV head, additional advancements will be forthcoming with the applications in large scale integrated circuits (microprocessors). Development as a Fast Fourier transform type LV processor with a microprocessor approach is recommended.

4. Expansion of the LV arrangement to include a multivector output arrangement is desirable.

APPENDIX - LASER VELOCIMETER IN-JET VELOCITY TO FAR-FIELD ACOUSTIC CROSS-CORRELATION MEASUREMENTS FOR A COANNULAR PLUG NOZZLE

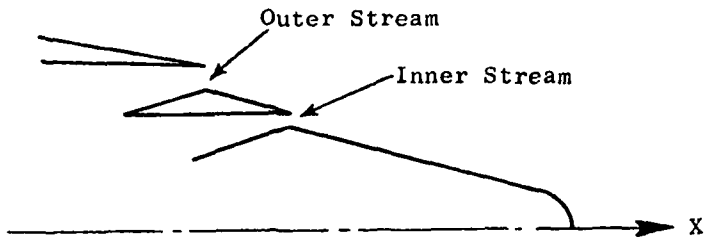

- Measurements Taken at: X/D_{eq} = 9.97; r/D_{eq} = 0, 0.246, 0.661
- D_{eq} = 5.519 inches
- Test Conditions:
  - Outer Stream: P_r = 2.7, T_T = 1650° R, V_j = 2216 fps
  - Inner Stream: P_r = 1.8, T_T = 850° R, V_j = 1250 fps

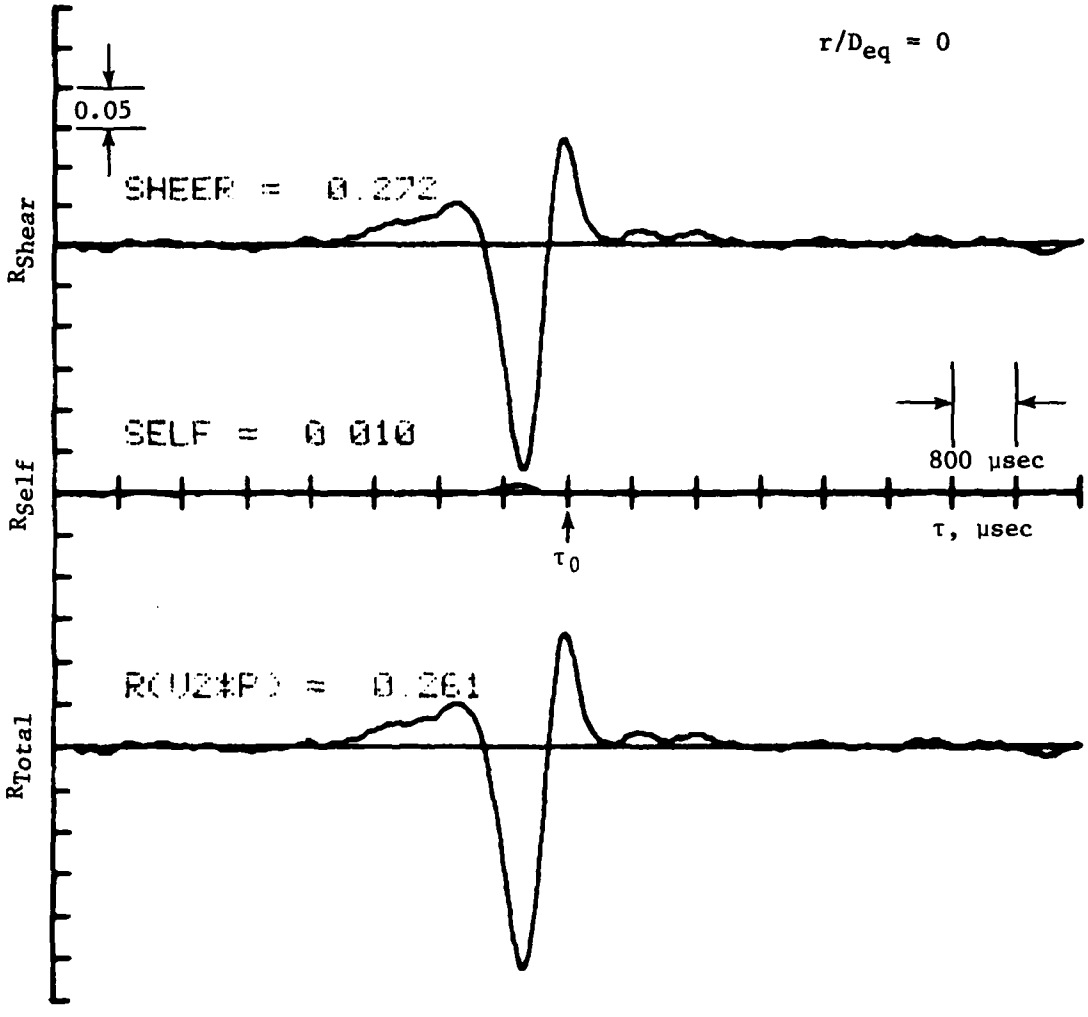
r/Deq = 0
0.05
SHEER = 0.272
RShear
SELF = 0 010
RSelf
800 µsec
τ, µsec
τ0
R(U2+P) = 0.261
RTotal

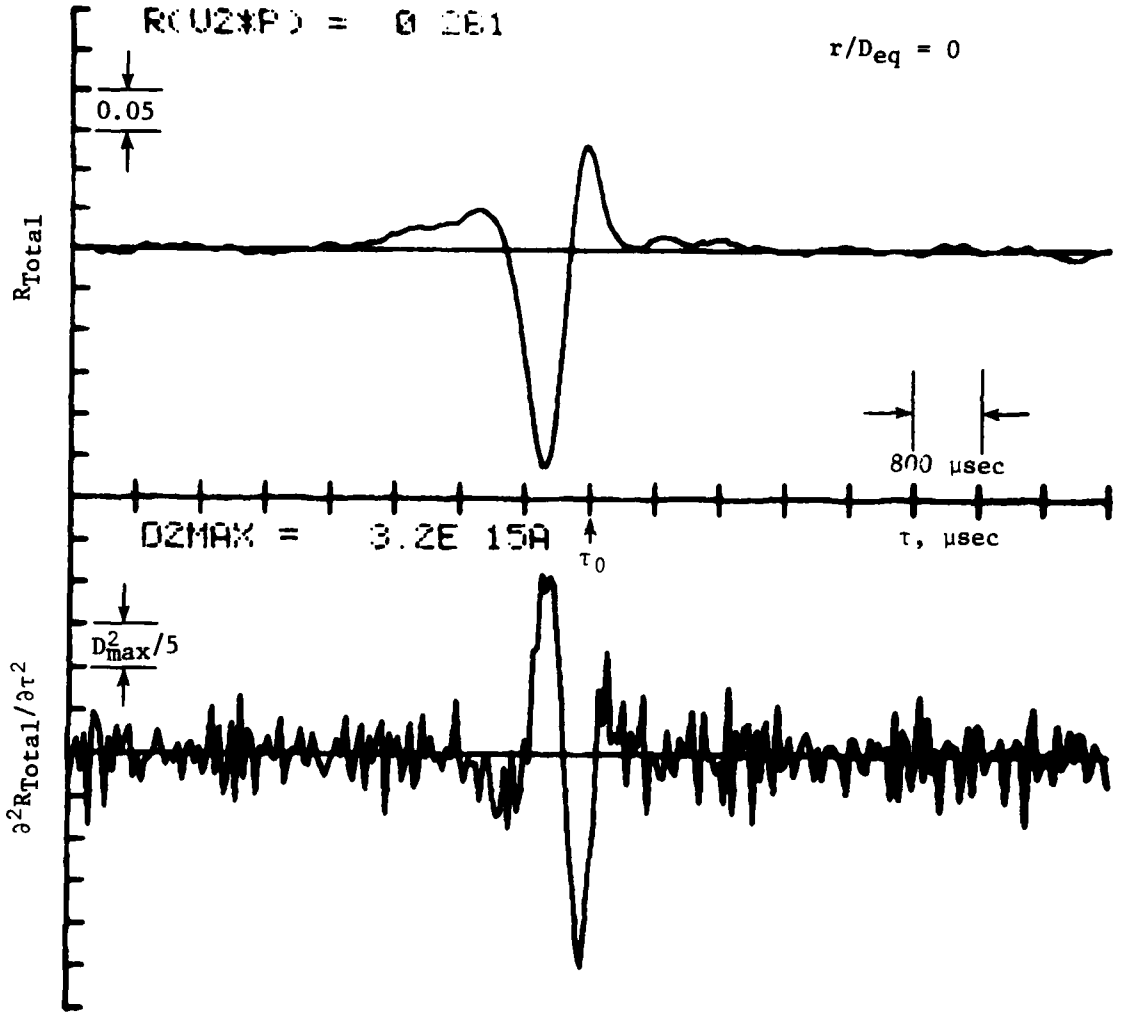
R(U2*P) = 0 2E1
r/Deq = 0
0.05
RTotal
800 μsec
DZMAX = 3.2E 15A
τ0
τ, μsec
D2max/5
∂2RTotal/∂τ2

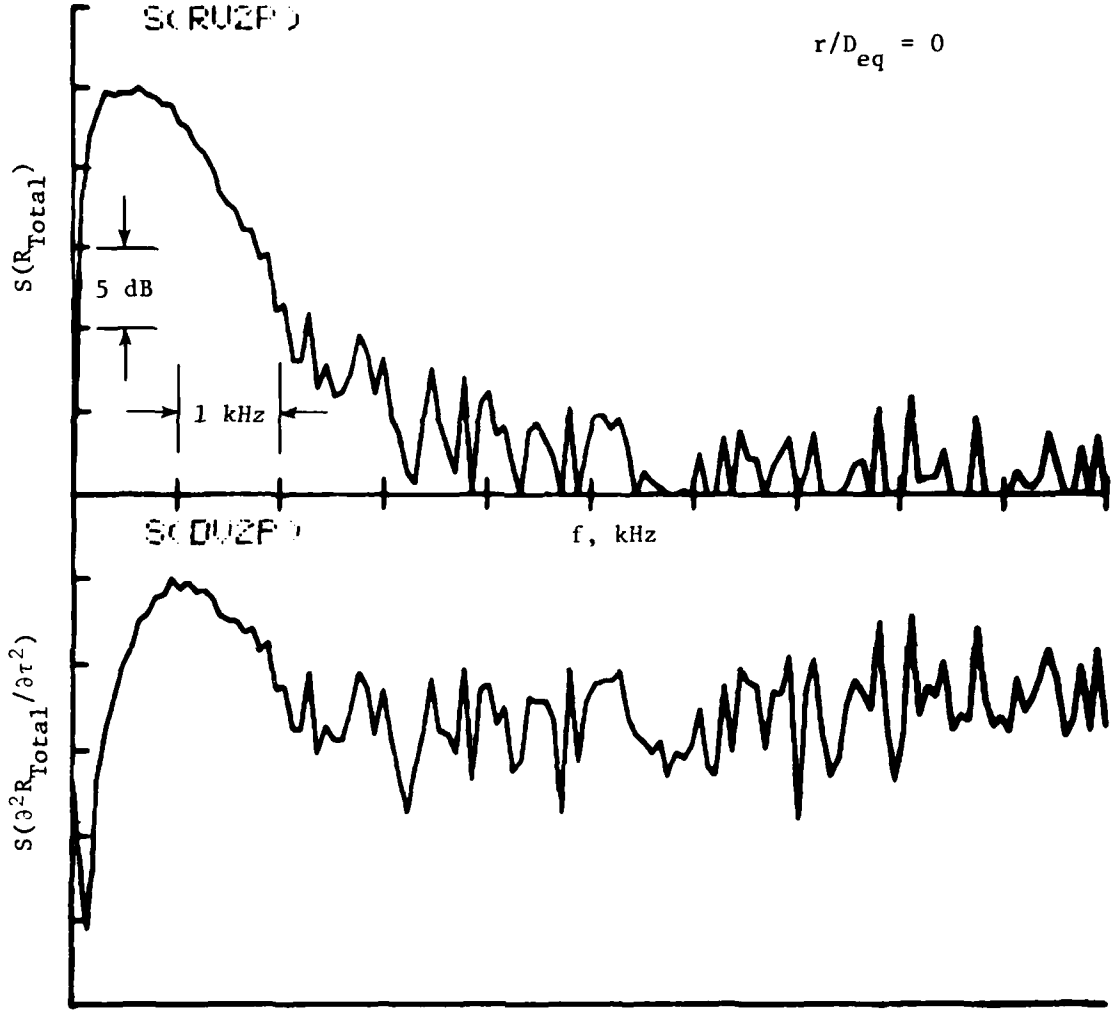
r/D_eq = 0
S(R_Total)
5 dB
1 kHz
f, kHz
S(∂²R_Total/∂τ²)

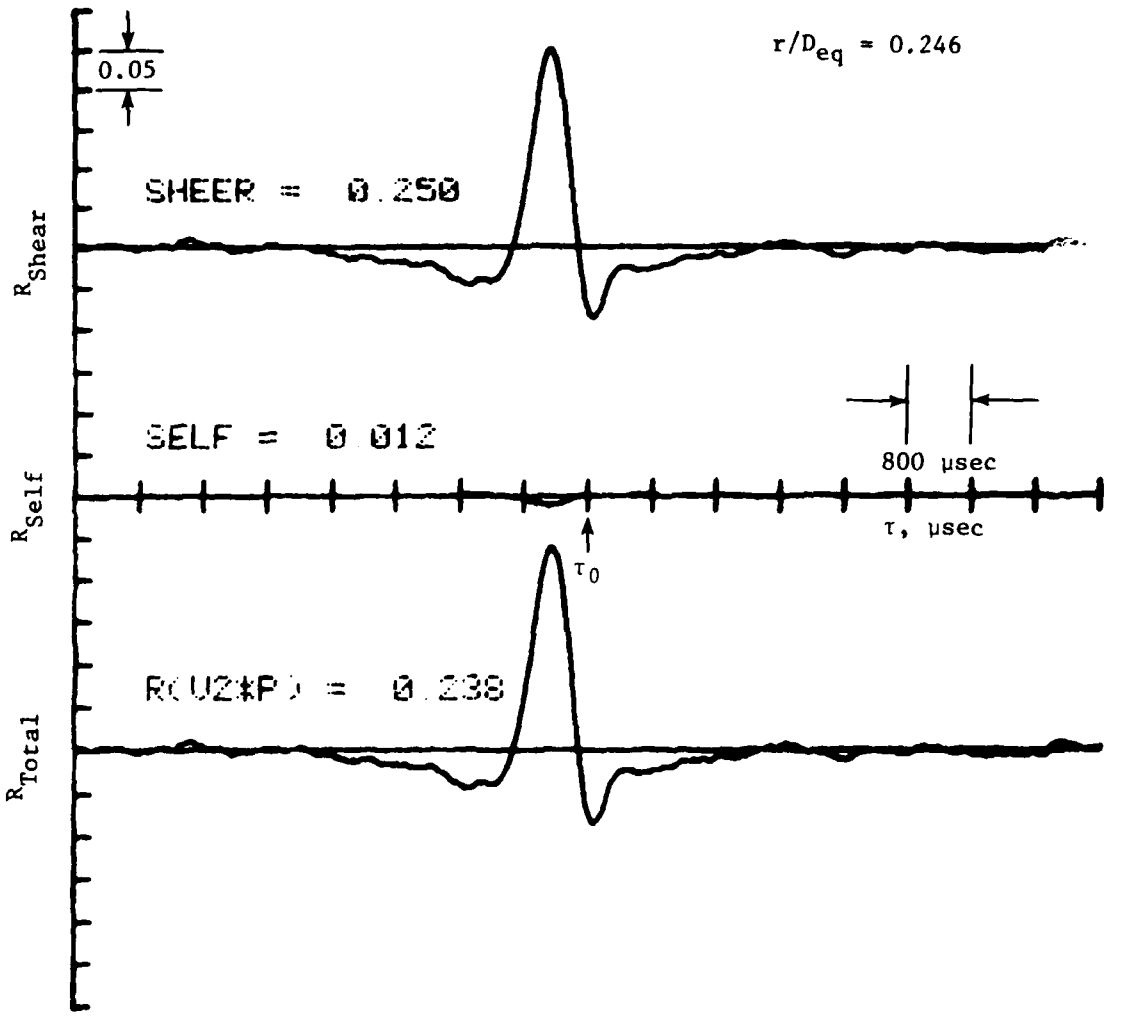
0.05
r/Deq = 0.246
SHEER = 0.250
RShear
SELF = 0.012
RSelf
800 μsec
τ, μsec
τ0
R(U2*P) = 0.238
RTotal

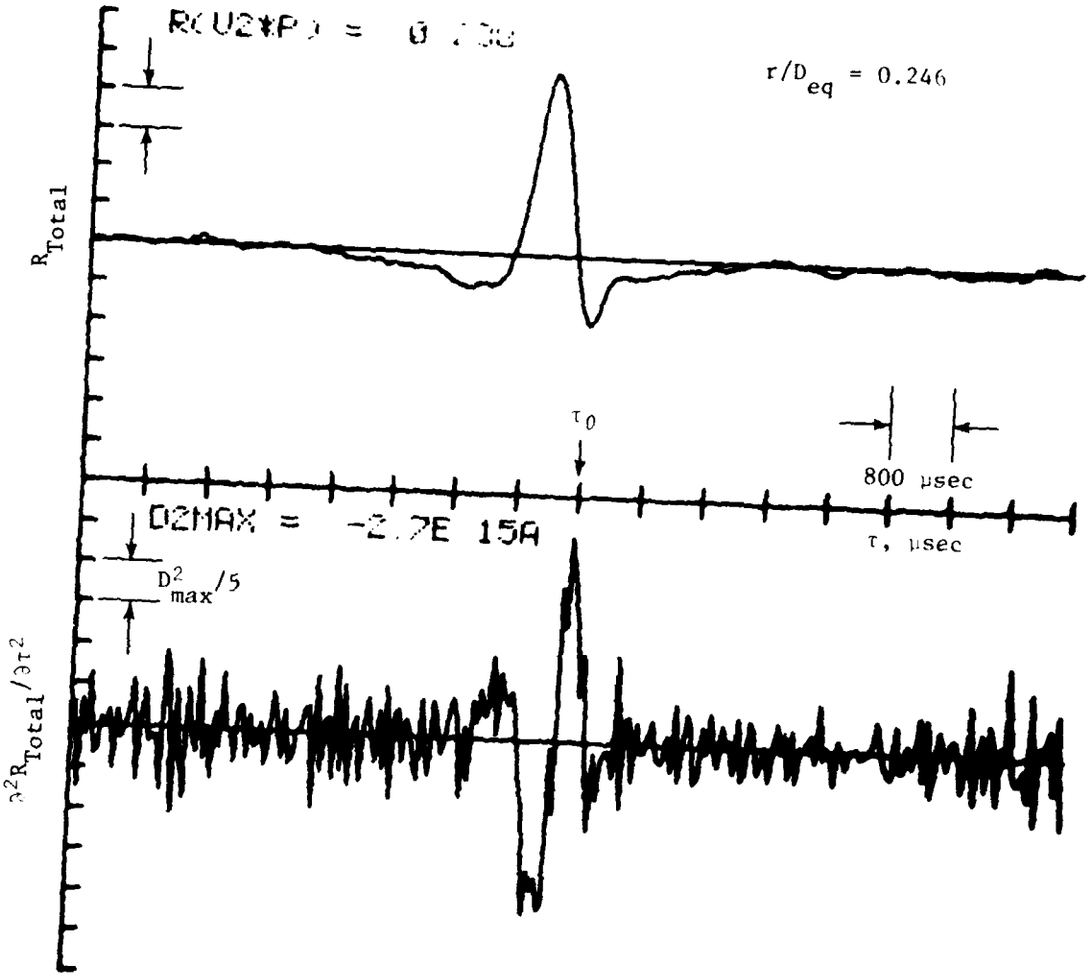
R(U2*P) = 0.238
r/D_eq = 0.246
R_Total
τ_0
800 μsec
τ, μsec
D2MAX = -2.2E 15A
D²max/5
∂²R_Total/∂τ²

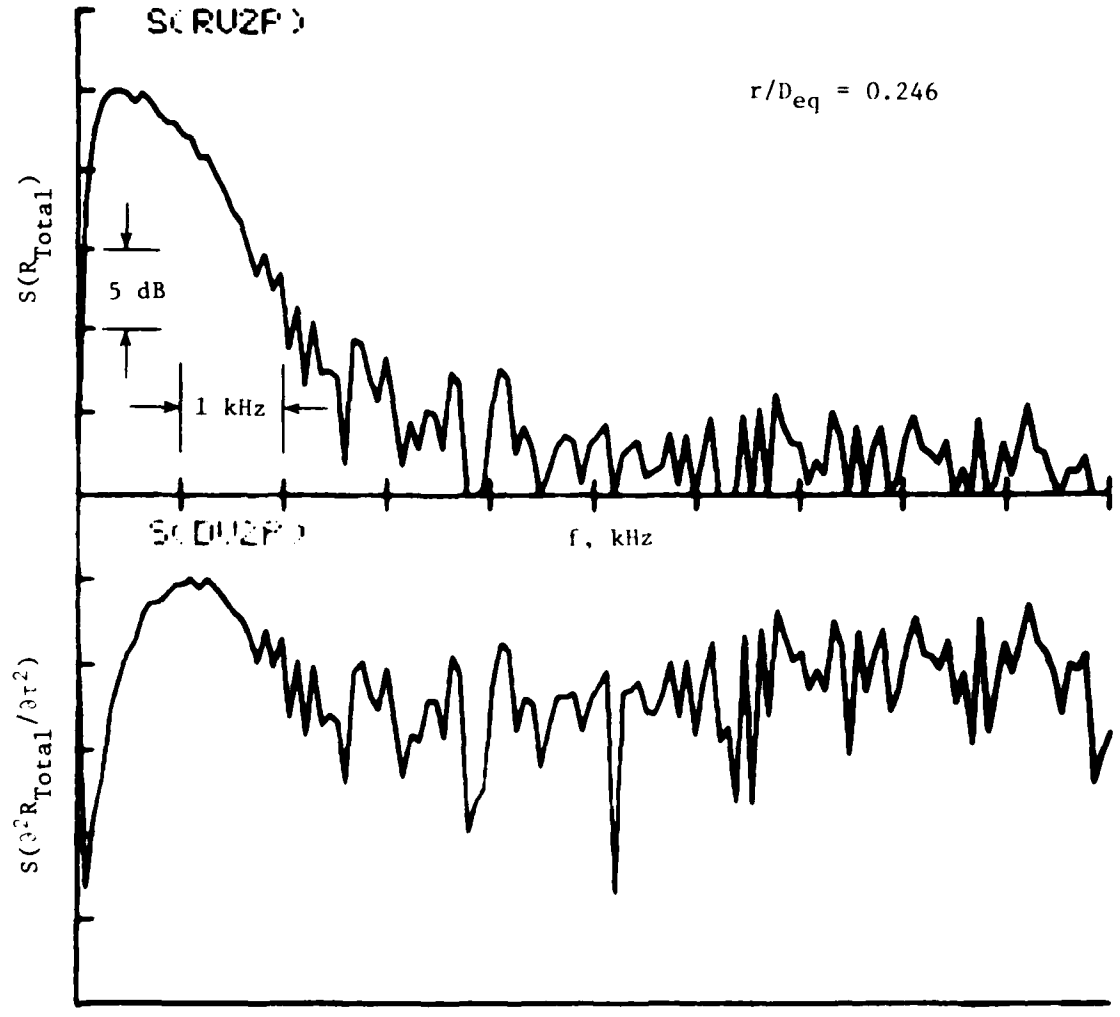
r/D_{eq} = 0.246
$S(R_{Total})$
5 dB
1 kHz
f, kHz
$S(\partial^2 R_{Total}/\partial r^2)$

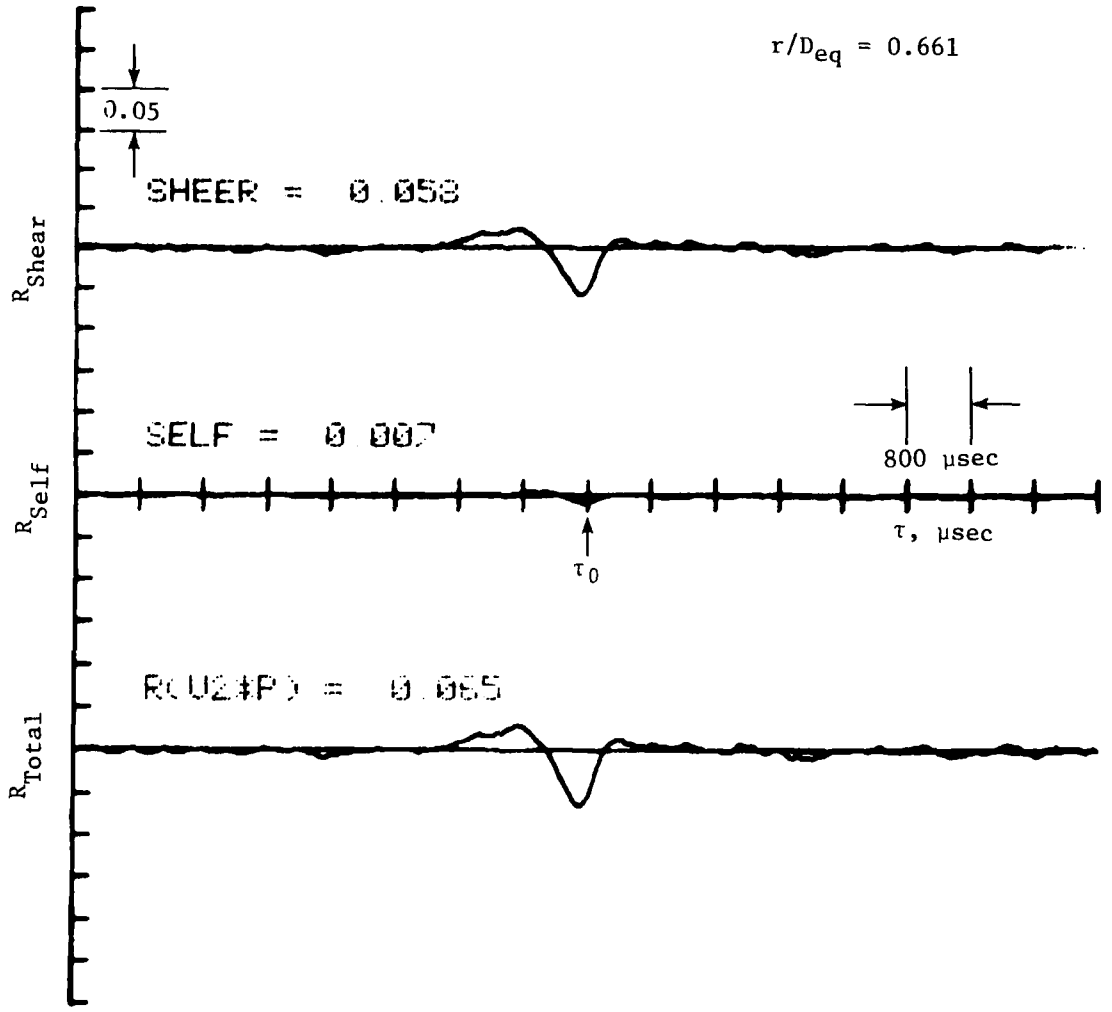
r/Deq = 0.661
0.05
SHEER = 0.058
RShear
SELF = 0.007
800 μsec
RSelf
τ, μsec
τ0
R(U2#P) = 0.065
RTotal

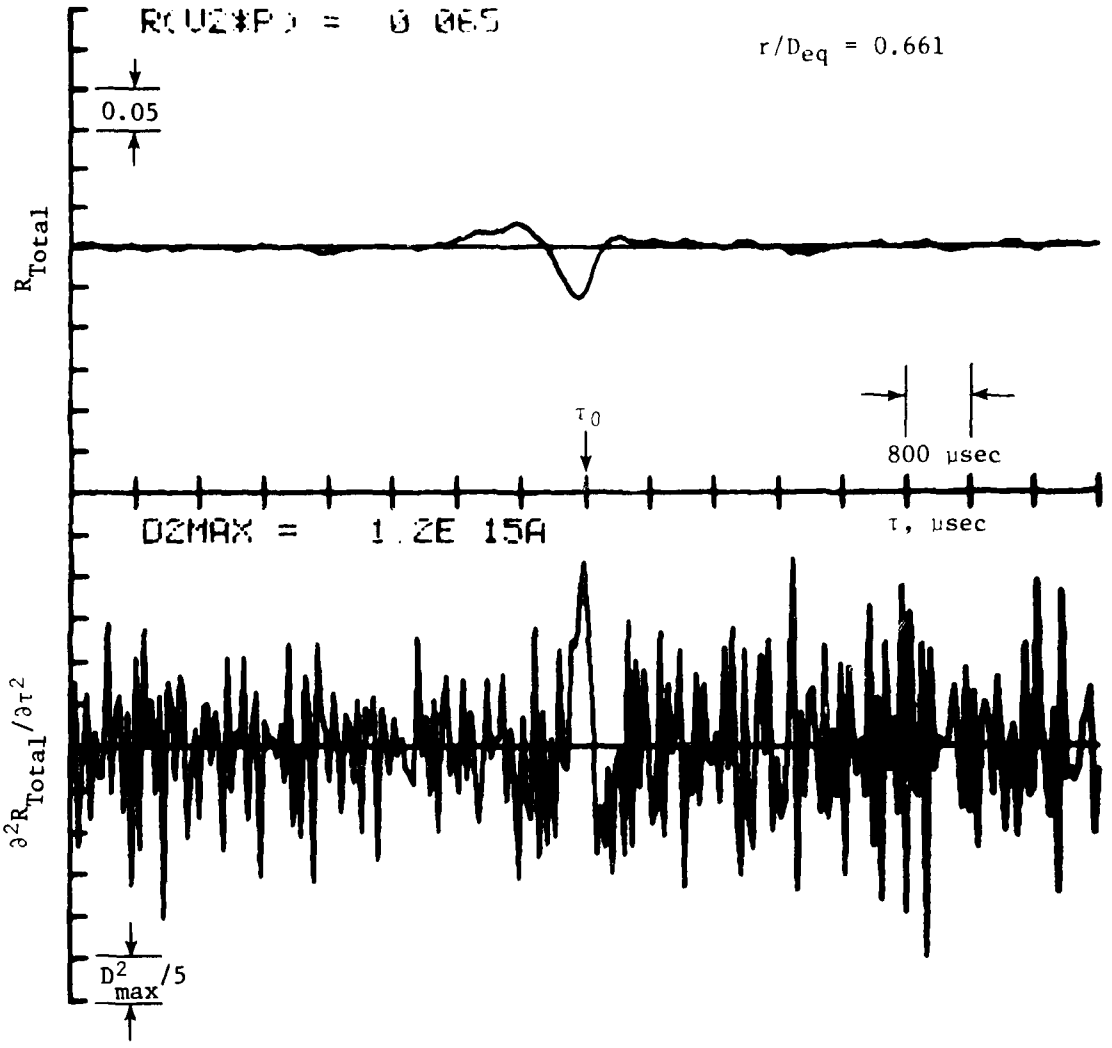
R(U2*P) = 0.065
r/Deq = 0.661
0.05
RTotal
τ0
800 μsec
τ, μsec
D2MAX = 1.2E 15A
∂2RTotal/∂τ2
D2max/5

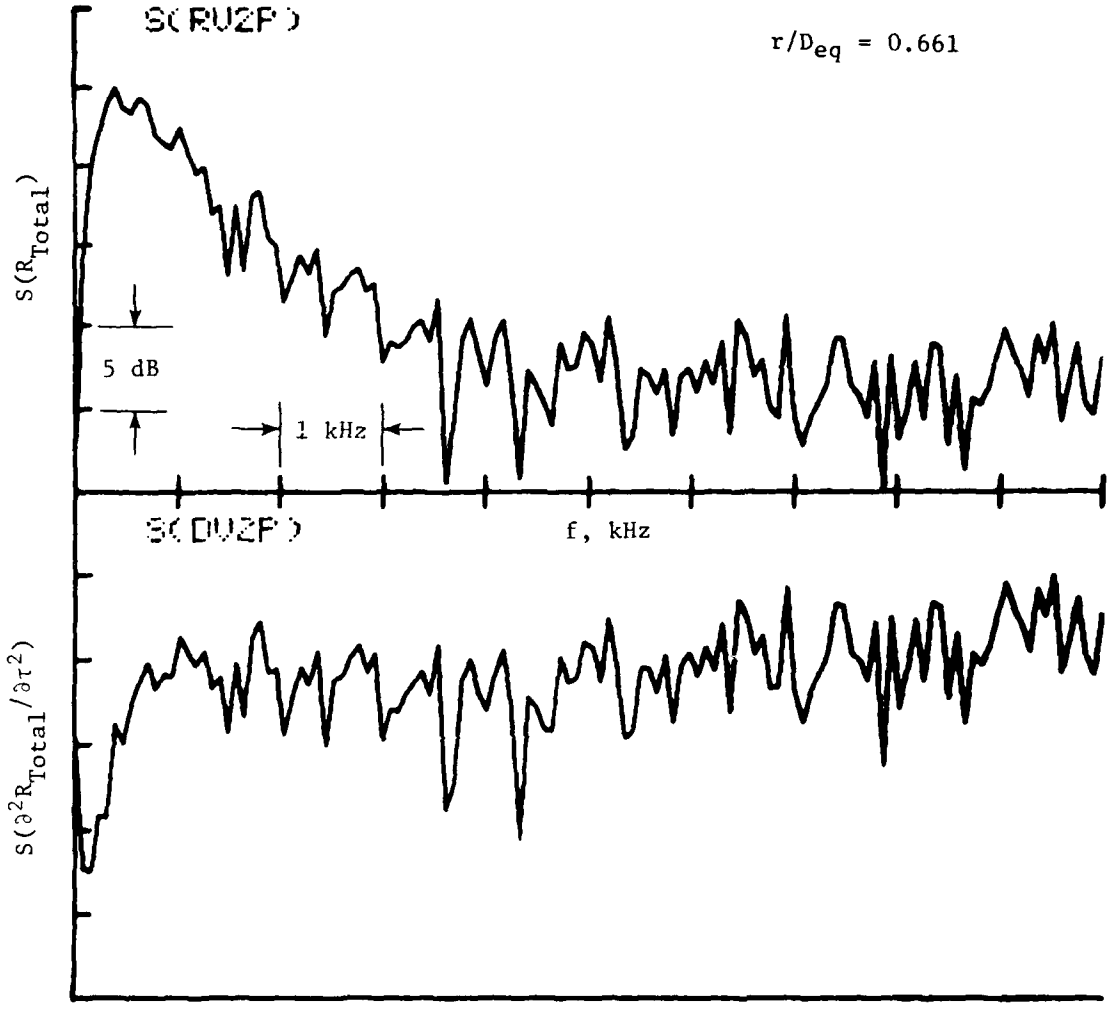
S(RU2P)
r/D_eq = 0.661
S(R_Total)
5 dB
1 kHz
S(DU2P)
f, kHz
S(∂²R_Total/∂τ²)

REFERENCES

1. Lee, R., Kendall, R.M., et al., "Research Investigation of the Generation and Suppression of Jet Noise," General Electric Company, NOAS 59-6160-C, January 1961.

2. Simcox, C.D., et al., "SST Technology Follow-On Program - Phase I - A Summary of the SST Jet Noise Suppression Test Program," Boeing Company, FAA-SS-72-41, February 1972.

3. Brausch, J.F. and Doyle, V.L., "Summary of GE4/SST Acoustic Suppression Research, Supersonic Transport Noise Reduction Technology Program, Phase I," General Electric Company, FAA-SS-72-42, December 1972.

4. Stringas, E.J. and Kazin, S.B., "Supersonic Transport Noise Reduction Technology Program - Phase II," General Electric Company, FAA-SS-73-29-1, September 1975.

5. Atvars, J., et al., "SST Technology Follow-On Program - Phase II," Boeing Company, FAA-SS-73-11, March 1975.

6. Hawkins, R. and Hoch, R., "Studies into Concorde's Engine Noise Reduction," NATO, AGARD-CPP-131.

7. Mani, R. and Stringas, E.J., "High Velocity Jet Noise Source Location and Reduction - Task 2 - Theoretical Developments and Basic Experiments," General Electric Company, FAA-RD-76-79, May 1978.

8. Bundy, F.P. and Strong, H.M., "Physical Measurements in Gas Dynamics and Combustion," Volume IX, Princeton University Press, 1954.

9. Yeh, Y., and Cummins, H.Z., "Localized Fluid Flow Measurements with He-Ne Laser Spectrometer," Applied Physics Letters, Vol. 4, 1964, p. 176.

10. Penney, C.M., "Differential Doppler Velocity Measurements," Paper No. 1.6 presented at the 1969 Institute of Electrical and Electronics Engineers, Conference on Laser Engineering and Application, Washington, D.C., May 26-28, 1969. Also IEE Journal of Quantum Electronics, Vol. QE-5, June 1969, p. 318.

11. Jenkins, F.A. and White, H.E., "Fundamental of Optics," McGraw-Hall, New York, New York, 1950.

12. Bloom, A.L., "Gas Laser," John Wiley & Sons, Inc., New York, New York, 1968.

13. Asher, J.A., Scott, P.F., and Wang, J.F.C., "Parameters Affecting Laser Velocimeter Turbulence Spectra Measuremnent," AEDC-TR-74-54 (1974).

14. Rolfe, E., Silk, J.K., Booth, S., Meister, K., and Young, R.M. "Laser Doppler Velocity Instrument," NASA Contractor Report CR-1199, Dec. 1968.

15. Lennert, A.E., Brayton, D.B., Crosswy, F.L., et al., "Summary Report of the Development of a Laser Velocimeter to be used in AEDC Wind Tunnels," ARO, Inc., Report No. AEDC-TR-70-101, July, 1970.

16. TSI, Inc. Catalog 900-477 "Laser Anemometer Systems," St. Paul, Minn., 1977.

17. DISA Electronics Catalog 5205E "Laser Doppler Anemometer Equipment," Franklin Lakes, N.J., 1977.

18. Jones, W.B., "Laser Fluid Velocity Sensor," Paper No. 2-8-82 Symposium on Flow, Pittsburg, Pa., sponsored by AIAA, AIP, and NBS, May, 1971.

19. Pike, E.R., "Photon Correlation Methods," Proceedings of the Second International Workshop on Laser Velocimetry, Purdue University, March 27-29, 1974.

20. Kalb, H.T., and Cline, V.A. "New Technique in the Processing and Handling of Laser Velocimeter Burst Data," pp. 708-711, Review of Scientific Instruments, Vol. 47, No. 6, June 1976.

21. Diermendjian, Closen, and Viegee, Journal of the Optical Society of America, 51, 621 (1961).

22. Engstrom, R.W., et al., Photomultiplier Manual, Chapter "Statistical Fluctuation and Noise," RCA Corporation, Harrison, N.J., 1970.

23. Benzakein, M.J. and Knott, P.R., "Supersonic Jet Exhaust Noise," Air Force Aero Propulsion Lab, AFAPL-TR-72-52, July, 1972.

24. Wisler, D.C., and Mossey, P.W. "Practical Applications of LV Systems to Aero Engine Research and Development," AGARD Lecture Series No. 90, "Laser Optical Measurement Methods for Aero Engine Research and Development," August - September, 1977.

25. Asher, J.A., "Laser Doppler Velocimeter System Development and Testing," GE Report 72CRD295, also published in AIAA Progress in Astronautics and Aeronautics, Vol. 34.

26. Whalen, A., "Detection of Signals in Noise," Academic Press, 1965.

27. Lighthill, M.J., 1952 Proceedings of the Royal Society A211, 564-587, "On Sound Generated Aerodynamically I. General Theory."

28. Lighthill, M.J., 1954 Proceedings of the Royal Society A222, 1-32. "On Sound Generated Aerodynamically II. Turbulence as a Source of Sound."

29. Knott, P.R., Benzakein, M.J., "Analytical and Experimental Supersonic Jet Exhaust Noise Research," AIAA 73-188 (1973).

30. Knott, P.R. et al., "Supersonic Jet Exhaust Noise Investigation," AFAPL-TR-74-25 (June 1974).

31. Knott, P.R. et al., "Supersonic Jet Exhaust Noise Investigation," Volume I, II, III and IV, AFAPL-TR-76-68 (July 1976).

32. Mani, R., "The Influence of Jet Flow on Jet Noise - Part I and II," Journal of Fluid Mechanics - Vol. 73, 1976, pp 753-793.

33. Balsa, T.F., "Fluid Shielding of Low Frequency Convected Sources by Arbitrary Jet," Journal of Fluid Mechanics, Vol. 70, 1975, pp 17-36.

34. Ribner, H.S., "The Generation of Sound by Turbulent Jets," Advances in Applied Mechanics, Vol. 3, Academic Press, New York, 1964, pp. 103-182.

35. Lee, H.K., "Correlation of Noise and Flow of a Jet," UTIAS Rep. 168, Aug. 1971.

36. Lee, H.K. and Ribner, H.S., "Direct Correlation of Noise and Flow of a Jet," AIAA 72-640.

37. Chu, W.T., "Turbulence Measurements Relevant to Jet Noise," UTIAS Report 119 (Nov. 1966).

38. Proudman, I., "The Generation of Noise by Isotropic Turbulence," Proc. Roy. Soc. A214, pp 119-132 (1952).

39. Clark, P.J.F. and Ribner, H.S., "Direct Correlation of Fluctuating Lift and Radiated Sound for an Airfoil in Turbulent Flow," Jour. of the Acoustical Society of America, Vol. 46, No. 3 (Part 2), 1969, pp 802-805.

40. Siddon, T.E., "Surface Dipole Strength for Flow Past Airfoils," Journ. of the Acoustical Society of America, Vol. 48, No. 1 (Part 1), 1970.

41. Meecham, W.C., and Forel, G.W., "Acoustic Radiation from Isotropic Turbulence," Journ. of the Acoustical Society of America, Vol. 30 No. 4, 1958, pp 318-322.

42. Seiner, J.M. and Reethof, G., "On the Distribution of Source Coherency in Subsonic Jets," AIAA 74-4 (1974).

43. Bendat, J.S. and Pierson, A., Random Data: Measurement & Analysis Procedures; Wiley; 1971; Sec. 6.3.

44. Enochsen, L. and Otnes, R. "Programming and Analysis for Digital Time Series Data," U.S. D.O.D., SUM-3, 1968 pg 215.

45. Hahn, G. and Shapiro, S., Statistical Models in Engineering, Wiley, 1967, Sec. 2-9.

46. Scott, P.F., "The Auto-Correlation Functions and Spectra of a Signal that has Been Randomly Sampled," Conference Record, IEEE76 CH1067-8. ASSP, pp 296-299.

47. Scott, P.F., "Distortion and Estimation of the Auto-Correlation Function and Spectrum of a Randomly Sampled Signal," General Electric, 76CR180, Class I, 1976.

48. Hinze, J.O., Turbulence; McGraw-Hill, 1959, pgs. 49-51.

49. Fletcher, R. and Reeves, C.M., "Function Minimization by Conjugate Gradients."

50. Scott, P., "The Theory and Implementation of LV Spectra Measurements," International Workshop on Laser Velocimeters, 23 March 1974.

51. Knott, P.R., Scott, P., Mossey, P., "Noise Source Diagnostic Methods with a Laser Velocimeter," 1977 Independent Research and Development Technical Plan, Volume III, March 1977, R77AEG326.

52. Knott, P.R., Blozy, J.T., Staid, P.S., "Acoustic and Performance Investigation of Coannular Plug Nozzle," NAS3-19777, May 1977.


DAT
FILM